

Manuscript Details

Manuscript number	AEOLIA_2018_87_R2
Title	Using GLUE to pull apart the provenance of atmospheric dust
Article type	Full Length Article

Abstract

Identifying the sources of aeolian dust is a crucial step in mitigating the associated hazards. We apply a Generalized Likelihood Uncertainty Estimation (GLUE) model to constrain the uncertainties associated with sediment fingerprinting of atmospheric dust in the Sistan region on the Iran-Afghanistan border, one of the world's dustiest places. 57 dust samples were collected from the rooftop of the Zabol Department of Environmental Protection during a summer dusty period from June to October 2014, in addition to 31 surface soil samples collected from potential sources nearby, including cultivated land (n=8), uncultivated rangeland (n=7), and two dry lakes: Hamoun Puzak (n=10) and Hamoun Saberi (n=6). Dust and soil samples were analyzed for 24 tracers including 16 geochemical elements and 8 water-soluble ions. Five optimum composite fingerprints (Fe, Sr, Mn, Cr and Pb) were selected for discriminating sources by a two-stage statistical process involving a Kruskal-Wallis test and stepwise discriminant function analysis (DFA). Uncertainty ranges for source contributions of dust determined by the GLUE model showed that the dry lake Hamoun Puzak is the dominant source for all dust samples from Zabol and cultivated land is a secondary source. We found marked spatial variance in the importance of regional dry lake beds as dust sources, and temporal persistence in dust emissions from Hamoun Puzak, despite very large areas of adjacent lake beds drying during the study period. Aeolian sediment fingerprinting studies can benefit considerably from the constraints provided by modelling frameworks, such as GLUE, for quantifying the uncertainty in dust provenance data.

Keywords	Sediment fingerprinting; uncertainty; GLUE; atmospheric dust; Iran
Corresponding Author	Matt Telfer
Corresponding Author's Institution	Plymouth University
Order of Authors	Reza Dahmardeh behrooz, hamid gholami, Matt Telfer, John Jansen, Abolhassan Fathabadi
Suggested reviewers	Jan-Berend Stuut, Richard Brazier

Submission Files Included in this PDF

File Name [File Type]

AEOLIA_2018_87_R2_Sistan_comments_addressed.pdf [Response to Reviewers (without Author Details)]

AEOLIA_2018_87_R1_Title_Page.docx [Title Page (with Author Details)]

AEOLIA_2018_87_R2_Manuscript.docx [Manuscript (without Author Details)]

Figure_3_R1.eps [Figure]

Figure_4_R1.eps [Figure]

Figure_5_R1.eps [Figure]

Figure_8_R1.eps [Figure]

Figure_9_R1.eps [Figure]

Figs 1-2-6-7-10-11_R2.docx [Figure]

AEOLIA_2018_87_R1_CRediT Author statement.docx [Author Statement]

To view all the submission files, including those not included in the PDF, click on the manuscript title on your EVISE Homepage, then click 'Download zip file'.

Research Data Related to this Submission

Data set

<https://data.mendeley.com/datasets/6672h2t3wb/draft?a=bf976f11-b4fa-4396-b6f0-61119f53049a>

Data for: Using GLUE to pull apart the provenance of atmospheric dust

The full distributions of Generalized Likelihood Uncertainty Estimate (GLUE) modelling used in Behrooz et al (submitted, Aeolian Research, 2018)

Manuscript Details

Manuscript number AEOLIA_2018_87
Title Using GLUE to pull apart the provenance of atmospheric dust

Abstract

We apply a Generalized Likelihood Uncertainty Estimation (GLUE) model to constrain the uncertainties associated with sediment fingerprinting aimed at source contributions of atmospheric dust in the Sistan region on the Iran-Afghanistan border. Fifty seven dust samples were collected from the rooftop of the Zabol Department of Environmental Protection during a summer dusty period from 23 June to 4 October 2014 in addition to thirty one surface soil samples collected from potential sources nearby, including cultivated land (n=8), uncultivated range land (n=7), and two dry lakes: Hamoun Puzak (n=10) and Hamoun Saberi (n=6). Dust and soil samples were analyzed for 24 tracers including 16 geochemical elements and 8 water-soluble ions. Based on our results, five optimum composite fingerprints (Fe, Sr, Mn, Cr and Pb) were selected for discriminating sources by a two-stage statistical processes involving a Kruskal-Wallis test and stepwise discriminant function analysis (DFA). Uncertainty ranges for source contributions of dust determined from our GLUE methodology showed that the dry lake Hamoun Puzak is the dominant source for all 57 dust samples from Zabol and cultivated land is a secondary source. We found marked spatial variance in the importance of regional dry lake beds as dust sources, and equally notable temporal persistence in dust emissions from Hamoun Puzak, despite very large areas of adjacent lake beds drying and becoming exposed during the study period. Aeolian sediment fingerprinting studies can benefit considerably from the constraints provided by modelling frameworks, such as GLUE, for quantifying uncertainty in dust provenance data.

Submission Files Included in this PDF

File Name [File Type]

Using_GLUE_to_to_pull_apart_aeolian_dust_provenance.pdf [Manuscript (without Author Details)]

To view all the submission files, including those not included in the PDF, click on the manuscript title on your EVISE Homepage, then click 'Download zip file'.

Research Data Related to this Submission

Data set <https://data.mendeley.com/datasets/6672h2t3wb/draft/b?a=YmY5NzZmMTetYjRmYS00Mzk2LWI2ZjAtNjExMTImNTMwNDIh>

Data for: Using GLUE to pull apart the provenance of atmospheric dust

The full distributions of Generalized Likelihood Uncertainty Estimate (GLUE) modelling used in Behrooz et al (submitted, Aeolian Research, 2018)

Using GLUE to pull apart the provenance of atmospheric dust

HIGHLIGHTS

- The GLUE model is applied to reveal the provenance of aeolian dust in Zabol, Iran.
- Quantitative estimates and uncertainties of four different dust sources are distinguished.
- One dry lake, Hamoun Puzak, is by far the dominant dust source, despite others nearby.
- The major dust source is insensitive to large changes in exposed local dry lake beds.
- Cultivated land is the second most important dust source, ahead of some playas.

Abstract

We apply a Generalized Likelihood Uncertainty Estimation (GLUE) model to constrain the uncertainties associated with sediment fingerprinting aimed at source contributions of atmospheric dust in the Sistan region of the Iran-Afghanistan border. Fifty seven dust samples were collected from the rooftop of the Zabol Department of Environmental Protection during a summer dusty period from 23 June to 4 October 2014 in addition to thirty one surface soil samples collected from potential sources nearby, including cultivated land (n=8), uncultivated range land (n=7), and two dry lakes: Hamoun Puzak (n=10) and Hamoun Saberi (n=6). Dust and soil samples were analyzed for 24 tracers including 16 geochemical elements and 8 water-soluble ions. Based on our results, five optimum composite fingerprints (Fe, Sr, Mn, Cr and Pb) were selected for discriminating sources by a two-stage statistical processes involving a Kruskal-Wallis test and stepwise discriminant function analysis (DFA). Uncertainty ranges for source contributions of dust determined from our GLUE methodology showed that the dry lake Hamoun Puzak is the dominant source for all dust samples from Zabol and cultivated land is a secondary source. We found marked spatial variance in the importance of regional dry lake beds as dust sources, and equally notable temporal persistence in dust emissions from Hamoun Puzak, despite very large areas of adjacent lake beds drying and becoming exposed during the study period. Aeolian sediment fingerprinting studies can benefit considerably from the constraints provided by modelling frameworks, such as GLUE, for quantifying uncertainty in dust provenance data.

60
61
62
63 29
64 30 **KEY WORDS:** sediment fingerprinting, uncertainty, GLUE, atmospheric dust, Iran
65
66 31

67 32 **1. Introduction**

68
69 33 Constraining the source of atmospheric dust particles circulating in the ancient past as well as the
70 34 present-day is central to understanding the manifold implications of dust in the Earth system
71
72 35 (Ridgwell, 2002; Goudie and Middleton, 2006; Shao et al., 2011). Ancient dust deposits are archives of
73
74 36 long-term environmental change (Dietze et al., 2016); the best-known and longest being the >8 Myr
75
76 37 loess record in China (Sun & Zhu 2010). Present-day dust storms trigger a series of negative off-site
77
78 38 and on-site repercussions (Goossens, 2003). Off-site effects include respiratory disease in humans and
79
80 39 non-humans, contamination of food and water supplies, and interference with traffic safety,
81
82 40 machinery, and electronics. On-site effects include the loss of soil organic matter, nutrients, and
83
84 41 overall agricultural productivity (Goudie and Middleton, 2006). From this perspective, identifying
85
86 42 sources of dust and quantifying multi-source contributions and their uncertainties is a key step
87
88 43 towards hazard mitigation, especially in drylands.

89
90 44
91
92 45 A diverse range of techniques have been employed for tracing sources of atmospheric dust, including
93
94 46 isotopic ratios (e.g., Krom et al., 1999; Nakano et al., 2004; Grousset and Biscaye, 2005; Chen et al.,
95
96 47 2007; Cao et al., 2008; Wang et al., 2005; Rio-Salas et al., 2012; Yang et al., 2009); mineralogical and
97
98 48 chemical characteristics (Shen et al., 2009); meteorological data (Rezazadeh et al., 2013; Nabavi et al.,
99
100 49 2016; Ge et al., 2016; Rashki et al., 2017); synthesis of isotopic and geochemical data (e.g., Aarons et
101
102 50 al., 2017; Wei et al., 2017; Chavagnac et al., 2008); synthesis of trace element and water-soluble ion
103
104 51 analyses (Dahmardeh Behrooz et al., 2017a,b); numerical simulation (Hamidi et al., 2014; Nabavi et
105
106 52 al., 2017); satellite data (Long et al., 2016; Cherboudj et al., 2016; Schepanski et al., 2012); and
107
108 53 multidisciplinary approaches (Yan et al., 2015; Cao et al., 2015). While most of the studies listed above
109
110 54 are highly successful at inferring dust sources, we note that in many cases the uncertainties associated
111
112 55 with ascribing provenance are not considered formally. We see this an important omission for two
113
114 56 reasons: 1) airborne dust is commonly generated simultaneously from multiple populations and areas
115
116 57 of fine-grained particles; and 2) these multiple populations are, in turn, typically an amalgam
117
118 58 generated from different sources and mixed to differing degrees over timescales ranging from
59 geological to individual storm events. In other words, dust provenance presents a diabolical mixing-
60 problem and hence uncertainty is fundamental. These two points ultimately stem from geomorphic
61 processes of fine-particle production, transport, deposition, and reworking.

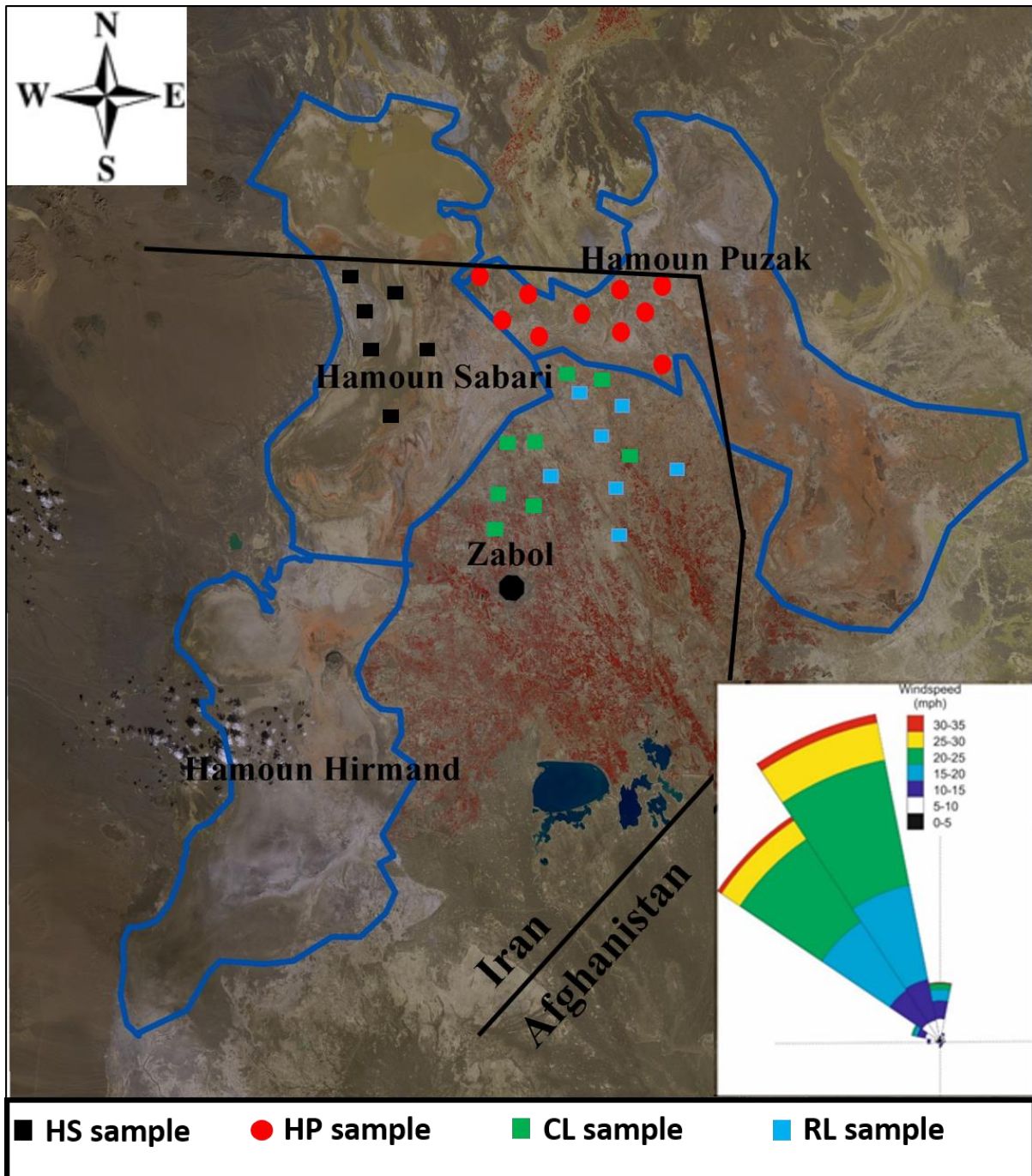
119
120
121
122 63 Sediment fingerprinting is widely used to quantify source contributions of fluvial sediments (e.g.,
123 64 Collins et al., 1997; Walling, 2005; Stone et al., 2014; Zhou et al., 2016a; and Manjoro et al., 2017) and
124 65 its application to aeolian problems is growing (e.g., Liu et al., 2016; and Gholami et al., 2017a,b).
126 66 Moreover, the uncertainties involved with this method are gaining increased attention (Walling,
127 67 2013). In order to manage and quantify the uncertainty in fluvial sediment fingerprinting, some studies
129 68 have applied a Monte Carlo simulation framework (e.g., Motha et al., 2003; Collins et al., 2012; Voli et
130 69 al., 2013; Smith and Blake, 2014; Stone et al., 2014; Sherriff et al., 2015; and Vale et al., 2016).
132 70 Similarly, Bayesian approaches are also applied to fingerprinting aeolian sands (Gholami et al., 2017b)
133 71 and fluvial sediments (e.g., Massoudieh et al., 2013; Cooper et al., 2014; Cooper et al., 2015; Stewart
135 72 et al., 2015; and Abban et al., 2016). Yet, several challenges remain in adequately capturing the
137 73 uncertainty associated with diverse aeolian dust sources and pathways (Walling, 2013) and we suggest
138 74 that techniques developed in other disciplines may offer a way forward (Gholami et al., 2017b).
139
140 75

141
142 76 First proposed for hydrological modelling by Beven and Binley (1992), GLUE (Generalised Likelihood
143 77 Uncertainty Estimation) has gained much favour as a tool for evaluating uncertainty estimates (e.g.,
144 78 Hassan et al., 2008; Zhou et al., 2016b; Viola et al., 2009; Mantovan and Todini, 2006; and Gong et al.,
146 79 2011). Here, we apply GLUE to the problem of dust provenance in the Sistan Hamoun region on the
148 80 Iran-Afghanistan border. Since it constitutes a major dust source for south-west Asia, Sistan has been
149 81 the focus of numerous previous investigations, (e.g., Goudie and Middleton, 2006; Rashki et al., 2012,
150 82 2013 a,b, 2015; Alizadeh Choobari et al., 2014). Recent work has generated an important geochemical
152 83 dataset of dust samples from a meteorological station at Zabol which has been analyzed geochemically
154 84 to provide qualitative estimates of source (Dahmardeh Behrooz et al., 2017a) and the temporal
155 85 variability of dust emissions (Dahmardeh Behrooz et al., 2017b). Here we provide the first attempt to
157 86 formally quantify aeolian dust provenance and associated uncertainties with this dataset using
158 87 (Dahmardeh Behrooz et al., 2017a; 2017b).

163 90 2. Study area

164
165 91 The Sistan-Hamoun study area (Fig. 1) straddles the border between Afghanistan and the Sistan and
166 92 Baluchestan province of south-eastern Iran (30°5' to 31°28' N and 61°15' to 61°50' E) (Rashki et al.,
168 93 2012, 2013a). The Hamoun lakes complex comprises three main lakes: Hamoun Hirmand, Hamoun
169 94 Saberi, and Hamoun Puzak, which are recharged primarily from Afghanistan by the Hirmand
171 95 (Helmand) River with smaller contributions from streams to the north and west (Esmaeili and Omrani,
172 96 2007). Following exceptionally high runoff, the lakes form a single body of water ~5700 km² in area
174
175
176
177

178
 179
 180 and ~13 Mm³ in volume (Sharifikia, 2013), though such events have become rare in recent decades
 181
 182 while dust emissions have grown correspondingly in magnitude (Goudie and Middleton, 2006; Rashki
 183
 184 et al., 2012).



100

101 *Figure 1: Sampling sites in the Sistan region: the dry-bed of Hamoun Puzak (HP); the dry-bed of Hamoun*
 102 *Sabari (HS); uncultivated range land (RL); and cultivated land (CL). Inset shows the hourly averaged*
 103 *wind regime for the period June-October 2014 (data source: National Climatic Data Centre, Climate*
 104 *Data Online).*

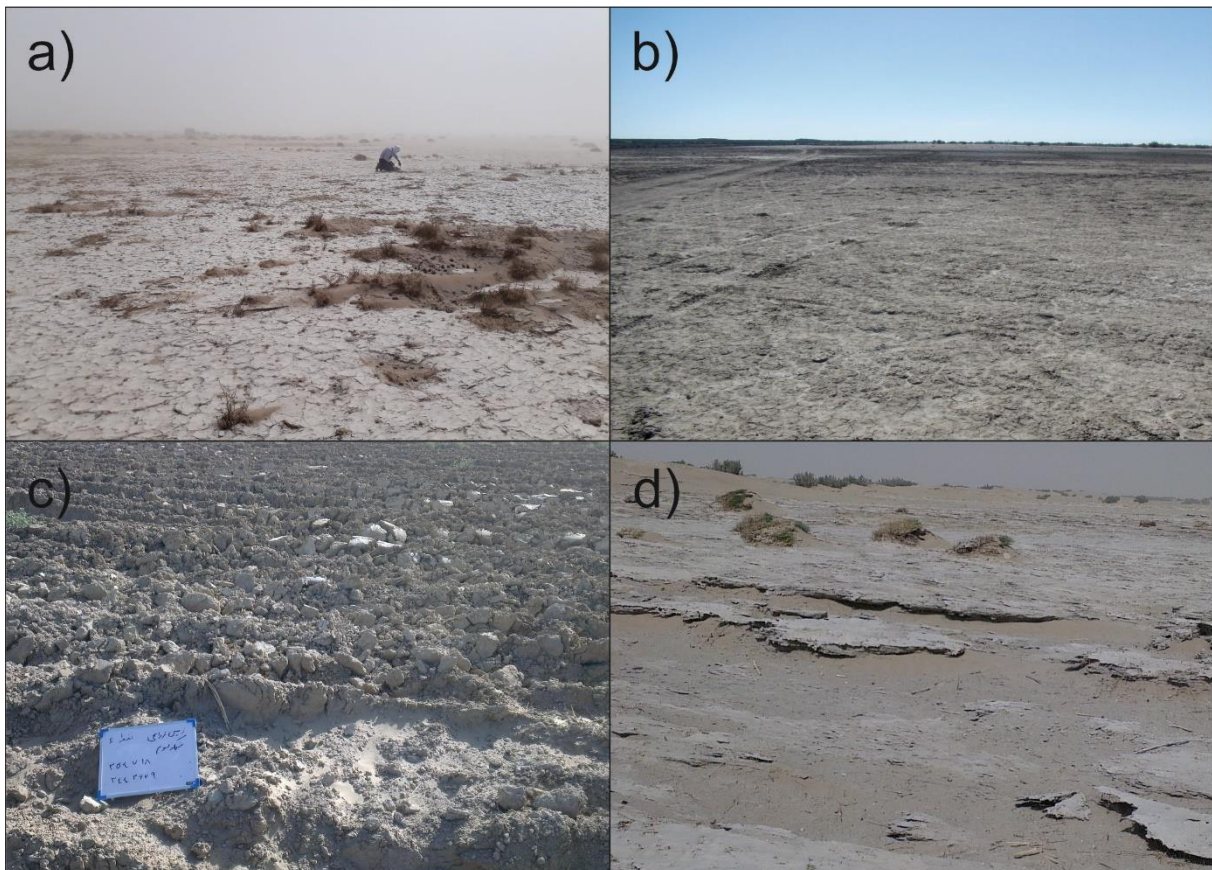
105 The climate in the Sistan region is arid to hyper-arid, and land-use is chiefly linked to agriculture and
 106 fishing. At Zabol meteorological station (Fig. 1), mean rainfall is 55 mm/y and mean evaporation is

237
238
239 107 >4000 mm/y (Moghaddamnia et al., 2009). The prevailing wind is the notorious “Wind of 120 Days”
240
241 108 from the north, which in the summer is accelerated into a Low-Level Jet (LLJ) by a persistent high-
242
243 109 pressure system over the Hindu Kush and the channeling effect of the surrounding topography
244
245 110 (Alizadeh-Choobari et al., 2014). As a result, the city of Zabol and its ~135,000 inhabitants experience
246 111 dust storms of catastrophic proportions, resulting in Zabol ranking as the world's most polluted city
247 112 for particulate matter less than 2.5 μm (PM2.5) in size (World Health Organisation, 2016).
248
249 113

250 114 3. Methods

251 115 3.1 Field sampling

252 116 We set out to characterise the soil materials for four different potential sources of atmospheric dust
253 117 emissions to the north of Zabol city (Fig. 1): 1) the dry lake-bed of Hamoun Puzak (Fig. 2a); 2) the dry
254 118 lake-bed of Hamoun Saberi (Fig. 2b); 3) cultivated arable farmland generally without crop-cover in
255 119 summer (Fig. 2c); and 4) bare land surfaces with sparse to negligible natural vegetation cover (Fig. 2d).
256 120 A total of 31 sufficient soil samples (<5 cm depth in a 30 cm² area) were collected from the four potential
257 121 sources (Table 1). We sieved the soil samples with a 400-mesh sieve, retaining particles with a nominal
258 122 geometric diameter of < 38.5 μm , which is equivalent to the aerodynamic diameter of dust (Cao et al.,
259 123 2008). After sieving we retained about 5 g of dust-sized material from each sample.
260
261
262
263
264
265



296
297
298
299
300
301
302
303
304
305
306
307
308
309
310
311
312
313
314
315
316
317
318
319
320
321
322
323
324
325
326
327
328
329
330
331
332
333
334
335
336
337
338
339
340
341
342
343
344
345
346
347
348
349
350
351
352
353
354

125 *Figure 2. Typical examples of the land surfaces we sampled. a) Hamoun Puzak dry lake-bed, b) Hamoun*
126 *Saberi dry lake-bed, c) close-up view of cultivated agricultural land surface during the summer months,*
127 *and d) sparsely vegetated, uncultivated rangeland.*


129 During an exceptionally dusty summer period in Zabol (23 June to 4 October 2014), 57 atmospheric
130 dust samples were collected at one- to four day intervals (Table 1) with sampling apparatus fitted to
131 the rooftop of the Department of Environmental Protection (5 m above ground level, 31°N, 61.3°E) in
132 an outer suburban area with no major industrial activities nor local fugitive dust sources. Our two dust
133 samplers (Model Chrono, Zambelli, Milan) were equipped with cyclones operating at a flow rate of
134 16.7 L/min as per the EU norms (Dahmardeh Behrooz et al, 2017a; 2017b). Total suspended-particle
135 (TSP) samples were collected in Teflon filters (0.45 µm pore size and 47 mm diameter) and then
136 desiccated for 24-hours at 25 °C. Dust mass concentrations were measured gravimetrically by
137 weighing the Teflon filters before and after sampling using an analytical balance (Adam model) with
138 ±0.1 mg precision. We refrigerated all dust samples at 4°C until chemical analysis (Dahmardeh Behrooz
139 et al., 2017 a).

141 **3.2 Laboratory analysis of water-soluble ions and trace elements**

142 We measured the concentrations of 8 water-soluble ions in our samples (viz., Na⁺, NH₄⁺, K⁺, Ca²⁺, Mg²⁺,
143 Cl⁻, NO₃⁻, NO₂⁻). Three cations (Na⁺, NH₄⁺ and K⁺) were measured with a Shim-pack IC-C1 (Shimadzu
144 DGU-12A) using 5-mM HNO₃ solution as eluent. Three anions (Cl⁻, NO₃⁻ and NO₂⁻) were measured with
145 a Shim-pack ICA1 (Shimadzu DGU-12A), using 2.5-mM phthalic acid combined with 2.4-mM tris-
146 (hydroxymethyl) aminomethane as eluent (Lin, 2002). Two cations (Ca²⁺ and Mg²⁺) were measured via
147 flame atomic absorption spectrometry (Philips, PU9400X, England).

149 After acid digestion, all samples were analyzed to determine the concentrations of 16 trace elements
150 (viz., Al, As, Au, Co, Cr, Cu, Fe, Li, Mg, Mn, Ni, Pb, Pt, Sn, Sr, and Zn) via Inductively Coupled Plasma
151 Atomic Emission Spectroscopy (ICP-OES, Perkin Elmer, Optima 2000, USA). Further details of
152 sampling and laboratory procedures are given in Dahmardeh Behrooz et al. (2017a,b).

154 **3.3 Two-stage method: Kruskal-Wallis test and discriminant function analysis**

155 Our  surements of 8 water-soluble ions and 16 trace elements form the basis of the sediment
156 fingerprinting method aimed at identifying the source contribution of the Zabol dust samples. We
157 adopt a two-stage statistical procedure following the approach of Collins et al. (1997). In stage one we
158 tested the primary ability of tracers to discriminate dust sources using the Kruskal-Wallis H test.

355
356
357 159 Tracers with critical values at the 95 % confidence levels or better were taken to the second stage in
358
359 160 which we identified optimum composite fingerprints using a stepwise discriminant function analysis
360
361 161 based on minimization of Wilk's lambda.

362 162 363 163 **3.4 Generalised Likelihood Uncertainty Estimation (GLUE)**

364 164 GLUE was first devised by Beven and Binley (1992) as a means of sensitivity analysis and uncertainty
365
366 165 estimation in environmental model outputs. We use GLUE to quantify the uncertainty in the sediment
367
368 166 fingerprinting results via the following five steps:

369
370 167
371 168 1) Random sampling of parameter sets (300,000 iterations) are conducted using the Latin Hypercube
372
373 169 Sampling (LHS) method (Zhou et al, 2016b) and assuming source contributions from each source are
374
375 170 non-negative and total contributions sum to unity. Due to the lack of prior information, we used a
376
377 171 uniform distribution as the prior distribution for all parameters.

378 172
379 173 2) Selection of a likelihood function and behavioral parameter thresholds. Here, we adopt the Nash–
380
381 174 Sutcliffe coefficient (ENS) as the likelihood function (Jin et al, 2010):

$$382 175
383
384 176 ME = 1 - \frac{\sum(O_{obs} - O_{sim})}{\sum(O_{obs} - \hat{Q}_{obs})} = 1 - \frac{\sigma_i^2}{\sigma_{obs}^2} \quad (eq.1),$$

385
386 177
387 178 where \hat{Q}_{obs} is the mean value of the observed tracer concentration; O_{sim} is the simulated tracer
388
389 179 concentration; O_{obs} is the observed tracer concentration; σ_i^2 is the error variance for the i th model
390
391 180 (i.e., the combination of the model and the i th parameter set) and σ_{obs}^2 is the variance of the
392
393 181 observations.

394 182
395 183 3) Sampled parameter sets from step 1 are input to the mixing model (equation 2) and the likelihood
396
397 184 function is calculated for each parameter set as:

$$398 185
399
400 186 C_{dust} = C_{Sources} \times P \quad (eq. 2)$$

401 187
402
403 188 where P is an m dimensional column vector of sources contribution (sampled parameter sets), C_{dust}
404
405 189 is an n-dimensional column vector of element concentration in sediment sample, $C_{Sources}$ is an $n \times m$ -
406
407 190 dimensional matrix representing mean tracer concentration in sources (each row represents mean
408
409 191 tracer concentration in each source), where n is the number of optimum composite fingerprints (n=5)
410
411 192 and m is the number of dust sources (m=4).

414
415
416
417
418
419
420
421
422
423
424
425
426
427
428
429
430
431
432
433
434
435
436
437
438
439
440
441
442
443
444
445
446
447
448
449
450
451
452
453
454
455
456
457
458
459
460
461
462
463
464
465
466
467
468
469
470
471
472

193
194
195
196
197
198
199
200
201
202
203
204
205
206
207
208
209
210
211
212
213
214
215
216
217
218
219
220
221
222
223

4) Parameter sets are divided into behavioural and nonbehavioural types with respect to a threshold value (Zhou et al, 2016). In this step, those parameter sets that have likelihood functions greater than a threshold value were classified as behavioural parameter sets. For the next step, nonbehavioural parameter sets were discarded.

5) For behavioural parameter sets, likelihood weights are rescaled such that they sum to one, then each parameter is sorted and we calculate cumulative distributions for each parameter. Quintiles and uncertainty intervals are calculated via the cumulative distributions.

3.5 Geospatial analysis and climate data

Landsat data were downloaded from the United States Geological Survey's Earth Explorer, and all analysis was conducted within ArcGIS 10.3. Quantitative analysis of water extent was conducted using a modified Normalized Difference Water Index (NDWI), based on the green (Band 3) and short-wave infrared (Band 6) bands of Landsat 8 data (Xu, 2006). Climate data are taken from the Hourly Global Surface Data (DS3505) dataset for the Zabol station (World Meteorological Organization ID: 40829), accessed via the legacy Climate Data Online (CDO) portal of the National Oceanic and Atmospheric Administration's (NOAA) National Climatic Data Centre (NCDC) online (available at <https://www7.ncdc.noaa.gov/CDO/dataproduct>).

4. Results

4.1 Kruskal-Wallis test and discriminant function analysis

The results of the Kruskal-Wallis tests (Table 2) indicate that among the twenty-four measured properties (8 water-soluble ions and 16 element concentrations), thirteen trace elements (Mg, Sr, Li, Fe, Cr, Cu, As, Ni, Pb, Mn and Sn) and one ion (Ca^{2+}) show statistically significant differences at the 95 %-level between our four potential dust sources (the two dry lake beds, cultivated farmland, and areas of natural vegetation cover). Trace elements clearly out-performed water-soluble ions for tracking spatial sources of dust. We passed the thirteen trace elements to stage-two for stepwise discriminant function analysis (DFA). The DFA yielded five trace elements (Fe, Sr, Mn, Cr and Pb) with optimum composite fingerprints that correctly discriminate 87 % of our source samples (Table 2 and Fig. 3).

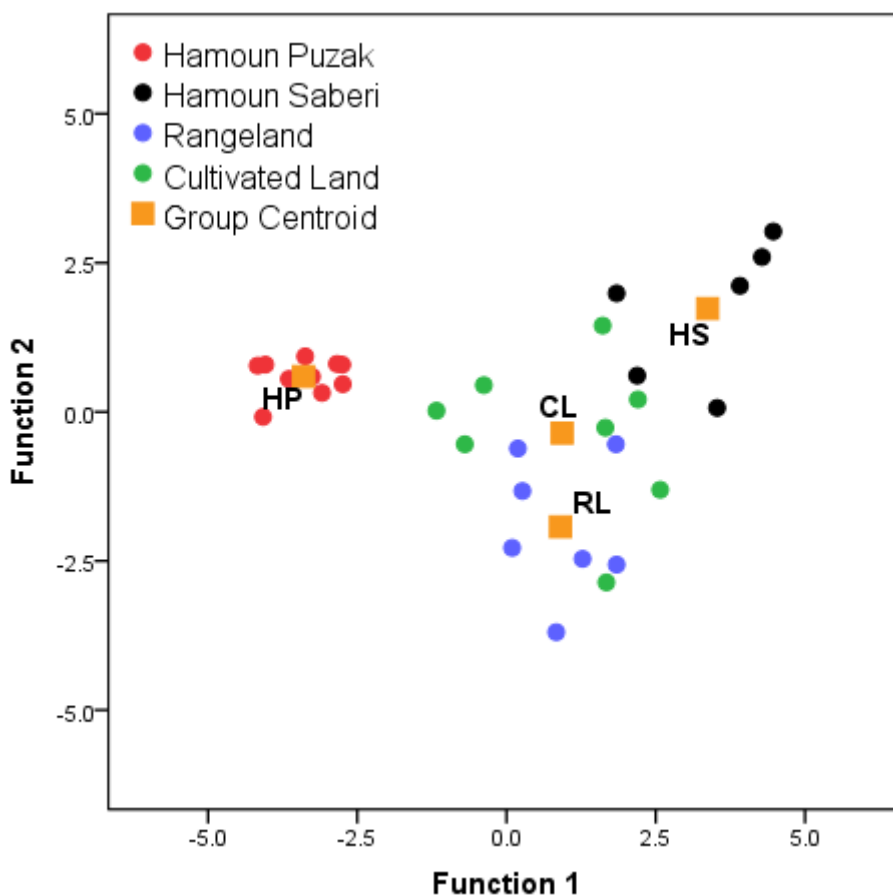


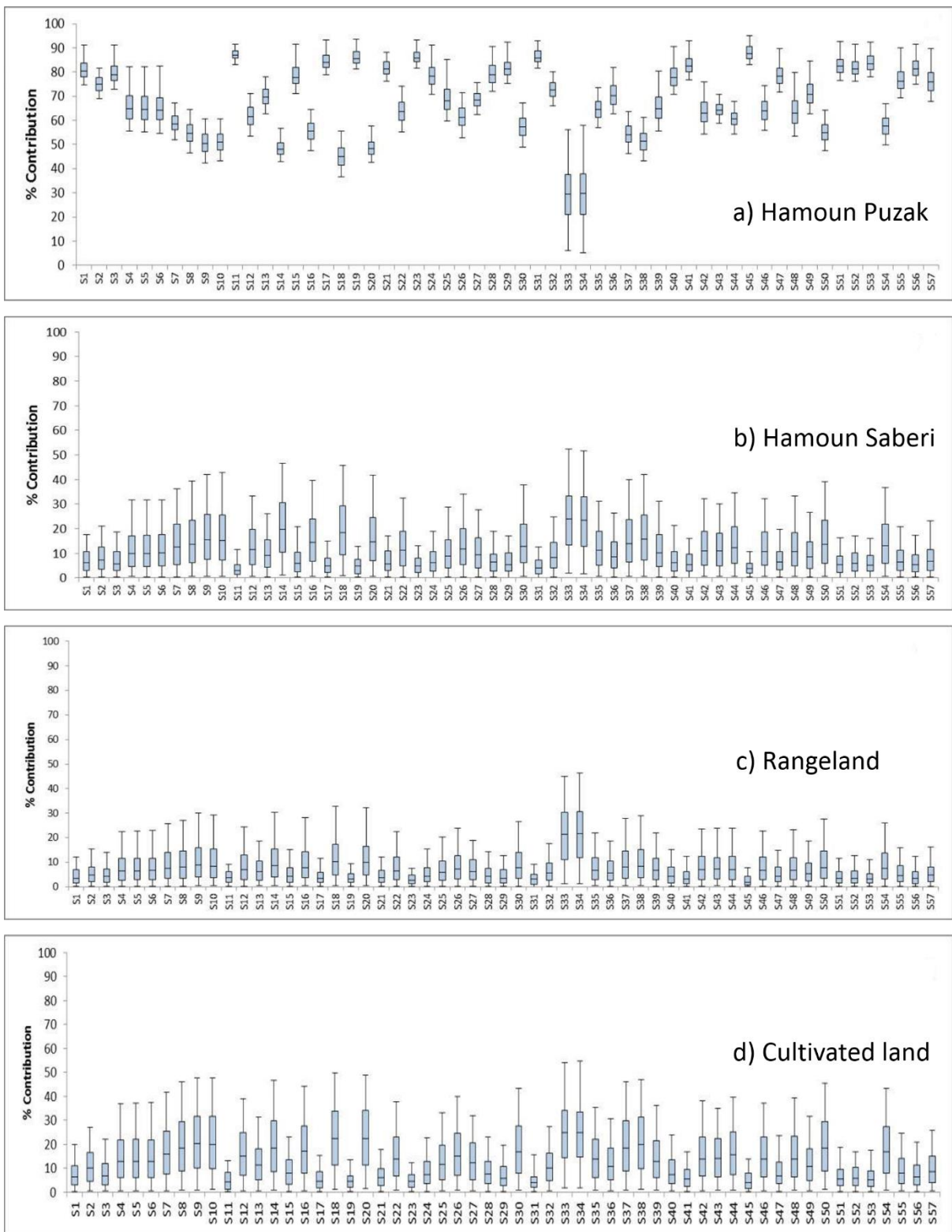
Figure 3. Scatterplot constructed from the first and second functions derived from a stepwise DFA for the source groups including the four land (i.e. Hamoun Puzak (HP), Hamoun Saberi (HS), cultivated land (CL) and uncultivated rangeland (RL). Five optimum fingerprints (Fe, Sr, Mn, Cr and Pb) were used to construct the scatterplot and 87% of the source samples are discriminated, correctly.

4.2 Using GLUE to constrain uncertainty in the source contributions of dust

Uncertainty intervals of source contributions estimated by our GLUE-mixing model at the 95 % confidence level are presented in Figure 4. These results show that the most important dust source is clearly Hamoun Puzak (Figs 4a and 5). Median contributions from this lake-bed span 29 to 88 % (samples 33 and 45, respectively). Hamoun Saberi is a less important source for our samples. Median contributions from this lake bed span 3 to 24 % (samples 11 and 33, respectively) (Figs. 4b). The sparsely vegetated rangeland is the least active dust source. Median contributions span 2 to 22 % (samples 45 and 34, respectively) (Fig. 4c). Cultivated farmland is recognized as the second-most important source for all of 57 samples. Median contributions from farmland span 4 to 25 % (samples 23 and 34, respectively) (Figs. 4d). We note that for most samples, the lower-limit of predicted uncertainty is zero for contributions from the three sources other than Hamoun Puzak (Figs. 4b-d).

532
533
534
535
536
537
538
539
540
541
542
543
544
545
546
547
548
549
550
551
552
553
554
555
556
557
558
559
560
561
562
563
564
565
566
567
568
569
570
571
572
573
574
575
576
577
578
579
580
581
582
583
584
585
586
587
588
589
590

241 Figure. 5 presents an overview of the source contributions with all samples plotted together as a
242 frequency histogram.



243
244 Figure 4. GULE results for dust source contributions yielding 95% confidence limits (with percentiles
245 2.5, 25, 50, 75 and 97.5). A) Hamoun Puzak; B) Hamoun Saberi; C) uncultivated rangeland; and d)
246 cultivated land.

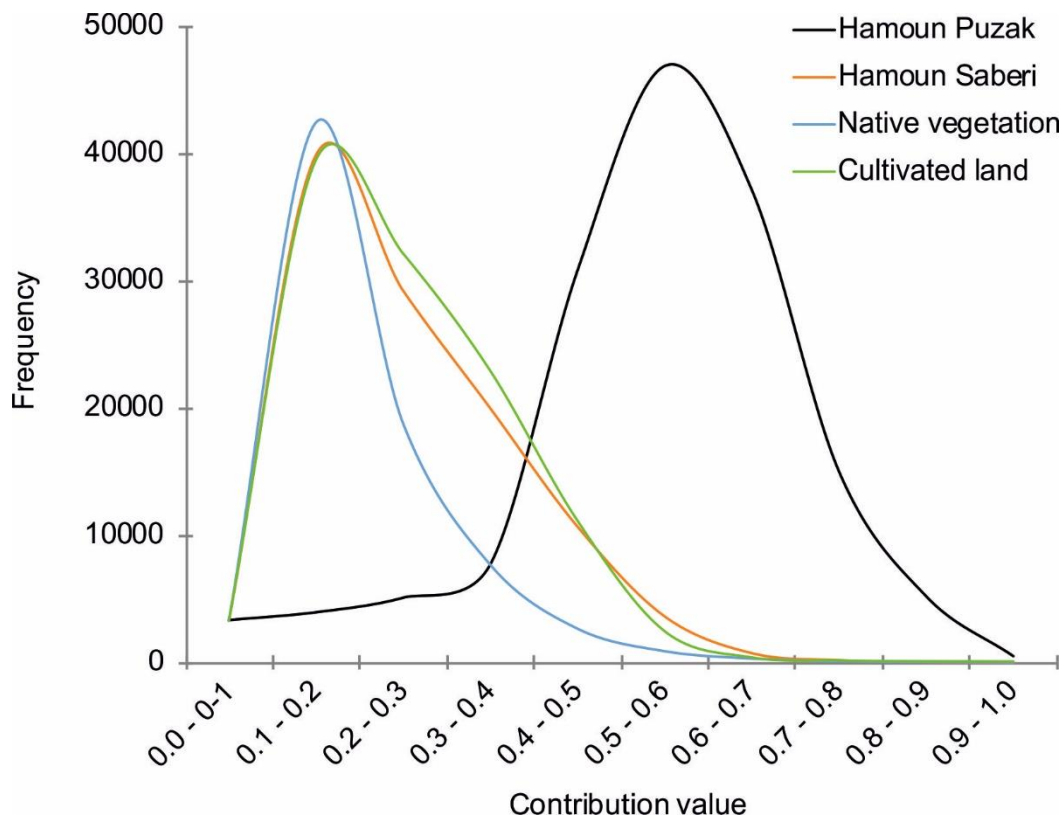


Figure 5. Summary of all source contributions plotted as a probability density function.

5. Discussion

Sediment fingerprinting is a highly effective technique for quantifying source contributions of fluvial sediments (e.g. Collins et al., 1997; Walling, 2005; Stone et al., 2014; Zhou et al., 2016a; Manjoro et al., 2017) and aeolian sands (e.g. Liu et al., 2016; Gholami et al., 2017a,b). Here we build upon this approach by exploring the potential of the GLUE methodology for distinguishing spatially proximate aeolian dust sources with similar underlying geology and geomorphology. We demonstrate its efficacy at formally quantifying the uncertainty distributions associated with aeolian dust fingerprinting due to spatial and temporal variation in the dust cycle, and use the method to reveal spatial complexity - alongside an unexpected lack of temporal complexity - in the nature of the dust sources.

5.1 Environmental context of dust emissions

The strong interannual correlation between dusty days and the surface area of exposed lake floors indicates that i) dust storms in the Sistan-Hamoun region are directly related to the dryness of the Hamoun lakes, and ii) these lake beds are the main source of dust emissions (Goudie and Middleton 2006; Rashki et al., 2012; 2013a; 2013b; 2015). Such relationships are not uncommon, as worldwide observations suggest that exposed dry lake beds can govern the frequency and intensity of dust

650
651
652
653
654
655
656
657
658
659
660
661
662
663
664
665
666
667
668
669
670
671
672
673
674
675
676
677
678
679
680
681
682
683
684
685
686
687
688
689
690
691
692
693
694
695
696
697
698
699
700
701
702
703
704
705
706
707
708

266 storms; for example, at Owens Lake, USA (Reheis et al., 2009), Aral Sea, Uzbekistan (Breckle et al.,
267 2012), Makgadikgadi pan complex; Etosha Pan, southern Africa (Prospero et al., 2002; Mahowald et
268 al., 2003; and Washington et al., 2003); and Lake Eyre, Australia (Baddock et al., 2009).

270 The frequency and magnitude of dust emissions from the Hamoun Lakes has also been related to
271 annual/decadal scale variations in the surface area of the lakes, which varies dramatically. **At its**
272 **maximum extent, observed** following the 1998 spring-melt Hirmand River floods (Rashki et al.,
273 2012a), the Hamoun lake complex forms a single body of water ~4500 km² in area. This is comprised
274 of Hamoun Hirmand (~1400 km²), Hamoun Saberi (~1400 km²) and Hamoun Puzak (~1700km²). During
275 more typical lake-full episodes, these bodies of water are not conjoined; for instance, during the spring
276 of 1996 (Figure 6a), Hamoun Saberi spanned ~815km² and Hamoun Puzak spanned 375km². Hamoun
277 Hirmand lies mostly downwind of Zabol, and hence is not considered further. Between 1999 and 2010
278 a prolonged drought, likely related to the El Nino Southern Oscillation, resulted in the rapid **and**
279 **sustained** desiccation of the Hamoun lakes, with a concomitant increase in the frequency of dusty
280 days (Rashki et al., 2012; 2013). Since 2010, lake levels have been highly variable (Fig. 6), with returns
281 to lake-full conditions experienced around 2011, **but a subsequent return to large areas of exposed**
282 **dry lake beds in recent years.**
283 **The implications of such changes can develop rapidly.** Within the timeframe of this study (June-
284 October 2014), Hamoun Puzak and Hamoun Saberi lost around 295 km² and 640 km² of water surface
285 area, respectively (i.e. 98.5% and 99.9% of their extent on June 14th) (Fig. 7). This desiccation affected
286 Hamoun Saberi and Puzak proportionally at very similar rates, but Saberi's larger surface area at the
287 start of this study led to greater absolute change in lake floor exposure area **at Saberi**. During this
288 period, there was no rainfall recorded at the Zabol meteorological station, but the persistent 'Wind of
289 120 Days' blew from 327° ± 36° during June-October, with daily average windspeeds up to 35 mph,
290 and 50 of the 138 days of the study period exceeding daily averages of 20 mph.

709
710
711
712
713
714
715
716
717
718
719
720
721
722
723
724
725
726
727
728
729
730
731
732
733
734
735
736
737
738
739
740
741
742
743
744
745
746
747
748
749
750
751
752
753
754
755
756
292
757
293
758
294
759
295
760
296
761
297
762
763
764
765
766
767

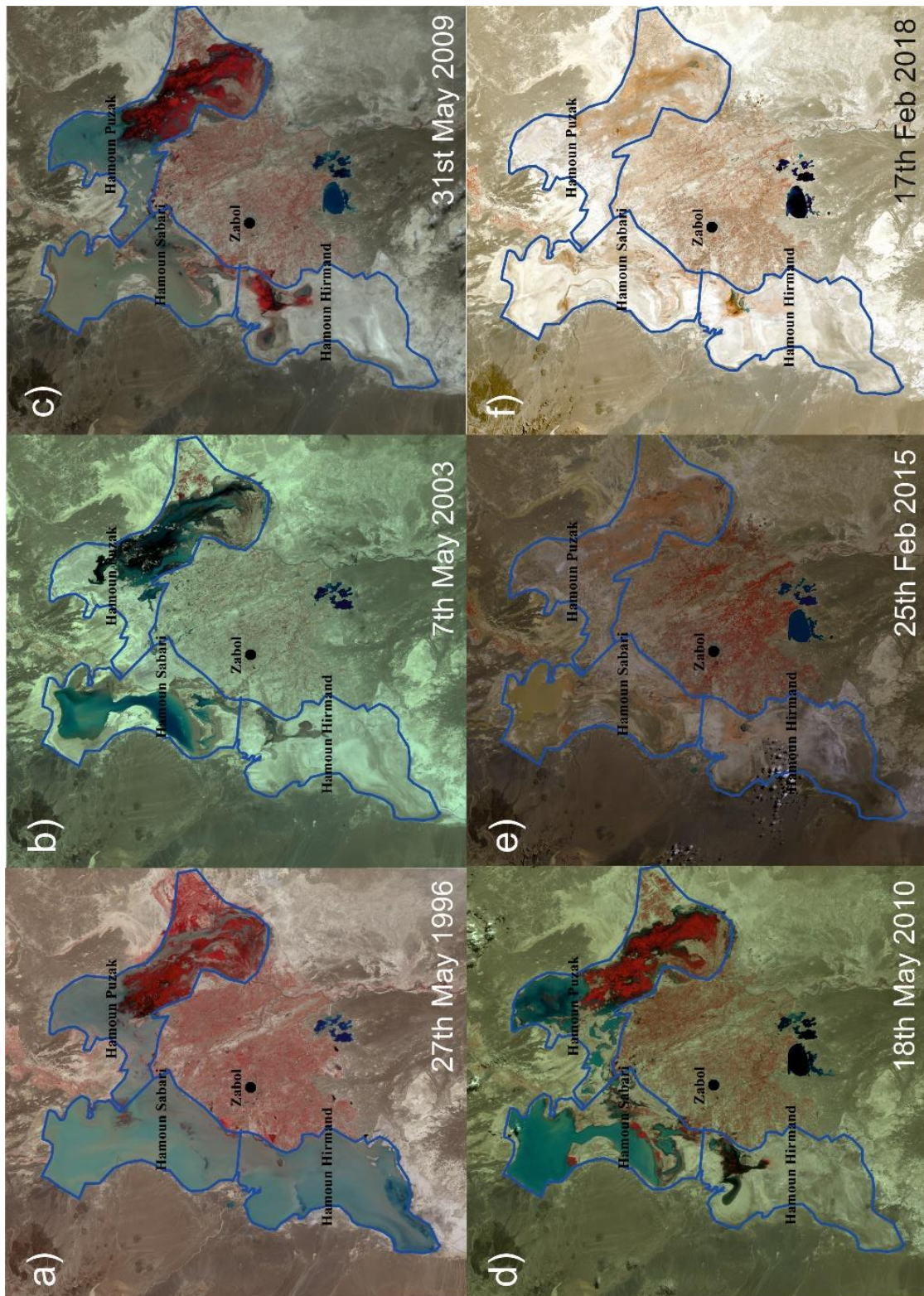
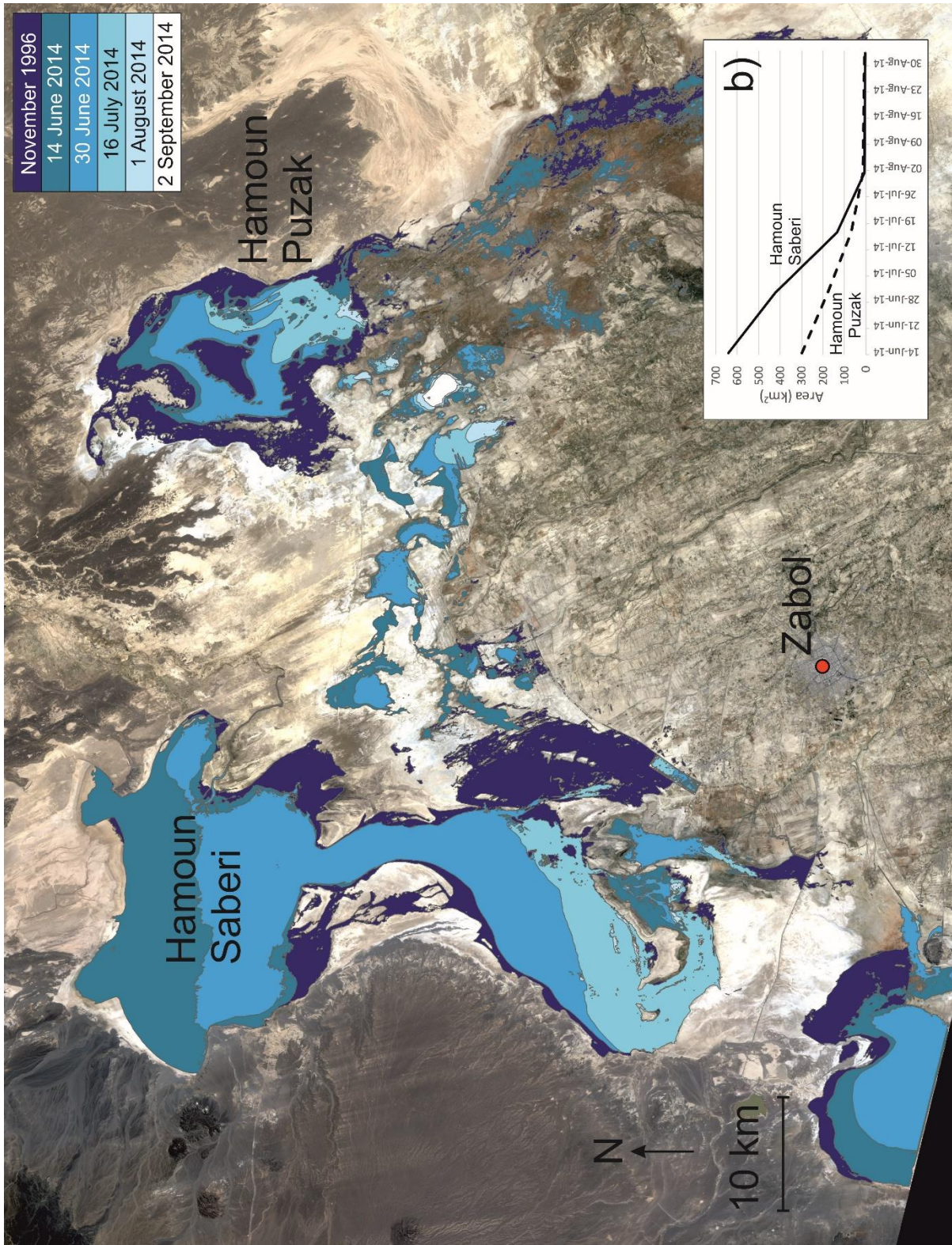


Figure 6. Decadal scale changes in the Hamoun Lakes. Following lake-full conditions in the late 1990s (a), a sustained decade of drought (b and c) resulted in the exposure of large areas of dry lake-beds and therefore potential dust sources. Since then, levels have varied and often changed rapidly (d, e and f). All images are infrared/red/green composites based on Landsat 5 and 8 imagery, using Bands 4/3/2 and 5/4/3 respectively. Vegetation is shown as red tones.










768
769
770
771
772
773
774
775
776
777
778
780
781
782
783
784
785
786
787
788
789
790
791
792
793
794
795
796
797
798
799
800
801
802
803
804
805
806
807
808
809
810
811
812
813
814
815
816
817
818
819
820
821
822
823
824
825
826




298
299 *Figure 7. Changes in the surface extent of the Hamoun Lakes between June and September, 2014.*
300 *Note the rapid desiccation during June and July, and resultant exposure of new surfaces for potential*
301 *deflation.*

827
828
829
830
831
832
833
834
835
836
837
838
839
840
841
842
843
844
845
846
847
848
849
850
851
852
853
854
855
856
857
858
859
860
861
862
863
864
865
866
867
868
869
870
871
872
873
874
875
876
877
878
879
880
881
882
883
884
885

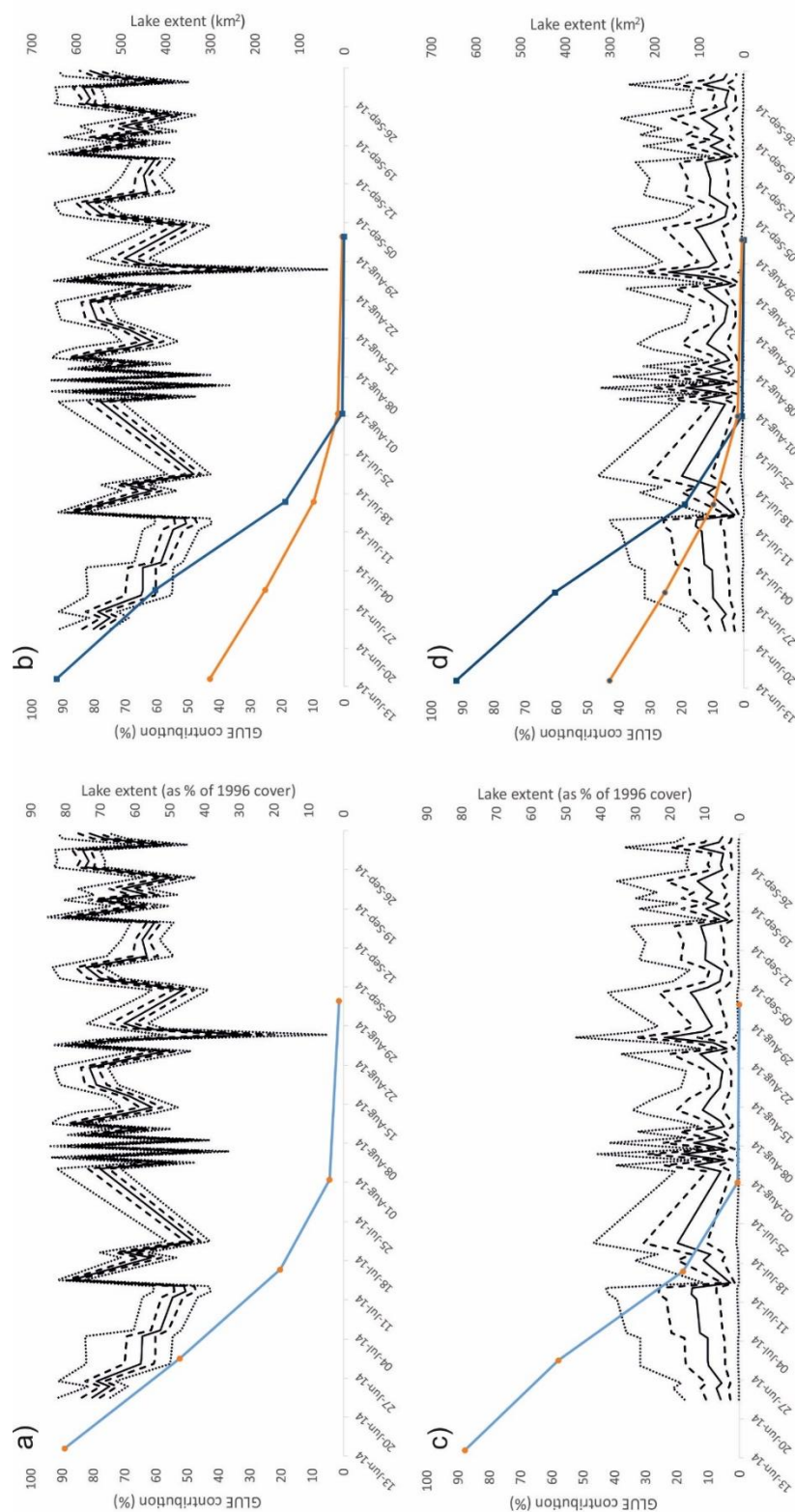
304 **5.2. Dust sources: dry beds of Hamoun Lakes**

305 The GLUE results (Figs 4 and 5) reveal  the dominant source of dust collected at Zabol is Hamoun
306 Puzak, and also that in general,  the sources of the dust vary little over the three month period from
307 June to the beginning of October, 2014. This finding is unexpected  for a number of reasons. Firstly,
308 with the wind at Zabol  during this period coming from  the northwest to north-northwest  ($327^\circ \pm 36^\circ$),
309 the most  obvious candidate  source of the Zabol dust is the upwind Hamoun Saberi (Figures. 1 and 7).
310 Yet, consistently, Hamoun Puzak  contributes ~40-90% (uncertainties included) of the dust received at
311 Zabol. Furthermore, given the rapid increase in Saberi's exposed dry bed during the early period of
312 sampling, its contribution would be expected to increase proportionally over this period. But Saberi's
313 contributions actually vary little during the season (Fig. 4). When the surface area of the lakes is
314 considered, either relative to lake-full conditions (Figure 8a and 8c), or as absolute surface areas
315 (Figure 8b and 8d), there is little temporal relationship with the relative dust contributions of the two
316 lake beds.

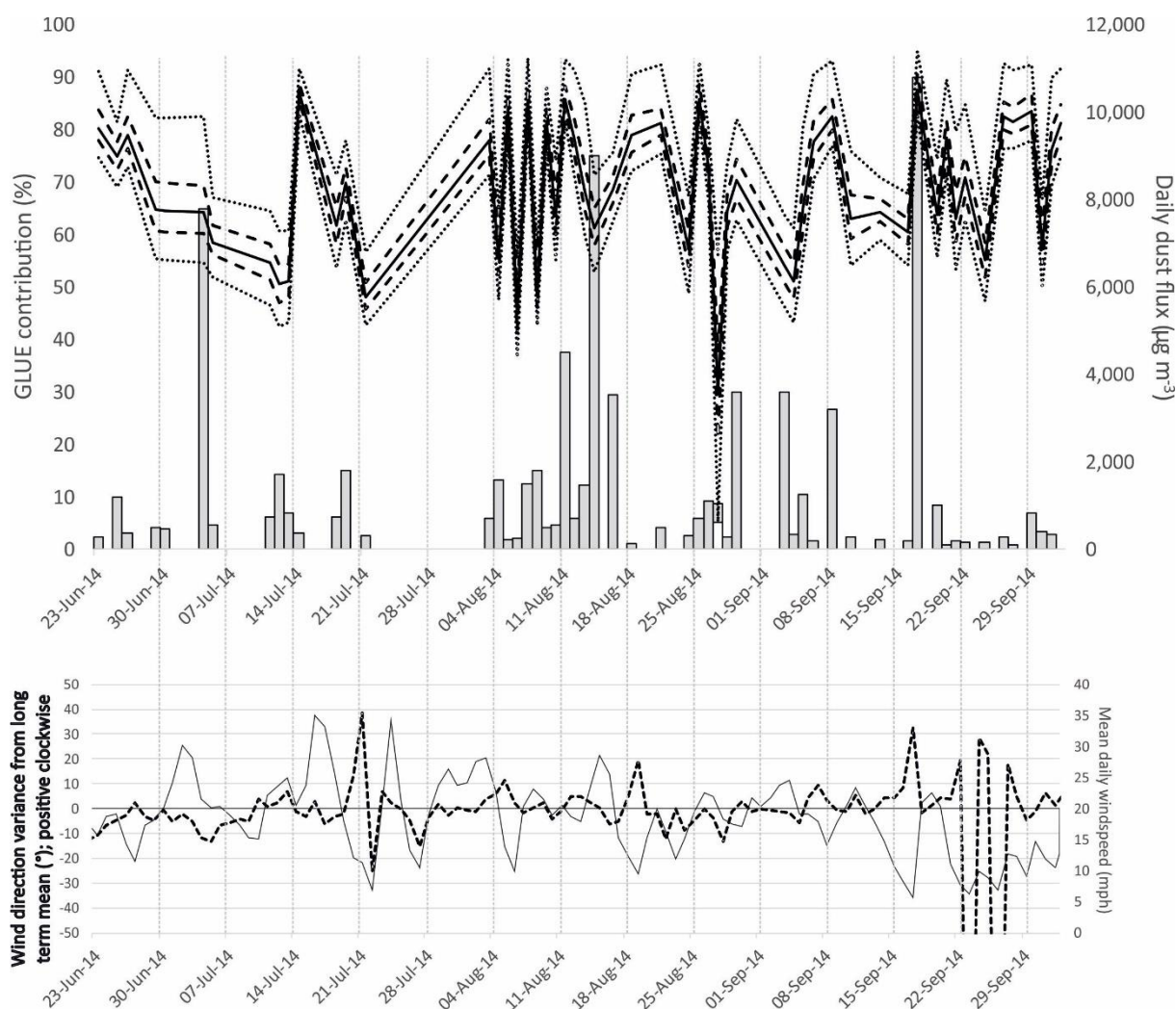
317
318 Similarly, investigation of the meteorological conditions during June-October do not readily explain
319 the dominance of Hamoun Puzak. There is no clear correlation with either wind magnitude, or
320 direction, that can readily explain the dominance of Puzak, and no obvious explanation arise for the
321 occasional excursions when other sources contribute markedly more. For instance, on August 27th
322 replicate samples were collected (S33 and S34 in Fig. 4) and yield consistent results- note that, for
323 consistency, only one of these samples is included in Figs. 8 and 9.

324
325 These result suggest that Hamoun Puzak – or at least the western margin of Hamoun Puzak, where
326 the source samples were collected (Fig. 1) - is a prolific and persistent source of dust over Zabol
327 irrespective of the existence of large adjacent alternative sources. Why is Hamoun Puzak such an
328 effective dust emitter? And why, despite its size and position directly upwind of Zabol, does Hamoun
329 Saberi contribute relatively little? We propose that several factors may  play, as follows.

886
887
888
889
890
891
892
893
894
895
896
897
898
899
900
901
902
903
904
905
906
907
908
909
910
911
912
913
914
915
916
917
918
919
920
921
922
923
924
925
926
927
928
929
930
931
932
933
934
935
936
937
938
939
940
941
942
943
944



330
331 *Figure 8. The relative contributions of a) and b) Hamoun Puzak and c) and d) Hamoun Saberi, plotted*
332 *alongside a) and c) the surface area of the lakes (expressed as a percentage of the 1996 lake-full*
333 *condtions) and b) and d) the absolute surface area of the lakes. There is no consistent trend in dust*
334 *provenance, despite the changing area of the potential sources. Solid lines indicate the median*
335 *estimate, dashed lines the first and third quartiles and dotted lines the 2.5% and 97.5% bounds.*



336
 337 *Figure 9. The dominant dust contribution from Hamoun Puzak (top; key for lines as in Figure 8), shown*
 338 *alongside the magnitude of dust collected at Zabol (bars), and the mean daily wind speed (thin solid*
 339 *line) and variance in mean wind direction (bold dashed line).*

340
 341 First, let us consider the hydrological setting and sedimentology of the area. The Hamoun Lakes are
 342 predominantly fed with water from the Hirmand River to the east, with the Khash River also feeding
 343 directly into Hamoun Puzak from the east. Hamoun Saberi is fed largely from the north by the Harut
 344 and Farah rivers. The sampled region at the western margin at Hamoun Puzak lies in series of channels
 345 and small closed basins which act as spillways connecting the lakes during lake-full episodes, and thus
 346 is likely to have distinctly different sedimentology from lake bed areas subject to direct lacustrine
 347 sedimentation (King et al., 2011, Sweeney et al., 2011). Evidence that these sediments are distinct
 348 from those of Hamoun Saberi is implicitly provided in the primary function of the DFA used here to
 349 define the characteristics of these dusts (Fig. 3). The wind regime necessary for aeolian transport to
 350 Zabol from western Hamoun Puzak is compatible with this zone being a dominant source, as northerly
 351 orientation lies well within the $327^\circ \pm 36^\circ$ (one sigma) direction of the observed winds. It may also be



1004
1005
1006 352 that the transport pathways associated with the low-level jet from the north are strongly affected by
1007 topography. We note that wind streaks evident on the satellite imagery of the region suggest that
1008 353 topography is steering and deflecting local winds in a complex manner.
1009 354

1010
1011 355
1012 356 This orientation, however, raises another question: Why does Hamoun Saberi, which lies directly
1013 357 upwind of Zabol, not contribute more to Zabol's dust flux, especially during the latter part of our study
1014 358 when an additional 640 km² of dry lake bed became exposed? It is well-reported that dust production
1015 359 can be spatially highly variable, even at sub-basin scales (Mahowald et al., 2003, Reheis et al., 2002,
1016 360 Bullard et al., 2008). One possibility relates to the differing geochemistry of the sediments that can
1017 361 promote the formation of protective crusts. Field experiments have shown that, dry river courses that
1018 362 are replenished frequently with fine-grained sediment can be much more effective at producing
1019 363 deflatable dust relative to playas and, counter-intuitively, playa centres are relatively low emission
1020 364 sources (Sweeney et al., 2011, King et al., 2011). Dry lake-bed deposits from the M...ve, for instance,
1021 365 have been reported to yield less dust than those with fluctuating water-levels (Reynolds et al., 2007),
1022 366 and the progressive and rapid desiccation of Hamoun Saberi during the study period may have been
1023 367 simply unfavourable for the generation of deflatable dust.
1024 368

1025 369 Conversely, it may be that exogenic water supply from the northerly channels sufficiently dampened
1026 370 the surface to limit additional deflation. We note that shallow flooding was observed during the field
1027 371 sample collection, despite the lack of rain observed either in Zabol, or the fortnightly Landsat images.
1028 372 Over longer timescales, rates of aeolian erosion have been shown to inversely relate to soil moisture
1029 373 (Whitney et al., 2015). Although the whole region is sparsely vegetated, the role of vegetation in
1030 374 influencing surface roughness and thus susceptibility to aeolian erosion also cannot be overlooked
1031 375 (e.g. Cowie et al., 2013, Li et al., 2007). Lastly, we point to the cause of the additional 13% of variability,
1032 376 which was not well explained by the discriminant function analysis of the source sediments. This
1033 377 variability may imply that a significant component of Zabol dust derives from outside the immediate
1034 378 area of the Hamoun Lakes. Dust plumes transported from Karakum desert in Turkmenistan may affect
1035 379 the Sistan region (Kaskaoutis et al., 2015) and may be a source of exogenous dust not accounted for
1036 380 among the four potential sources we sampled. In short, further work is needed to identify precisely
1037 381 why Hamoun Puzak dominates the aeolian dust flux at Zabol.

1038 382 1039 383 **5.3. Dust sources: cultivated and uncultivated land**

1040 384 The connection between land management, agriculture and aeolian dust emissions are well
1041 385 documented (Wiggs and Holmes, 2011, Okin et al., 2001), and the role of agriculture in exacerbating

1063
1064
1065 386 drought-driven dust events such as the decade-scale ‘Dust Bowl’ of 1930s USA is clearly established
1066
1067 387 (Worster, 2004). We find that the cultivated cropland in the north of Zabol is the region’s second
1068 largest overall source of dust (Fig. 4), slightly out-stripping Hamoun Saberi, and contributing
1069 388
1070 389 substantially more than uncultivated rangeland with sparse vegetation. Desertification (i.e. semi-arid
1071 and arid land degradation) has been recognized in other regions of Iran (Sepehr et al., 2007), and given
1072 390 the difficulties of agriculture in such an extremely dry and hot climate, it is unsurprising that
1073 391 sustainable land management is difficult to achieve. The spread of wind erosion is challenging land
1074 392 managers worldwide - from the Argentinian Pampas (Buschiazzi and Zobeck, 2008) to the Tibetan
1075 393 Plateau (Zhang et al., 2012); and even temperate regions such as southern Sweden (Barring et al.,
1076 394 2003). The findings here that cultivation-based farming is the second largest contributor to Zabol’s
1077 395 dust flux (with median contributions of 4-25% for individual samples) highlights an anthropogenic dust
1078 396 source that may be quelled through more considered farming practices in the future.
1079
1080
1081
1082
1083
1084
1085

1086 399 6. Conclusion

1087 400 Identifying source(s) of aeolian sediments (sand and dust) is essential to improve planning and
1088 401 management of arid and semi-arid regions. Here we present a quantitative sediment fingerprinting
1089 402 approach coupled with the GLUE methodology to quantify source contributions of dust to the city of
1090 403 Zabol in the Sistan-Hamoun region of south-east Iran. Zabol consistently ranks globally as one of the
1091 404 most susceptible to fine (PM2.5 and PM10) aerosol pollutants. Using GLUE, we have assigned
1092 405 quantitative estimates of the relative contributions of four potential dust sources; two dry lake beds
1093 406 (Hamoun Puzak and Hamoun Saberi), cultivated land, and sparsely-vegetated uncultivated rangeland.
1094 407 The dry bed of Hamoun Puzak is the major source supplying sediment for dust samples, with cultivated
1095 408 land contributing more than Hamoun Saberi or uncultivated areas. Robust estimates of uncertainty
1096 409 reveal that whilst the other three dust sources are broadly similar in magnitude, the western end of
1097 410 Hamoun Puzak is undoubtedly the main source.
1098
1099
1100
1101
1102
1103
1104
1105

1106 412 The samples used for these analyses were collected over a three-month period, during the first half of
1107 413 which the surface water extent of both Puzak and Saberi lakes decreased by > 98%. Yet, the relative
1108 414 contributions from the different land classes remained remarkably consistent. We also note that
1109 415 despite a persistent seasonal wind bearing NW-NNW upon Zabol, the main dust source lies to the
1110 416 northerly segment of the winds observed. This suggests that either the median wind direction is not
1111 417 the most dust-bearing, or the transport pathways are more complex than suspected.
1112
1113
1114
1115
1116
1117
1118
1119
1120
1121

1122
1123
1124 419 Our results demonstrate both the potential and the necessity of combining quantitative provenancing
1125
1126 420 techniques with robust uncertainty methods and, ultimately, improved land management. The
1127
1128 421 straightforward approach of linking the main wind direction to a large and rapidly-drying lake bed
1129 422 (Hamoun Saberi) does not yield a good outcome, in this case. Spatial variation in dust sources has
1130
1131 423 been identified elsewhere, most strikingly at the Bodélé Depression in the Chadian Sahara
1132 424 (Washington et al., 2003); here we demonstrate the application of methods with the scope to identify
1133
1134 425 such spatial variation from the point of receipt of the dust. We are unable to outline the exact reasons
1135 426 for Hamoun Puzak's susceptibility to aeolian erosion. However, we attribute notable influence to the
1136
1137 427 geomorphological conditions of the western arm of the Puzak, with its array of interconnected small
1138 428 basins and spillways proving more prone to generating dusts emissions.
1139
1140 429

1141 430 REFERENCES

- 1143 431 Aaron, S. M., Blakowski, M. A., Aciego, S. M., Stevenson, E. I., Sims, K. W. W., Scott, S. R., and Aarons,
1144 432 C. (2017). Geochemical characterization of critical dust source regions in the American West.
1145
1146 433 *Geochimica et Cosmochimica Acta* 215; 141-161.
1147
1148 434 <http://dx.doi.org/10.1016/j.gca.2017.07.024>
- 1149 435 Abban, B., Papanicolaou, A. N., Cowles, M. K., Wilson, C. G., Abaci, O., Wacha, K., Schilling, and K.,
1150 436 Schnobelen, D. (2016). An enhanced Bayesian fingerprinting framework for studying
1151
1152 437 sediment source dynamics in intensively managed landscapes. *Water Resource Research*, 52,
1153
1154 438 4646-4673. doi:10.1002/2015WR018030.
- 1155 439 Alizadeh Choobari, O., Zawar-Reza, P., and Sturman, A. (2014). The "wind of 120 days" and dust
1156
1157 440 storm activity over the Sistan Basin. *Atmospheric Research*, 143; 328-341.
1158
1159 441 <http://dx.doi.org/10.1016/j.atmosres.2014.02.001>
- 1160 442 Baddock, M. C., Bullard, J. E., and Bryant, R. G (2009). Dust source identification using MODIS: a
1161
1162 443 comparison of techniques applied to the Lake Eyre Basin, Australia. *Remote Sens Environ*,
1163 444 113:1511–28.
- 1164 445 Barring, L., Jonsson, P., Mattsson, J. O. & Ahman, R. 2003. Wind erosion on arable land in Scania,
1166 446 Sweden and the relation to the wind climate - a review. *Catena*, 52, 173-190.
- 1168 447 Beven, K. and Binley, A. (1992). The future of distributed models: Model calibration and uncertainty
1169 448 prediction. *Hydrological Processes*, 6(3), 279-298. doi: 10.1002/hyp.3360060305.
- 1171 449 Breckle, S.W., Wucherer, W., Liliya, A., Dimeyeva, L. A., Nathalia, P., and Ogar, N.P. (2012). Aralkum -
1172 450 a man-made desert: the desiccated floor of the Aral Sea (Central Asia). Springer; 2012486.
- 1174 451 Bullard, J., Baddock, M., Mctainsh, G. & Leys, J. 2008. Sub-basin scale dust source geomorphology
1175 452 detected using MODIS. *Geophysical Research Letters*, 35.

1181
1182
1183 453 Buschiazzo, D. E. & Zobeck, T. M. 2008. Validation of WEQ, RWEQ and WEPS wind erosion for
1184 454 different arable land management systems in the Argentinean Pampas. *Earth Surface*
1185 455 *Processes and Landforms*, 33, 1839-1850.
1186
1187
1188 456 Cao, H., Amiraslani, F., Liu, J., and Zhou, N. (2015). Identification of dust storm source areas in West
1189 457 Asia using multiple environmental datasets. *Science of the Total Environment*, 502; 224-235.
1190 458 <http://dx.doi.org/10.1016/j.scitotenv.2014.09.025>
1191
1192
1193 459 Cao, J. J., Zhu, C. S., Chow, J. C., Liu, W. G., Han, Y. M., and Watson, J. G. (2008). Stable carbon and
1194 460 oxygen isotopic composition of carbonate in fugitive dust in the Chinese Loess Plateau.
1195 461 *Atmospheric Environment*, 42; 9118-9122. doi:10.1016/j.atmosenv.2008.09.043
1196
1197 462 Chavagnac, V., Lair, M., Milton, J. A., Lloyd, A., Croudace, I .W., Palmer, M. R., Green, D. R. H., and
1198 463 Cherkashev, G. A. (2008). Tracing dust input to the Mid-Atlantic Ridge between 14°45'N and
1200 464 36°14'N: Geochemical and Sr isotope study. *Marine Geology*, 247; 208-225.
1201 465 doi:10.1016/j.margeo.2007.09.003
1202
1203 466 Chen, J., Li, G., Yang, J., Rao, W., Lu, H., Balsam, W., Sun, Y., and Ji, J. Nd and Sr isotopic
1204 467 characteristics of Chinese deserts: Implications for the provenances of Asian dust.
1205 468 *Geochimica et Cosmochimica Acta*, 71; 3904-3914.
1206
1207
1208 469 Cherboudj, I., Beegum, S. N., and Ghedira, H. (2016). Identifying natural dust source regions over the
1209 470 Middle-East and North-Africa: Estimation of dust emission potential. *Earth Science Review*.
1210 471 <http://dx.doi.org/10.1016/j.earscirev.2016.12.010>
1211
1212
1213 472 Collins, A. L., and Walling, D. E. (2007). Sources of fine sediment recovered from the channel bed of
1214 473 lowland groundwater-fed catchments in the UK. *Geomorphology*, 88, 120–138.
1215 474 doi:10.1016/j.geomorph.2006.10.018
1216
1217 475 Collins, A.L., Walling, D.E., and Leeks, G.J.L. (1997). Fingerprinting the origin of fluvial suspended
1218 476 sediment in larger river basins: combining assessment of spatial provenance and source
1219 477 type. *Geografiska Annaler*, 79, 239–254.
1220
1221
1222 478 Collins, A.L., Zhang, Y., Walling, D.E., Grenfell, S.E., Smith, P., Grischeff, J., ... Brogden, D. (2012).
1223 479 Quantifying fine-grained sediment sources in the River Axe Catchment, southwest England:
1224 480 Application of a Monte-Carlo numerical modelling framework incorporating local and
1225 481 genetic algorithm optimisation. *Hydrological Processes*, 26 (13), 1962–1983.
1226 482 doi:10.1002/hyp.8283.
1227
1228
1229
1230 483 Cooper, R. J., Krueger, T., Hiscock, K. M., & Rawlins, B. G. (2014). Sensitivity of fluvial sediment
1231 484 source apportionment to mixing model assumptions : A Bayesian model comparison. *Water*
1232 485 *Resources Research*, 9031–9047. doi:10.1002/2014WR016194.
1233
1234 486 Cooper, R. J., Krueger, T., Hiscock, K. M., & Rawlins, B. G. (2015). High-temporal resolution fluvial
1235
1236
1237
1238
1239

1240
1241
1242 487 sediment source fingerprinting with uncertainty: A Bayesian approach. *Earth Surface*
1243 Processes and Landforms, 40(1), 78–92. doi:10.1002/esp.3621
1244 488
1245 489 Cowie, S. M., Knippertz, P. & Marsham, J. H. 2013. Are vegetation-related roughness changes the
1246 cause of the recent decrease in dust emission from the Sahel? *Geophysical Research Letters*,
1247 490 40, 1868-1872.
1248 491
1249 492 Dahmardeh Behrooz, R., Esmaili-Sari, A., Bahramifar, N., and Kaskaoutis, D. G. (2017a). Analysis of
1250 the TSP, PM10 concentrations and water-soluble ionic species in airborne samples over
1251 Sistan, Iran during the summer dusty period. *Atmospheric Pollution Research*, 8; 403-417.
1252 493 http://dx.doi.org/10.1016/j.apr.2016.11.001
1253 494
1254 495 Dahmardeh Behrooz, R., Esmaili-Sari, A., Bahramifar, N., and Kaskaoutis, D. G., Saeb, K., and Rajaei,
1255 F. (2017b). Trace-element concentrations and water-soluble ions in size-segregated dust-
1256 borne and soil samples in Sistan, southeast Iran. *Aeolian Research*, 25; 87-105.
1257 496 http://dx.doi.org/10.1016/j.aeolia.2017.04.001
1258 497
1259 498 Del Rio-Salas, R., Ruiz, J., De la O-Villanueva, M., Valencia-Moreno, M., Moreno,-Rodriguez, V.,
1260 Gomez-Alvarez, A., Grijalva, T., Mendivil, H., Paz-Moreno, F., and Meza-Figueroa, D. (2012).
1261 499 Tracing geogenic and anthropogenic sources in urban dusts: Insights from lead isotopes.
1262 *Atmospheric Environment*, 60; 202-210. http://dx.doi.org/10.1016/j.atmosenv.2012.06.061
1263 500
1264 501 Esmaili, A. and Omrani, M. (2007). Efficiency analysis of fishery in Hamoon lake using DEA
1265 approach. *J. Appl. Sci*, 7; 2856-2860.
1266 502
1267 503 Ge, Y., Abuduwaili, J., Ma, L., Wu, N., and Liu, D. (2016). Potential transport pathways of dust
1268 emanating from the playa of Ebinur Lake, Xinjiang, in arid northwest China. *Atmospheric*
1269 *Research*, 178-179; 196-206. http://dx.doi.org/10.1016/j.atmosres.2016.04.002
1270 504
1271 505 Gholami, H., Middleton, N., Nzari Samani, A., and Wasson, R. (2017a). Determining contribution of
1272 sand dune potential sources using radionuclides, trace and major elements in central Iran.
1273 *Arab J Geosci*, 10:163. doi. 10.1007/s12517-017-2917-0.
1274 506
1275 507 Gholami, H., Telfer, M. W., Blake, W. H., and Fathabadi, A. (2017) Aeolian sediment fingerprinting
1276 using a Bayesian mixing model. *Earth Surf. Process. Landforms*, 42: 2365–2376. doi:
1277 508 10.1002/esp.4189.
1278 509
1279 510 Gong, Y., Shen, Zh, Hong, Q., Liu, R., and Liao, Q. (2011). Parameter uncertainty analysis in watershed
1280 total phosphorus modeling using the GLUE methodology. *Agriculture, Ecosystems and*
1281 *Environment* 142; 246-255. doi:10.1016/j.agee.2011.05.015
1282 511
1283 512 Goossens, D. (2003). On-site and off-site effects of wind erosion. In: Warren A (ed) *Wind erosion on*
1284 *agricultural land in Europe*. European Commission, Luxembourg, pp. 29–38
1285 513
1286 514 Goudie, A. S. and Middleton, N. J. (2006). *Desert dust in the global system*. Springer.
1287 515
1288 516
1289 517
1290 518
1291 519
1292 520
1293
1294
1295
1296
1297
1298

1299
1300
1301
1302
1303
1304
1305
1306
1307
1308
1309
1310
1311
1312
1313
1314
1315
1316
1317
1318
1319
1320
1321
1322
1323
1324
1325
1326
1327
1328
1329
1330
1331
1332
1333
1334
1335
1336
1337
1338
1339
1340
1341
1342
1343
1344
1345
1346
1347
1348
1349
1350
1351
1352
1353
1354
1355
1356
1357

521 Grousset, F. E. and Biscaye, P. E. (2005). Tracing dust sources and transport patterns using Sr, Nd and
522 Pb isotopes. *Chemical Geology*, 222; 149-167. doi:10.1016/j.chemgeo.2005.05.006
523 Hamidi, M., Kavianpour, M. R., and Shao, Y. (2014). Numerical simulation of dust events in the
524 Middle East. *Aeolian Research*, 13; 59-70. <http://dx.doi.org/10.1016/j.aeolia.2014.02.002>
525 Hassan, A. E., Bekhit, H. M., and Chapman, J. B. (2008). Uncertainty assessment of a stochastic
526 groundwater flow model using GLUE analysis. *Journal of Hydrology*, 362; 89-109.
527 doi:10.1016/j.jhydrol.2008.08.017
528 Kaskaoutis, D.G., Rashki, A., Francois, P., Dumka, U.C., Houssos, E.E., and Legrand, M. (2015).
529 Meteorological regimes modulating dust outbreaks in southwest Asia: the role of pressure
530 anomaly and Inter-Tropical Convergence Zone on the 1–3 July 2014 case. *Aeolian Research*.
531 18, 83–97.
532 Kaskaoutis, D.G., Rashki, A., Houssos, E. E., Goto, D., and Nastos, P. T. (2014). Extremely high aerosol
533 loading over Arabian Sea during June 2008: the specific role of the atmospheric dynamics
534 and Sistan dust storms. *Atmospheric Environment*. Doi: 10.1016/j.atmosenv.2014.05.012
535 King, J., Etyemezian, V., Sweeney, M., Buck, B. J. & Nikolich, G. 2011. Dust emission variability at the
536 Salton Sea, California, USA. *Aeolian Research*, 3, 67-79.
537 Krom, M.D., Cliff, R. A., Eijsink, L. M., Herut, B., and Chester, R. (1999). The characterisation of
538 Saharan dusts and Nile particulate matter in surface sediments from the Levantine basin
539 using Sr isotopes. *Marine Geology*, 155; 319-330.
540 Li, J., Okin, G. S., Alvarez, L. & Epstein, H. 2007. Quantitative effects of vegetation cover on wind
541 erosion and soil nutrient loss in a desert grassland of southern New Mexico, USA.
542 *Biogeochemistry*, 85, 317-332.
543 Liu, B., Niu, Q., Qu, J., and Zu, R. (2016). Quantifying the provenance of aeolian sediments using
544 multiple composite fingerprints. *Aeolian Research*, 22, 117-122.
545 dx.doi.org/10.1016/j.aeolia.2016.08.002
546 Long, X., Li, N., Tie, X., Cao, J., Zhao, Sh., Huang, R., Zhao, M., Li, G., and Feng, Tian. (2016). Urban
547 dust in the Guanzhong Basin of China, part I: A regional distribution of dust sources retrieved
548 using satellite data. *Science of the Total Environment*, 541; 1603-1613.
549 <http://dx.doi.org/10.1016/j.scitotenv.2015.10.063>
550 Mahowald, N. M., Bryant, R. G., del Corral, J., and Steinberger, L. (2002). Ephemeral lakes and desert
551 dust sources. *Geophys Res Lett*, 30:1074. <http://dx.doi.org/10.1029/2002GL016041>
552 Manjoro, M., Rowntree, K., Kakembo, V., Foster, I., and Collins, A. L. (2016). Use of sediment source
553 fingerprinting to assess the role of subsurface erosion in the supply of fine sediment in a



1358
1359
1360 554 degraded catchment in the Eastern Cape, South Africa. *Journal of Environmental*
1361 Management, xxx, 1-15. [dx.doi.org/10.1016/j.jenvman.2016.07.019](https://doi.org/10.1016/j.jenvman.2016.07.019)
1362 555
1363 556 Massoudieh, A., Gellis, A., Banks, W. S., & Wieczorek, M. E. (2013). Suspended sediment source
1364 apportionment in Chesapeake Bay watershed using Bayesian chemical mass balance
1365 557 receptor modeling. *Hydrological Processes*, 27(24), 3363–3374. doi:10.1002/hyp.9429
1366 558
1367 Middleton NJ. (1986). Dust storms in the Middle East. *J Arid Environ*,10:83–96
1368 559
1369 560 Moghaddamnia, A., Ghafari, M.B., Piri, J., Amin, S., and Han, D. (2009). Evaporation
1370 estimation using artificial neural networks and adaptive neuro-fuzzy inference
1371 561 system techniques. *Adv. Water Resour.* 32, 88–97
1372 562
1373 563 Montovan, P. and Todini, E. (2006). Hydrological forecasting uncertainty
1374 564 assessment: Incoherence of the GLUE methodology. *Journal of Hydrology*, 330; 368-381.
1375 565 doi:10.1016/j.jhydrol.2006.04.046
1376 566
1377 566 Motha, J.A., Wallbrink, P.J., Hairsine, P.B., and Grayson, R.B. (2003). Determining the sources of
1380 567 suspended sediment in a forested catchment in southeastern Australia. *Water Resources*, 39
1381 568 (3), 1056. doi:10.1029/2001wr000794.
1382 569
1383 569 Nabavi, S. O., Haimberger, L., and Samimi, C. (2016). Climatology of dust distribution over West Asia
1384 570 from homogenized remote sensing data. *Aeolian Research*, 21; 93-107.
1385 571 <http://dx.doi.org/10.1016/j.aeolia.2016.04.002>
1386 572
1387 572 Nabavi, S. O., Haimberger, L., and Samimi, C. (2017). Sensitivity of WRF-chem predictions to dust
1388 573 source function specification in West Asia. *Aeolian Research*, 24; 115-131.
1389 574 <http://dx.doi.org/10.1016/j.aeolia.2016.12.005>
1390 575
1391 575 Nakano, T., Yokoo, Y., Nishikawa, M., and Koyanagi, H. (2004). Regional Sr–Nd isotopic ratios of soil
1392 576 minerals in northern China as Asian dust fingerprints. *Atmospheric Environment*, 38; 3061-
1393 577 3067. doi:10.1016/j.atmosenv.2004.02.016
1394 578
1395 578 Okin, G. S., Murray, B. & Schlesinger, W. H. 2001. Degradation of sandy arid shrubland
1396 579 environments: observations, process modelling, and management implications. *Journal of*
1397 580 *Arid Environments*, 47, 123-144.
1398 581
1399 581 Rashki, A., Arjmand, A., and Kaskaoutis, D. G. (2017). Assessment of dust activity and dust-plume
1400 582 pathways over Jazmurian Basin, southeast Iran. *Aeolian Research*, 24; 145-160.
1401 583 <http://dx.doi.org/10.1016/j.aeolia.2017.01.002>
1402 584
1403 584 Rashki, A., Eriksson, P. G., Rautenbach, C. J. D., Kaskaoutis, D. G., Grote, W., and Dykstra, J. (2013a).
1404 585 Assessment of chemical and mineralogical characteristics of airborne dust in the Sistan
1405 586 region, Iran. *Aeolian Research*, 90; 227-236.
1406 587 <http://dx.doi.org/10.1016/j.chemosphere.2012.06.059>
1407
1408
1409
1410
1411
1412
1413
1414
1415
1416

1417
1418
1419 588 Rashki, A., Kaskaoutis, D. G., Francois, P., Kosmopoulos, P. G., and Legrand, M. (2015). Dust-storm
1420 dynamics over Sistan region, Iran: Seasonality, transport characteristics and affected areas.
1421 589 Aeolian Research, 16; 35-48.
1422 590
1423
1424 591 Rashki, A., Kaskaoutis, D. G., Goudie, A. S., and Kahn, R. A. (2013b). Dryness of ephemeral lakes and
1425 consequences for dust activity: The case of the Hamoun drainage basin, southeastern Iran.
1426 592 Science of the Total Environment, 463-464; 552-564.
1427 593
1428 594 <http://dx.doi.org/10.1016/j.scitotenv.2013.06.045>
1429
1430 595 Rashki, A., Kaskaoutis, D. G., Rautenbach, C. J. D., Eriksson, P. G. (2012a). Changes of Permanent Lake
1431 Surfaces, and Their Consequences for Dust Aerosols and Air Quality: The Hamoun Lakes of
1432 596 the Sistan Area, Iran. In: Hayder Abdul-Razzak (Eds.), Atmospheric Aerosols - Regional
1433 597 Characteristics. DOI: 10.5772/48776
1434 598
1435 599 Rashki, A., Kaskaoutis, D. G., Rautenbach, C. J. D., Eriksson, P. G., Qiang, M., and Gipta, P. (2012b).
1436 Dust storms and their horizontal dust loading in the Sistan region, Iran. Aeolian Research, 5;
1437 600 51-62. doi:10.1016/j.aeolia.2011.12.001
1438 601
1439 602 Reheis, M. C., Budahn, J. R. & Lamothe, P. J. 2002. Geochemical evidence for diversity of dust
1440 603 sources in the southwestern United States. *Geochimica Et Cosmochimica Acta*, 66, 1569-
1441 604 1587.
1442
1443 605 Reheis, M., Budahn, J. R., Lamothe, P. J., and Reynolds, R. L. (2009). Compositions of modern dust
1444 606 and surface sediments in the Desert Southwest United States. J Geophys Res, 114: F01028.
1445 607 <http://dx.doi.org/10.1029/2008JF001009>
1446
1447 608 Reynolds, R.L., Yount, J.C., Reheis, M., Goldstein, H, Chavez Jr, P., Fulton, R, Whitney, J., Fuller, C.,
1448 609 Forester, R.M. (2007). Dust emission from wet and dry playas in the Mojave Desert, USA.
1449 610 Earth Surface Processes and Landforms, 3; 1811-1827. <https://doi.org/10.1002/esp.1515>
1450 611
1451 612 Rezazadeh, M., Irannejad, P., and Shao, Y. (2013). Climatology of the Middle East dust events.
1452 613 Aeolian Research, 10; 103-109. <http://dx.doi.org/10.1016/j.aeolia.2013.04.001>
1453 614
1454 615 Schepanski, K., Tegen, I., and Macke. A. (2012). Comparison of satellite based observations of
1455 616 Saharan dust source areas. Remote Sensing of Environment, 123; 90-97.
1456 617
1457 618 doi:10.1016/j.rse.2012.03.019
1458 619
1459 620 Sepehr, A., Hassanli, A. M., Ekhtesasi, M. R. & Jamali, J. B. 2007. Quantitative assessment of
1460 621 desertification in south of Iran using MEDALUS method. *Environmental Monitoring and*
1461 622 *Assessment*, 134, 243.
1462
1463 623 Shen, Z., Caquineau, S., Cao, J., Zhang, X., Han, Y., Gaudichet, A., and Gomes, L. (2009). Mineralogical
1464 624 characteristics of soil dust from source regions in northern China. Particology, 7; 507-512.
1465 625
1466 626 doi:10.1016/j.partic.2009.10.001
1467
1468
1469
1470
1471
1472
1473
1474
1475

1476
1477
1478 622 Sherriff, S. C., Franks, S. W., Rowan, J. S., Fenton, O., & Ó'hUallacháin, D. (2015). Uncertainty-based
1479
1480 623 assessment of tracer selection, tracer non-conservativeness and multiple solutions in
1481 624 sediment fingerprinting using synthetic and field data. *Journal of Soils and Sediments*,
1482
1483 625 15(10), 2101–2116. doi:10.1007/s11368-015-1123-5
1484
1485 626 Smith, H.G., and Blake, W.H. (2014). Sediment fingerprinting in agricultural catchments: A critical re-
1486 627 examination of source discrimination and data corrections. *Geomorphology*, 204, 177–191.
1487 628 doi:10.1016/j.geomorph.2013.08.003.
1489 629 Stewart, H. A., Massoudieh, A., & Gellis, A. (2015). Sediment source apportionment in Laurel Hill
1490 630 Creek, PA, using Bayesian chemical mass balance and isotope fingerprinting. *Hydrological*
1491 631 *Processes*, 29(11), 2545–2560. doi:10.1002/hyp.10364
1494 632 Stone, M., Collins, A.L., Silins, U., Emelko, M.B., and Zhang, Y.S. (2014). The use of composite
1495 633 fingerprints to quantify sediment sources in a wildfire impacted landscape, Alberta, Canada.
1496 634 *Science of the Total Environment*, 473-474, 642–650. doi:10.1016/j.scitotenv.2013.12.052.
1498 635 Sweeney, M. R., Mcdonald, E. V. & Etyemezian, V. 2011. Quantifying dust emissions from desert
1499 636 landforms, eastern Mojave Desert, USA. *Geomorphology*, 135, 21-34.
1501 637 Sweeney, M. R., Zlotnik, V. A., Joeckel, R. M. & Stout, J. E. 2016. Geomorphic and hydrologic controls
1502 638 of dust emissions during drought from Yellow Lake playa, West Texas, USA. *Journal of Arid*
1503 639 *Environments*, 133, 37-46.
1506 640 United Nations Environment Programme (UNEP) (2006). History of environmental change in
1507 641 the Sistan basin based on satellite image analysis: 1976–2005; 200660.
1509 642 Vale, S. S., Fuller, I. C., Procter, J. N., Basher, L. R., and Smith, I. E. (2016). Characterization and
1510 643 quantification of suspended sediment sources to the Manawatu River, New Zealand. *Science*
1511 644 *of the Total Environment*, 543, 171–186. doi:10.1016/j.scitotenv.2015.11.003
1514 645 Viola, F., Noto, L. V., Cannarozzo, G., and Loggia, G. L. (2009). Daily streamflow prediction with
1515 646 uncertainty in ephemeral catchments using the GLUE methodology. *Physics and Chemistry of*
1517 647 *the Earth* 34; 701-706.
1518 648 Voli, M.T., Wegmann, K.W., Bohnenstiehl, D.R., Leithold, E., Osburn, C.L., and Polyakov, V. (2013).
1519 649 Fingerprinting the sources of suspended sediment delivery to a large municipal drinking
1520 650 water reservoir: Falls Lake, Neuse River, North Carolina, USA. *Journal of Soils and Sediments*,
1521 651 13 (10), 1692–1707. doi:10.1007/s11368-013-0758-3.
1525 652 Walling, D.E. (2005). Tracing suspended sediment sources in catchments and river systems. *Science*
1526 653 *of the Total Environment*, 344 (1-3), 159–184. doi:10.1016/j.scitotenv.2005.02.011.
1527 654 Walling, D.E. (2013). The evolution of sediment source fingerprinting investigations in fluvial
1528 655 systems. *Journal of Soils and Sediments*, 13 (10), 1658–1675. doi:10.1007/s11368-013-0767-

1535
1536
1537 656 2.
1538
1539 657 Wang, Y. Q., Zhang. X. Y., Arimoto, R., Cao, J. J., and Shen, Z. X. (2005). Characteristics of carbonate
1540 658 content and carbon and oxygen isotopic composition of northern China soil and dust aerosol
1541 659 and its application to tracing dust sources. *Atmospheric Environment*, 39; 2631-2642.
1542 660 doi:10.1016/j.atmosenv.2005.01.015
1543
1544 661 Washington, R., Todd, M., Middleton, N.J., and Goudie, A. S. (2003). Dust storm source areas
1545 662 determined by the Total Ozone Monitoring Spectrometer and surface observations. *Ann*
1546 663 *Assoc Am Geogr*, 93: 297–313.
1547
1548 664 Wei, T., Dong, Z., Kang, Sh., Qin, X., and Guo, Zh. (2017). Geochemical evidence for sources of
1549 665 surface dust deposited on the Laohugou glacier, Qilian Mountains. *Applied Geochemistry*;
1550 666 79; 1-8. <http://dx.doi.org/10.1016/j.apgeochem.2017.01.024>
1551
1552
1553 667 Whitney, J. W., Breit, G. N., Buckingham, S. E., Reynolds, R. L., Bogle, R. C., Luo, L., Goldstein, H. L. &
1554 668 Vogel, J. M. 2015. Aeolian responses to climate variability during the past century on
1555 669 Mesquite Lake Playa, Mojave Desert. *Geomorphology*, 230, 13-25.
1556
1557
1558 670 Wiggs, G. & Holmes, P. 2011. Dynamic controls on wind erosion and dust generation on west-central
1559 671 Free State agricultural land, South Africa. *Earth Surface Processes and Landforms*, 36, 827-
1560 672 838.
1561
1562
1563 673 World Health Organisation (2016). WHO Global Urban Ambient Air Pollution Database. URL:
1564 674 http://www.who.int/phe/health_topics/outdoorair/databases/cities/en/ (Accessed
1565 675 23/06/2018).
1566
1567
1568 676 Worster, D. 2004. *Dust bowl: the southern plains in the 1930s*, Oxford University Press.
1569
1570 677 Xu, H. (2006). Modification of normalised difference water index (NDWI) to enhance open water
1571 678 features in remotely sensed imagery. *International Journal of Remote Sensing*, 27; 3025–
1572 679 3033. doi: 10.1080/01431160600589179
1573
1574 680 Yan, Y., Sun, Y., Ma., L., and Long, X. (2015). A multidisciplinary approach to trace Asian dust storms
1575 681 from source to sink. *Atmospheric Environment*, 105; 43-52.
1576 682 <http://dx.doi.org/10.1016/j.atmosenv.2015.01.039>
1577
1578
1579 683 Yang, J., Li, G., Rao, W., and Ji, J. (2009). Isotopic evidences for provenance of East Asian Dust.
1580 684 *Atmospheric Environment*, 43; 4481-4490. doi:10.1016/j.atmosenv.2009.06.035
1581
1582 685 Zhang, D., Zhou, Z. H., Zhang, B., Du, S. H. & Liu, G. C. 2012. The effects of agricultural management
1583 686 on selected soil properties of the arable soils in Tibet, China. *Catena*, 93, 1-8. Prospero, J. M.,
1584 687 Ginoux, P., Torres, O., Nicholson, S. E., and Gill, T. E. (2002). Environmental characterization
1585 688 of global sources of atmospheric soil dust identified with the Nimbus 7 total ozone mapping
1586 689 spectrometer absorbing aerosol product. *Rev Geophys*, 40: 2–31
1587
1588
1589
1590
1591
1592
1593

1594
1595
1596
1597
1598
1599
1600
1601
1602
1603
1604
1605
1606
1607
1608
1609
1610
1611
1612
1613
1614
1615
1616
1617
1618
1619
1620
1621
1622
1623
1624
1625
1626
1627
1628
1629
1630
1631
1632
1633
1634
1635
1636
1637
1638
1639
1640
1641
1642
1643
1644
1645
1646
1647
1648
1649
1650
1651
1652

690 Zhou, H., Chang, W., and Zhang, L. (2016a). Sediment sources in a small agricultural catchment: A
691 composite fingerprinting approach based on the selection of potential sources.
692 *Geomorphology*, 266, 11-19. dx.doi.org/10.1016/j.geomorph.2016.05.007
693 Zhou, R., Li, Y., Lu, D., Liu, H., and Zhou, H. (2016b). An optimization based sampling approach for
694 multiple metrics uncertainty analysis using generalized likelihood uncertainty estimation.
695 *Journal of Hydrology*, 540; 274-286. <http://dx.doi.org/10.1016/j.jhydrol.2016.06.030>.

1653
1654
1655
1656
1657
1658
1659
1660
1661
1662
1663
1664
1665
1666
1667
1668
1669
1670
1671
1672
1673
1674
1675
1676
1677
1678
1679
1680
1681
1682
1683
1684
1685
1686
1687
1688
1689
1690
1691
1692
1693
1694
1695
1696
1697
1698
1699
1700
1701
1702
1703
1704
1705
1706
1707
1708
1709
1710
1711

697 *Table 1: Summery characteristics of dust samples collected in Zabol during 21 June to 4 October,*
698 *2014.*

dust sample no	Sampling date	W V* (m/s)	dust mass (ug/m ³)	dust sample no	Sampling date	W V* (m/s)	dust mass (ug/m ³)
1	23 June 2014	7.1	270.2	30	24 August 2014	6.5	300.15
2	25 June 2014	8.6	1180.5	31	25 August 2014	9	695.65
3	26 June 2014	6.3	380	32	26 August 2014	10.4	1100.15
4	29 June 2014	8.1	500.6	33	27 August 2014**	9.8	1052
5	30 June 2014	9	458	34	27 August 2014***	9.8	922.39
6	4 July 2014	9.5	7800	35	28 August 2014	8	606.29
7	5 July 2014	8.9	570.2	36	29 August 2014	7.4	271.3
8	11 July 2014	10.3	724	37	3 Sep 2014	10	3594.92
9	12 July 2014	10.5	1700.7	38	4 Sep 2014	11.4	3594.92
10	13 July 2014	10.5	831	39	5 Sep 2014	8.1	339.56
11	14 July 2014	8.9	370.3	40	6 Sep 2014	8.5	1243.88
12	18 July 2014	11.3	740.2	41	8 Sep 2014	6.1	186.21
13	19 July 2014	8.3	1800	42	10 Sep 2014	9.1	3188.85
14	21 July 2014	4.8	320.8	43	13 Sep 2014	7.4	296.8
15	3 August 2014	12.3	715.3	44	16 Sep 2014	4.6	213.77
16	4 August 2014	10	1600	45	17 Sep 2014	4.3	192.4
17	5 August 2014	5.1	216	46	19 Sep 2014	10.1	10785.5
18	6 August 2014	6.6	246.4	47	20 Sep 2014	8.5	1013.43
19	7 August 2014	10	1500	48	21 Sep 2014	4.9	111.76
20	8 August 2014	10	1803	49	22 Sep 2014	2.8	179.61
21	9 August 2014	10	480.04	50	24 Sep 2014	3.4	155.98
22	10 August 2014	8	560.04	51	26 Sep 2014	2.3	165.52
23	11 August 2014	9.1	4500	52	27 Sep 2014	5.5	274.83
24	12 August 2014	8.3	720	53	29 Sep 2014	4	90.31
25	13 August 2014	8.3	1480	54	30 Sep 2014	7.1	814.46
26	14 August 2014	11.5	9004.58	55	1 Oct 2014	5.1	413.15
27	16 August 2014	10.9	3529.4	56	2 Oct 2014	5.3	331.67
28	18 August 2014	5.1	126.74	57	3 Oct 2014	7.5	597.6
29	21 August 2014	8.3	498.5				

* W V indicates Wind Velocity; ** Sample collected on the day; *** Sample collected on the night.

701
702
703

1712
1713
1714
1715
1716
1717
1718
1719
1720
1721
1722
1723
1724
1725
1726
1727
1728
1729
1730
1731
1732
1733
1734
1735
1736
1737
1738
1739
1740
1741
1742
1743
1744
1745
1746
1747
1748
1749
1750
1751
1752
1753
1754
1755
1756
1757
1758
1759
1760
1761
1762
1763
1764
1765
1766
1767
1768
1769
1770

704 *Table 2: Results of a two-stage statistical process for selecting optimum composite fingerprints for*
705 *distinguishing sources of dust.*

Kruskal-Wallis H test			Stepwise DFA		
Fingerprint property	Chi-Square	P-value	Step	Entered fingerprint	Wilk's lambda
Trace elements			1	Fe	0.356
Au	6.79	0.079	2	Sr	0.188
Pt	1.58	0.664	3	Mn	0.081
Mg	20.83	0.000**	4	Cr	0.053
Al	1.48	0.686	5	Pb	0.033
Sr	20.6	0.000**	*Statistically significant at P<0.05 ** Statistically significant at P<0.01		
Li	22	0.000**			
Fe	20.9	0.000**			
Cr	19.5	0.000**			
Cu	19.5	0.000**			
Zn	5.16	0.16			
As	9.9	0.019*			
Ni	20.75	0.000**			
Pb	9.58	0.022*			
Mn	20.24	0.000**			
Co	18.73	0.000**			
Sn	12.9	0.005**			
Ions					
Na ⁺	7.24	0.065			
NH ₄ ⁺	2.6	0.456			
K ⁺	4	0.254			
Cl ⁻	0.4	0.941			
NO ₂ ⁻	3.3	0.358			
NO ₃ ⁻	7.01	0.072			
Mg ²⁺	1.38	0.709			
Ca ⁺	14.5	0.002**			

1771
1772
1773 706
1774
1775
1776
1777
1778
1779
1780
1781
1782
1783
1784
1785
1786
1787
1788
1789
1790
1791
1792
1793
1794
1795
1796
1797
1798
1799
1800
1801
1802
1803
1804
1805
1806
1807
1808
1809
1810
1811
1812
1813
1814
1815
1816
1817
1818
1819
1820
1821
1822
1823
1824
1825
1826
1827
1828
1829

1 Using GLUE to pull apart the provenance of atmospheric dust

2

3 Reza Dahmardeh Behrooz¹, Hamid Gholami^{2*}, Matt W. Telfer^{3*}, John D. Jansen^{4*}, Abolhassan

4 Fathabadi⁵

5

6 1. Department of Environmental Sciences, Faculty of Natural Resources, University of Zabol, Zabol,
7 Sistan, Iran

8 2. Department of Natural Resources Engineering, University of Hormozgan, Bandar-Abbas,
9 Hormozgan, Iran.

10 3. School of Geography, Earth and Environmental Sciences, Plymouth University, Plymouth, Devon
11 PL4 8AA, UK

12 4. Department of Geoscience, Aarhus University, Aarhus, 8000, Denmark.

13 5. Department of Range and Watershed Management, University of Gonbad-e-Kavoos, Gonbad-e-
14 Kavoos, Golestan, Iran

15

16 Corresponding Authors: Hamid Gholami, hgholami@hormozgan.ac.ir; Matt W Telfer,

17 matt.telfer@plymouth.ac.uk; John Jansen, jdj@geo.au.dk

18

19 HIGHLIGHTS

- 20 • The GLUE model is applied to reveal the provenance of aeolian dust in Zabol, Iran.
- 21 • Quantitative estimates and uncertainties of four different dust sources are discriminated.
- 22 • One dry lake, Hamoun Puzak, is by far the dominant dust source, despite others nearby.
- 23 • The major dust source is insensitive to large changes in exposed local dry lake beds.
- 24 • Cultivated land is the second most important dust source, ahead of some playas.

25

Using GLUE to pull apart the provenance of atmospheric dust

HIGHLIGHTS

- The GLUE model is applied to reveal the provenance of aeolian dust in Zabol, Iran.
- Quantitative estimates and uncertainties of four different dust sources are discriminated.
- One dry lake, Hamoun Puzak, is by far the dominant dust source, despite others nearby.
- The major dust source is insensitive to large changes in exposed local dry lake beds.
- Cultivated land is the second most important dust source, ahead of some playas.

Abstract

Identifying the sources of aeolian dust is a crucial step in mitigating the associated hazards. We apply a Generalized Likelihood Uncertainty Estimation (GLUE) model to constrain the uncertainties associated with sediment fingerprinting of atmospheric dust in the Sistan region on the Iran-Afghanistan border, one of the world's dustiest places. 57 dust samples were collected from the rooftop of the Zabol Department of Environmental Protection during a summer dusty period from June to October 2014, in addition to 31 surface soil samples collected from potential sources nearby, including cultivated land (n=8), uncultivated rangeland (n=7), and two dry lakes: Hamoun Puzak (n=10) and Hamoun Saberi (n=6). Dust and soil samples were analyzed for 24 tracers including 16 geochemical elements and 8 water-soluble ions. Five optimum composite fingerprints (Fe, Sr, Mn, Cr and Pb) were selected for discriminating sources by a two-stage statistical process involving a Kruskal-Wallis test and stepwise discriminant function analysis (DFA). Uncertainty ranges for source contributions of dust determined by the GLUE model showed that the dry lake Hamoun Puzak is the dominant source for all dust samples from Zabol and cultivated land is a secondary source. We found marked spatial variance in the importance of regional dry lake beds as dust sources, and temporal persistence in dust emissions from Hamoun Puzak, despite very large areas of adjacent lake beds drying during the study period. Aeolian sediment fingerprinting studies can benefit considerably from the constraints provided by modelling frameworks, such as GLUE, for quantifying the uncertainty in dust provenance data.

60
61
62 29
63
64 30 **KEY WORDS:** Sediment fingerprinting, uncertainty, GLUE, atmospheric dust, Iran
65
66 31

67 32 **1. Introduction**

68
69 33 Constraining the source of atmospheric dust particles circulating in the ancient past as well as the
70 34 present-day is essential to understand the manifold implications of dust in the Earth system (Ridgwell,
71 35 2002; Goudie and Middleton, 2006; Shao et al., 2011). Ancient dust deposits are also archives of long-
72 36 term environmental change (Dietze et al., 2016); the best-known and longest being the >8 Myr loess
73 37 record in China (Sun & Zhu 2010). Present-day dust storms trigger a series of negative off-site and on-
74 38 site repercussions (Goossens, 2003). Off-site effects include respiratory disease in humans and
75 39 animals, contamination of food and water supplies, and interference with traffic safety, machinery,
76 40 and electronics. On-site effects include the loss of soil organic matter, nutrients, and overall
77 41 agricultural productivity (Goudie and Middleton, 2006). From this perspective, identifying sources of
78 42 dust and quantifying multi-source contributions and their uncertainties is a key step towards hazard
79 43 mitigation, especially in drylands.
80
81
82
83
84
85
86 44

87 45 A diverse range of techniques have been employed for tracing sources of atmospheric dust, including
88 46 isotopic ratios (e.g., Krom et al., 1999; Nakano et al., 2004; Grousset and Biscaye, 2005; Chen et al.,
89 47 2007; Cao et al., 2008; Wang et al., 2005; Rio-Salas et al., 2012; Yang et al., 2009); mineralogical and
90 48 chemical characteristics (Shen et al., 2009); meteorological data (Rezazadeh et al., 2013; Nabavi et al.,
91 49 2016; Ge et al., 2016; Rashki et al., 2017); synthesis of isotopic and geochemical data (e.g., Aarons et
92 50 al., 2017; Wei et al., 2017; Chavagnac et al., 2008); synthesis of trace element and water-soluble ion
93 51 analyses (Dahmardeh Behrooz et al., 2017a,b); numerical simulation (Hamidi et al., 2014; Nabavi et
94 52 al., 2017); satellite data (Long et al., 2016; Cherboudj et al., 2016; Schepanski et al., 2012); and
95 53 multidisciplinary approaches (Yan et al., 2015; Cao et al., 2015). While most of the studies listed above
96 54 are highly successful at inferring dust sources, we note that in many cases the uncertainties associated
97 55 with ascribing provenance are not considered formally. This is an important omission for two reasons:
98 56 1) airborne dust is commonly generated simultaneously from multiple populations and areas of fine-
99 57 grained particles; and 2) these multiple populations are, in turn, typically an amalgam generated from
100 58 different sources and mixed to differing degrees over timescales ranging from geological to individual
101 59 storm events. In other words, dust provenance presents a very challenging mixing problem and hence
102 60 uncertainty is fundamental. These two points ultimately stem from geomorphic processes of fine-
103 61 particle production, transport, deposition, and reworking.
104
105
106
107
108
109
110
111
112
113
114 62
115
116
117
118

119
120
121 63 Sediment fingerprinting is widely used to quantify source contributions of fluvial sediments (e.g.,
122 64 Collins et al., 1997; Walling, 2005; Stone et al., 2014; Zhou et al., 2016a; and Manjoro et al., 2017) and
123 65 its application to aeolian studies is growing (e.g., Liu et al., 2016; and Gholami et al., 2017a,b).
124 66 Moreover, the uncertainties involved with this method are gaining increased attention (Walling,
125 67 2013). In order to manage and quantify the uncertainty in fluvial sediment fingerprinting, some studies
126 68 have applied a Monte Carlo simulation framework (e.g., Motha et al., 2003; Collins et al., 2012; Voli et
127 69 al., 2013; Smith and Blake, 2014; Stone et al., 2014; Sherriff et al., 2015; and Vale et al., 2016).
128 70 Similarly, Bayesian approaches are also applied to fingerprinting aeolian sands (Gholami et al., 2017b)
129 71 and fluvial sediments (e.g., Massoudieh et al., 2013; Cooper et al., 2014; Cooper et al., 2015; Stewart
130 72 et al., 2015; and Abban et al., 2016). Yet, several challenges remain in adequately capturing the
131 73 uncertainty associated with diverse aeolian dust sources and pathways (Walling, 2013) and we suggest
132 74 that techniques developed in other disciplines may offer a way forward (Gholami et al., 2017b).
133
134
135
136
137
138
139
140
141

142 76 First proposed for hydrological modelling by Beven and Binley (1992), GLUE (Generalized Likelihood
143 77 Uncertainty Estimation) has gained much favour as a tool for evaluating uncertainty estimates (e.g.,
144 78 Hassan et al., 2008; Zhou et al., 2016b; Viola et al., 2009; Mantovan and Todini, 2006; Gong et al.,
145 79 2011). Here, we apply GLUE to the problem of dust provenance in the Sistan-Hamoun region on the
146 80 Iran-Afghanistan border. Since it constitutes a major dust source for south-west Asia, Sistan has been
147 81 the focus of numerous previous investigations (e.g., Goudie and Middleton, 2006; Rashki et al., 2012,
148 82 2013 a,b, 2015; Alizadeh Choobari et al., 2014). Recent work has generated an important dataset of
149 83 dust samples from a meteorological station at Zabol, which has been analyzed geochemically to
150 84 provide qualitative estimates of source (Dahmardeh Behrooz et al., 2017a) and the temporal
151 85 variability of dust emissions (Dahmardeh Behrooz et al., 2017b). Here we provide the first attempt to
152 86 formally quantify aeolian dust provenance and associated uncertainties with this dataset using GLUE.
153
154
155
156
157
158
159

160 88 **2. Study area**

161
162 89 The Sistan-Hamoun study area (Fig. 1) straddles the border between Afghanistan and the Sistan and
163 90 Baluchestan province of south-eastern Iran (30°5' to 31°28' N and 61°15' to 61°50' E) (Rashki et al.,
164 91 2012, 2013a). The Hamoun Lakes complex comprises three main lakes: Hamoun Hirmand, Hamoun
165 92 Saberi, and Hamoun Puzak, which are recharged primarily from Afghanistan by the Hirmand
166 93 (Helmand) River with smaller contributions from streams to the north and west (Esmaeili and Omrani,
167 94 2007). Following exceptionally high runoff, the lakes form a single body of water ~5700 km² in area
168 95 and ~13 Mm³ in volume (Sharifikia, 2013), though such events have become rare in recent decades
169
170
171
172
173
174
175
176
177

178
179
180 96 while dust emissions have grown correspondingly in magnitude (Goudie and Middleton, 2006; Rashki
181 et al., 2012).
182 97
183 98

184
185 99 *[Approximate location of figure 1]*
186

187 100 The climate in the Sistan region is arid to hyper-arid, and land-use is chiefly linked to agriculture and
188 101 fishing. At Zabol meteorological station (Fig. 1), mean rainfall is 55 mm y⁻¹ and mean evaporation is
189 102 >4000 mm y⁻¹ (Moghaddamnia et al., 2009). The prevailing wind is the notorious Levar or “Wind of
190 103 120 Days” from the north, which in the summer is accelerated into a Low-Level Jet (LLJ) by a persistent
191 104 high-pressure system over the Hindu Kush and the channeling effect of the surrounding topography
192 105 (Alizadeh-Choobari et al., 2014; Kaskaoutis et al., 2016, 2017). As a result, the city of Zabol and its
193 106 ~135,000 inhabitants experience dust storms of catastrophic proportions, resulting in Zabol ranking
194 107 as the world's most polluted city for particulate matter less than 2.5 µm (PM2.5) in size (World Health
195 108 Organisation, 2016).
196
197
198
199
200
201 109

202 110 **3. Methods**

203 111 **3.1 Field sampling**

204 112 We set out to characterise the soil materials for four different potential sources of atmospheric dust
205 113 emissions to the north of Zabol city (Fig. 1): 1) the dry lake-bed of Hamoun Puzak (Fig. 2a); 2) the dry
206 114 lake-bed of Hamoun Saberi (Fig. 2b); 3) cultivated arable farmland generally without crop-cover in
207 115 summer (Fig. 2c); and 4) bare rangeland surfaces with sparse to negligible natural vegetation cover
208 116 (Fig. 2d). A total of 31 surficial soil samples (<5 cm depth in a 30 cm² area) were collected from the
209 117 four potential sources (Table 1). We sieved the soil samples with a 400-mesh sieve, retaining particles
210 118 with a nominal geometric diameter of < 38.5 µm, which is roughly equivalent to the aerodynamic
211 119 diameter of dust (Cao et al., 2008). After sieving, we retained about 5 g of dust-sized material from
212 120 each sample.
213
214
215
216
217
218
219
220 121

221 122 *[Approximate location of Figure 2]*
222
223 123

224 124 During an exceptionally dusty summer period in Zabol (23 June to 4 October 2014), 57 atmospheric
225 125 dust samples were collected at one- to four-day intervals (Table 1) with sampling apparatus fitted to
226 126 the rooftop of the Department of Environmental Protection (5 m above ground level, 31°N, 61.3°E) in
227 127 an outer suburban area with no major industrial activities nor local fugitive dust sources. Our two dust
228 128 samplers (Model Chrono, Zambelli, Milan) were equipped with cyclones operating at a flow rate of
229 129 16.7 L/min as per the EU norms (Dahmardeh Behrooz et al, 2017a; 2017b). Total suspended-particle
230
231
232
233
234
235
236

237
238
239
240
241
242
243
244
245
246
247
248
249
250
251
252
253
254
255
256
257
258
259
260
261
262
263
264
265
266
267
268
269
270
271
272
273
274
275
276
277
278
279
280
281
282
283
284
285
286
287
288
289
290
291
292
293
294
295

130 (TSP) samples were collected in Teflon filters (0.45 μm pore size and 47 mm diameter) and then
131 desiccated for 24-hours at 25 $^{\circ}\text{C}$. Dust mass concentrations were measured gravimetrically by
132 weighing the Teflon filters before and after sampling using an analytical balance (Adam model) with
133 ± 0.1 mg precision. We refrigerated all dust samples at 4 $^{\circ}\text{C}$ until chemical analysis (Dahmardeh Behrooz
134 et al., 2017 a).

135

136 **3.2 Laboratory analysis of water-soluble ions and trace elements**

137 We measured the concentrations of 8 water-soluble ions in our samples (viz., Na^+ , NH_4^+ , K^+ , Ca^{2+} , Mg^{2+} ,
138 Cl^- , NO_3^- , NO_2^-). Three cations (Na^+ , NH_4^+ and K^+) were measured with a Shim-pack IC-C1 (Shimadzu
139 DGU-12A) using 5-mM HNO_3 solution as eluent. Three anions (Cl^- , NO_3^- and NO_2^-) were measured with
140 a Shim-pack ICA1 (Shimadzu DGU-12A), using 2.5-mM phthalic acid combined with 2.4-mM tris-
141 (hydroxymethyl) aminomethane as eluent (Lin, 2002). Two cations (Ca^{2+} and Mg^{2+}) were measured via
142 flame atomic absorption spectrometry (Philips, PU9400X, England).

143

144 After acid digestion, all samples were analyzed to determine the concentrations of 16 trace elements
145 (viz., Al, As, Au, Co, Cr, Cu, Fe, Li, Mg, Mn, Ni, Pb, Pt, Sn, Sr, and Zn) via Inductively Coupled Plasma
146 Atomic Emission Spectroscopy (ICP-OES, Perkin Elmer, Optima 2000, USA). Further details of
147 sampling and laboratory procedures are given in Dahmardeh Behrooz et al. (2017a, b).

148

149 **3.3 Two-stage method: Kruskal-Wallis test and discriminant function analysis**

150 The measurements of 8 water-soluble ions and 16 trace elements form the basis of the sediment
151 fingerprinting method aimed at identifying the source contribution of the Zabol dust samples. We
152 adopt a two-stage statistical procedure following the approach of Collins et al. (1997) to identify the
153 most suitable tracers for source discrimination. In stage one we tested the primary ability of tracers
154 to discriminate dust sources using the Kruskal-Wallis H test. Tracers with critical values at the 95 %
155 confidence levels or better were taken to the second stage in which we identified optimum composite
156 fingerprints using a stepwise discriminant function analysis based on minimization of Wilk's lambda.

157

158 **3.4 Generalised Likelihood Uncertainty Estimation (GLUE)**

159 GLUE was first devised by Beven and Binley (1992) as a means of sensitivity analysis and uncertainty
160 estimation in environmental model outputs. We use GLUE to quantify the uncertainty in the sediment
161 fingerprinting results via the following five steps:

162

296
297
298
299
300
301
302
303
304
305
306
307
308
309
310
311
312
313
314
315
316
317
318
319
320
321
322
323
324
325
326
327
328
329
330
331
332
333
334
335
336
337
338
339
340
341
342
343
344
345
346
347
348
349
350
351
352
353
354

163 1) Random sampling of parameter sets (300,000 iterations) are conducted using the Latin Hypercube
164 Sampling (LHS) method (Zhou et al, 2016b), by assuming source contributions from each source are
165 non-negative and that total contributions sum to unity. Due to the lack of prior information, we used
166 a uniform distribution as the prior distribution for all parameters.

167
168 2) Selection of a likelihood function and behavioral parameter thresholds. Here, we adopt the Nash-
169 Sutcliffe coefficient (ENS) as the likelihood function (Jin et al, 2010):

$$ME = 1 - \frac{\sum(O_{obs} - O_{sim})}{\sum(O_{obs} - \bar{O}_{obs})} = 1 - \frac{\sigma_i^2}{\sigma_{obs}^2} \quad (\text{eq.1})$$

172
173 where \bar{O}_{obs} is the mean value of the observed tracer concentration; O_{sim} is the simulated tracer
174 concentration; O_{obs} is the observed tracer concentration; σ_i^2 is the error variance for the i th model
175 (i.e., the combination of the model and the i th parameter set) and σ_{obs}^2 is the variance of the
176 observations.

177
178 3) Sampled parameter sets from step 1 are input to the mixing model (equation 2) and the likelihood
179 function is calculated for each parameter set as:

$$C_{dust} = C_{Sources} \times P \quad (\text{eq. 2})$$

182
183 where P is an m dimensional column vector of sources contribution (sampled parameter sets), C_{dust}
184 is an n -dimensional column vector of element concentration in sediment sample, $C_{Sources}$ is an $n \times m$ -
185 dimensional matrix representing mean tracer concentration in sources (each row represents mean
186 tracer concentration in each source), where n is the number of optimum composite fingerprints ($n=5$)
187 and m is the number of dust sources ($m=4$).

188
189 4) Parameter sets are divided into behavioural and non-behavioural types with respect to a threshold
190 value (Zhou et al, 2016). In this step, those parameter sets that have likelihood functions greater than
191 a threshold value were classified as behavioural parameter sets. For the next step, non-behavioural
192 parameter sets were discarded.

193
194 5) For behavioural parameter sets, likelihood weights are rescaled such that they sum to one, then
195 each parameter is sorted and we calculate cumulative distributions for each parameter. Quintiles and
196 uncertainty intervals are calculated via the cumulative distributions.

355
356
357
358
359
360
361
362
363
364
365
366
367
368
369
370
371
372
373
374
375
376
377
378
379
380
381
382
383
384
385
386
387
388
389
390
391
392
393
394
395
396
397
398
399
400
401
402
403
404
405
406
407
408
409
410
411
412
413

197
198
199
200
201
202
203
204
205
206
207
208
209
210
211
212
213
214
215

3.5 Geospatial analysis and climate data

Landsat data were downloaded from the United States Geological Survey's Earth Explorer, and all analysis was conducted within ArcGIS 10.3. Quantitative analysis of water extent was conducted using a modified Normalized Difference Water Index (NDWI), based on the green (Band 3) and short-wave infrared (Band 6) bands of Landsat 8 data (Xu, 2006). Climate data are taken from the Hourly Global Surface Data (DS3505) dataset for the Zabol station (World Meteorological Organization ID: 40829), accessed via the legacy Climate Data Online (CDO) portal of the National Oceanic and Atmospheric Administration's (NOAA) National Climatic Data Centre (NCDC) online (available at <https://www7.ncdc.noaa.gov/CDO/dataproduct>). To calculate back-trajectories for the air mass affecting Zabol during selected peak dust events of the observation period, we use NOAA's Hysplit model (summarized in Stein et al., 2015). Ensemble runs for the 24 hours preceding peak dust events were run based on airflow at 50, 100 and 500 m above the land surface. Additional remote sensing data regarding atmospheric dust flux and dust deposition was derived from NASA's Earthview platform in the form of a) visible MODIS imagery from July 2014, b) the MERRA-2 monthly PM2.5 dust deposition product for July 2014 (see Gelaro et al., 2017) and c) the AURA Ozone Monitoring Instrument (OMI) Aerosol Index product for July 2nd (Torres, 2006), near the start of the observed period of study.

4. Results

4.1 Kruskal-Wallis test and discriminant function analysis

The results of the Kruskal-Wallis tests (Table 2) indicate that among the twenty-four measured properties (8 water-soluble ions and 16 element concentrations), thirteen trace elements (Mg, Sr, Li, Fe, Cr, Cu, As, Ni, Pb, Mn, Co, and Sn) and one ion (Ca²⁺) show statistically significant differences at the 95 %-level between the four potential dust sources (the two dry lake beds, cultivated farmland, and rangeland areas of natural vegetation cover). Trace elements clearly out-performed water-soluble ions for tracking spatial sources of dust. Thirteen trace elements were passed to stage-two for stepwise discriminant function analysis (DFA). The DFA yielded five trace elements (Fe, Sr, Mn, Cr and Pb) with optimum composite fingerprints that correctly discriminate 87 % of our source samples (Table 2 and Fig. 3).

[Approximate location of Figure 3]

4.2 Using GLUE to constrain uncertainty in the source contributions of dust

414
415
416
417
418
419
420
421
422
423
424
425
426
427
428
429
430
431
432
433
434
435
436
437
438
439
440
441
442
443
444
445
446
447
448
449
450
451
452
453
454
455
456
457
458
459
460
461
462
463
464
465
466
467
468
469
470
471
472

231 Uncertainty intervals of source contributions estimated by the GLUE-mixing model at the 95 %
232 confidence level are presented in Figure 4. These results show that the most important dust source is
233 clearly Hamoun Puzak (Figs. 4a and 5). Median contributions from this lake-bed span 29 to 88 %
234 (samples 33 and 45, respectively). Hamoun Saberi is a less important source for our samples. Median
235 contributions from this lake bed span 3 to 24 % (samples 11 and 33, respectively) (Fig. 4b). The sparsely
236 vegetated rangeland is the least active dust source. Median contributions span 2 to 22 % (samples 45
237 and 34, respectively) (Fig. 4c). Cultivated farmland is recognized as the second-most important source
238 for all of 57 samples. Median contributions from farmland span 4 to 25 % (samples 23 and 34,
239 respectively) (Figs. 4d). For most samples, the lower-limit of predicted uncertainty is zero for
240 contributions from the three sources other than Hamoun Puzak (Figs. 4b-d). Figure 5 presents an
241 overview of the source contributions with all samples plotted together as a frequency histogram.

242
243 Overall, a strong correlation (Pearson's $r = 0.783$, $p < 0.001$) can, unsurprisingly, be seen between dust
244 flux and the logarithm of the windspeed, with a threshold of around 10 m s^{-1} . However, no significant
245 correlation is observed between the relative contribution of Hamoun Puzak and Saberi, and either the
246 windspeed (Pearson's $r = -0.06$, $p = 0.66$) or wind direction (Pearson's $r = 0.238$, $p = 0.07$).

247
248 *[Approximate location of Figure 4]*
249 *[Approximate location of Figure 5]*

250

251 **5. Discussion**

252 Sediment fingerprinting is a highly effective technique for quantifying source contributions of fluvial
253 sediments (e.g. Collins et al., 1997; Walling, 2005; Stone et al., 2014; Zhou et al., 2016a; Manjoro et
254 al., 2017) and aeolian sands (e.g. Liu et al., 2016; Gholami et al., 2017a,b). Here we build upon this
255 approach by exploring the potential of the GLUE methodology for distinguishing spatially proximal
256 aeolian dust sources with similar underlying geology and geomorphology. We demonstrate its efficacy
257 at formally quantifying the uncertainty distributions associated with aeolian dust fingerprinting due
258 to spatial and temporal variation in the dust cycle. Further, we use the method to reveal spatial
259 complexity—alongside an unexpected lack of temporal complexity—in the nature of the dust sources.

260

261 **5.1 Environmental context of dust emissions**

262 The strong correlation between dusty days and the surface area of exposed lake floors indicates that
263 i) dust storms in the Sistan-Hamoun region are directly related to the dryness of the Hamoun Lakes,
264 and ii) these lake beds are the main source of dust emissions (Goudie and Middleton 2006; Rashki et

473
474
475
476
477
478
479
480
481
482
483
484
485
486
487
488
489
490
491
492
493
494
495
496
497
498
499
500
501
502
503
504
505
506
507
508
509
510
511
512
513
514
515
516
517
518
519
520
521
522
523
524
525
526
527
528
529
530
531

265 al., 2012; 2013a; 2013b; 2015). Such relationships are not uncommon, as worldwide observations
266 suggest that exposed dry lake beds can govern the frequency and intensity of dust storms; for
267 example, at Owens Lake, USA (Reheis et al., 2009); Aral Sea, Uzbekistan (Breckle et al., 2012);
268 Makgadikgadi pan complex and Etosha Pan, southern Africa (Prospero et al., 2002; Mahowald et al.,
269 2003; and Washington et al., 2003); and Kata Thandi-Lake Eyre, Australia (Baddock et al., 2009).

270
271 The frequency and magnitude of dust emissions from the Hamoun Lakes has also been related to
272 annual/decadal scale variations in the surface area of the lakes, which varies dramatically. At its
273 maximum extent, observed following the 1998 spring-melt Hirmand River floods (Rashki et al., 2012a),
274 the Hamoun lake complex forms a single body of water ~4500 km² in area. This is comprised of
275 Hamoun Hirmand (~1400 km²), Hamoun Saberi (~1400 km²) and Hamoun Puzak (~1700km²), with
276 Hamoun Baringak forming a series of smaller lakes and spillways between Saberi and Puzak. During
277 more typical lake-full episodes, these bodies of water are not conjoined; for instance, during the spring
278 of 1996 (Figure 6a), Hamoun Saberi spanned ~815 km² and Hamoun Puzak spanned 375 km² (Hamoun
279 Baringak is here considered part of the western extent of the Puzak basin). Hamoun Hirmand lies
280 mostly downwind of Zabol, and hence is not considered further. Between 1999 and 2010, a prolonged
281 drought likely related to the El Nino Southern Oscillation resulted in the rapid and sustained
282 desiccation of the Hamoun Lakes, with a concomitant increase in the frequency of dusty days (Rashki
283 et al., 2012; 2013b). Since 2010, lake levels have been highly variable (Fig. 6), with a return to lake-full
284 conditions experienced around 2011, and a subsequent return to large areas of exposed dry lake beds
285 in more recent years.

286
287 Such changes can also develop rapidly. Within the timeframe of this study (June-October 2014),
288 Hamoun Puzak and Hamoun Saberi lost around 295 km² and 640 km² of water surface area,
289 respectively (i.e. 98.5% and 99.9% of their extent on June 14th) (Fig. 7). The small, shallow Hamoun
290 Baringak lakes, directly to the north of Zabol, dried especially early in the season, with almost all water
291 lost by July 2014. This desiccation affected Hamoun Saberi and Puzak proportionally at very similar
292 rates, but Saberi's larger surface area at the start of this study led to greater absolute change in the
293 lake floor exposure area. During this period, there was no rainfall recorded at the Zabol meteorological
294 station, but the persistent 'Wind of 120 Days' blew from 327° ± 36° during June-October, with daily
295 average windspeeds up to 15 m s⁻¹ (~35 mph) and 50 of the 138 days of the study period exceeding
296 daily averages of ~9 m s⁻¹ (~20 mph).

297
298 *[Approximate location of Figure 6]*

532
533
534
535
536
537
538
539
540
541
542
543
544
545
546
547
548
549
550
551
552
553
554
555
556
557
558
559
560
561
562
563
564
565
566
567
568
569
570
571
572
573
574
575
576
577
578
579
580
581
582
583
584
585
586
587
588
589
590

299 [Approximate location of Figure 7]

300

301 **5.2. Dust sources: dry beds of Hamoun Lakes**

302 The GLUE results (Figs 4 and 5) reveal that the dominant source of dust collected at Zabol is Hamoun
303 Puzak, and also that in general, the dust sources vary little over the three-month period from June to
304 the beginning of October, 2014. This finding is unexpected, for a number of reasons. Firstly, as the
305 wind at Zabol during this period comes from the northwest to north-northwest ($327^\circ \pm 36^\circ$), the most
306 obvious candidate source of Zabol dust is the upwind Hamoun Saberi (Figures. 1 and 7). Yet,
307 consistently, Hamoun Puzak contributes ~40-90% (uncertainties included) of the dust received at
308 Zabol. Furthermore, given the rapid increase in Saberi's exposed dry bed during the early period of
309 sampling, its contribution would be expected to increase proportionally over this period. But Saberi's
310 contributions actually vary little during the season (Fig. 4). When the surface area of the lakes is
311 considered, either relative to lake-full conditions (Figure 8a and 8c), or as absolute surface areas
312 (Figure 8b and 8d), there is little temporal relationship with the relative dust contributions of the two
313 lake beds.

314
315 [Approximate location of Figure 8]

316

317 Similarly, investigation of the meteorological conditions during June-October do not readily explain
318 the dominance of Hamoun Puzak. There is no clear correlation with either wind magnitude, or
319 direction, that can readily explain the dominance of Puzak, and no obvious explanation for the
320 occasional excursions when other sources contribute markedly more. For instance, on August 27th
321 replicate samples were collected (S33 and S34 in Fig. 4) and yield consistent results (note that, for
322 consistency, only one of these samples is included in Figs. 8 and 9). Satellite aerosol observations,
323 modelled dust deposition, and aerosols indices (Figure 10), whilst confirming the regional importance
324 of the Hamoun Lakes, do not readily identify localized sources due to their relative spatial coarseness.

325

326 These results suggest that Hamoun Puzak—or at least Hamoun Baringak at the western margin of
327 Hamoun Puzak, where the source samples were collected (Fig. 1)—is a prolific and persistent source
328 of dust over Zabol irrespective of the existence of large adjacent alternative sources. Why is Hamoun
329 Puzak such an effective dust emitter? And why, despite its size and position directly upwind of Zabol,
330 does Hamoun Saberi contribute relatively little? We propose that several factors have an influence,
331 as follows.

332

591
592
593
594
595
596
597
598
599
600
601
602
603
604
605
606
607
608
609
610
611
612
613
614
615
616
617
618
619
620
621
622
623
624
625
626
627
628
629
630
631
632
633
634
635
636
637
638
639
640
641
642
643
644
645
646
647
648
649

333 [Approximate location of Figure 9]

334 [Approximate location of Figure 10]

335

336 First, let us consider the hydrological setting and sedimentology of the area. The Hamoun Lakes are
337 predominantly fed with water from the Hirmand River to the east, with the Khash River also feeding
338 directly into Hamoun Puzak from the east. Hamoun Saberi is fed largely from the north by the Harut
339 and Farah rivers. The sampled region around Hamoun Baringak and Hamoun Puzak lies in series of
340 channels and small closed basins which act as spillways connecting the lakes during lake-full episodes.
341 Such areas are likely to have distinctly different sedimentology from lake bed areas subject to direct
342 lacustrine sedimentation (King et al., 2011, Sweeney et al., 2011). Evidence that these sediments are
343 distinct from those of Hamoun Saberi is implicitly provided in the primary function of the DFA used
344 here to define the characteristics of these dusts (Fig. 3). The wind regime necessary for aeolian
345 transport to Zabol from Hamoun Baringak is compatible with this zone being a dominant source, as
346 northerly orientation lies well within the $327^\circ \pm 36^\circ$ (one sigma) direction of the observed winds. It
347 may also be that the transport pathways associated with the low-level jet from the north are strongly
348 impacted by topography. We note that wind streaks evident on the satellite imagery of the region
349 (visible in the northern and western part of Figure 7) suggest that topography is steering and deflecting
350 local winds in a complex manner. For instance, topographic roughness caused by rocky hills around
351 Hamoun Saberi may reduce effective winds at the surface. Further detailed analysis of the possible
352 role of topographic steering of the winds in this, and other comparable studies, is clearly desirable,
353 but does require high-resolution data and sophisticated modeling of the wind field to achieve
354 substantial results.

355

356 The mean orientation of the seasonal winds, however, raises another question: Why does Hamoun
357 Saberi, which lies directly upwind of Zabol, not contribute more to Zabol's dust flux, especially during
358 the latter part of our study when an additional 640 km² of dry lake bed became exposed? It is well-
359 reported that dust production can be spatially highly variable, even at sub-basin scales (Mahowald et
360 al., 2003, Reheis et al., 2002, Bullard et al., 2008). One possibility relates to the differing geochemistry
361 of the sediments that can promote the formation of protective crusts. Field experiments have shown
362 that dry river courses when replenished frequently with fine-grained fluvial sediment can be much
363 more effective at producing deflatable dust relative to playas and, counter-intuitively, playa centres
364 are relatively low emission sources (Sweeney et al., 2011, King et al., 2011). Dry lake-bed deposits
365 from the Mojave in the western US, for instance, have been reported to yield less dust than those with
366 fluctuating water-levels (Reynolds et al., 2007), and the progressive and rapid desiccation of Hamoun

650
651
652
653
654
655
656
657
658
659
660
661
662
663
664
665
666
667
668
669
670
671
672
673
674
675
676
677
678
679
680
681
682
683
684
685
686
687
688
689
690
691
692
693
694
695
696
697
698
699
700
701
702
703
704
705
706
707
708

367 Saberi during the study period may have been simply unfavourable for the generation of deflatable
368 dust.

369
370 Conversely, it may be that exogenic water supply from the northerly channels sufficiently dampened
371 the surface to limit additional deflation. We note that shallow flooding was observed during the field
372 sample collection, despite the lack of rain observed either in Zabol, or the fortnightly Landsat images.
373 Over longer timescales, rates of aeolian erosion have been shown to inversely relate to soil moisture
374 (Whitney et al., 2015). Although the whole region is sparsely vegetated, the role of vegetation in
375 influencing surface roughness and thus susceptibility to aeolian erosion also cannot be overlooked
376 (e.g. Cowie et al., 2013, Li et al., 2007). Lastly, we point to the cause of the additional 13% of variability,
377 which was not well explained by the discriminant function analysis of the source sediments. This
378 variability may imply that a significant component of Zabol dust derives from outside the immediate
379 area of the Hamoun Lakes. Dust plumes transported from the Karakum desert in Turkmenistan are
380 also known to affect much of southwest Asia, including the Sistan region (Kskaoutis et al., 2015), and
381 may be a source of exogenous dust not accounted for among the four potential sources we sampled.
382 To address these questions, we use the Hysplit model to calculate back-trajectories for three intervals
383 characterized by high dust deposition during the study period (Figure 11). These confirm variability in
384 both localized and regional wind trajectories for the high dust-flux days during period July to
385 September 2014. The role of the Karakum in contributing long-distance flux is supported, over the 24-
386 hour transport window modelled here (Figure 11a). However, there is also evidence of local and
387 regional variability, with July and August winds coming locally via a north-northwesterly track (over a
388 still largely inundated Hamoun Saberi), and the September peak in dust emission driven near Zabol by
389 a due northerly wind, tracking directly over a desiccated Hamoun Baringak and Puzak (Figure 11b).
390 This is likely related to seasonal variation of the Caspian Sea - Hindu Kush Index (CasHKI), a broadly
391 east-west atmospheric pressure dipole between 40–50°N, 50–55°E and 35–40°N, 70–75°E (Kaskaoutis
392 et al., 2016, 2017). This suggests that the interplay of atmospheric and hydrological controls on dust
393 emission is crucial in this region.

394
395 [Approximate location of Figure 11]

396
397 **5.3. Dust sources: cultivated and uncultivated rangeland areas**
398 The connections between land management, agriculture and aeolian dust emissions are well
399 documented (Wiggs and Holmes, 2011, Okin et al., 2001), and the role of agriculture in exacerbating
400 drought-driven dust events such as the decade-scale 'Dust Bowl' of 1930s USA is clearly established

709
710
711
712
713
714
715
716
717
718
719
720
721
722
723
724
725
726
727
728
729
730
731
732
733
734
735
736
737
738
739
740
741
742
743
744
745
746
747
748
749
750
751
752
753
754
755
756
757
758
759
760
761
762
763
764
765
766
767

401 (Worster, 2004). We find that the cultivated cropland to the north of Zabol is the region's second-
402 largest overall source of dust (Fig. 4), slightly out-stripping Hamoun Saberi, and contributing
403 substantially more than uncultivated rangeland with sparse vegetation. Desertification, by which we
404 mean mainly arid land degradation, has been recognized in other regions of Iran (Sepehr et al., 2007),
405 and given the difficulties for agriculture in such an extremely dry and hot climate, it becomes apparent
406 that sustainable land management is difficult to achieve. The spread of wind erosion is challenging
407 land managers worldwide - from the Argentinian Pampas (Buschiazzo and Zobeck, 2008) to the
408 Tibetan Plateau (Zhang et al., 2012) and even temperate regions such as southern Sweden (Barring et
409 al., 2003). The findings here that cultivation-based farming is the second largest contributor to Zabol's
410 dust flux (with median contributions of 4-25% for individual samples) highlights an anthropogenic dust
411 source that could be quelled with alternative farming practices.

412

413 **6. Conclusion**

414 Identifying source(s) of aeolian sediments (sand and dust) is essential to improve planning and
415 management of arid and semi-arid regions. Here we present a quantitative sediment fingerprinting
416 approach coupled with the GLUE methodology to quantify source contributions of dust to the city of
417 Zabol in the Sistan-Hamoun region of south-east Iran. Zabol consistently ranks globally as one of the
418 most susceptible to fine (PM_{2.5} and PM₁₀) aerosol pollutants. Using GLUE, we have assigned
419 quantitative estimates of the relative contributions of four potential dust sources: two dry lake beds
420 (Hamoun Puzak and Hamoun Saberi), cultivated land, and sparsely-vegetated uncultivated rangeland.
421 The dry bed of Hamoun Puzak is the major source supplying sediment for dust samples, with cultivated
422 land contributing more than Hamoun Saberi or rangeland areas. Robust estimates of uncertainty
423 reveal that whilst the other three dust sources are broadly similar in magnitude, the western end of
424 Hamoun Puzak (Hamoun Baringak) is undoubtedly the main source.

425

426 The samples used for these analyses were collected over a three-month period, during the first half of
427 which the surface water extent of both Puzak and Saberi lakes decreased by > 98%. Yet, the relative
428 contributions from the different land classes remained remarkably consistent. We also note that
429 despite a persistent seasonal wind bearing NW-NNW upon Zabol, the main dust source lies to the
430 northerly segment of the winds observed. This suggests that either the median wind direction is not
431 the most dust-bearing, or the transport pathways are more complex than suspected. Hysplit analyses
432 suggest important temporal variations during the windy season.

433

768
769
770
771
772
773
774
775
776
777
778
779
780
781
782
783
784
785
786
787
788
789
790
791
792
793
794
795
796
797
798
799
800
801
802
803
804
805
806
807
808
809
810
811
812
813
814
815
816
817
818
819
820
821
822
823
824
825
826

434 Our results demonstrate both the potential and the necessity of combining quantitative provenancing
435 techniques with robust uncertainty methods and, ultimately, improved land management. The
436 straightforward approach of linking the main wind direction to a large and rapidly-drying lake bed
437 (Hamoun Saberi) does not yield a good predictive outcome, in this case. Spatial variation in dust
438 sources has been identified elsewhere, most strikingly at the Bodélé Depression in the Chadian Sahara
439 (Washington et al., 2003); here we demonstrate the application of methods with the scope to identify
440 such spatial variation from the point of receipt of the dust. We are unable to outline the exact reasons
441 for Hamoun Puzak's susceptibility to aeolian erosion. However, we attribute notable influence to the
442 geomorphological conditions of the western arm of the Puzak, with its array of interconnected small
443 basins (Hamoun Baringak) and spillways proving more prone to generating dust emissions.

445 REFERENCES

- 446 Aaron, S. M., Blakowski, M. A., Aciego, S. M., Stevenson, E. I., Sims, K. W. W., Scott, S. R., and Aarons,
447 C. (2017). Geochemical characterization of critical dust source regions in the American West.
448 *Geochimica et Cosmochimica Acta* 215; 141-161.
449 <http://dx.doi.org/10.1016/j.gca.2017.07.024>
- 450 Abban, B., Papanicolaou, A. N., Cowles, M. K., Wilson, C. G., Abaci, O., Wacha, K., Schilling, and K.,
451 Schnobelen, D. (2016). An enhanced Bayesian fingerprinting framework for studying
452 sediment source dynamics in intensively managed landscapes. *Water Resource Research*, 52,
453 4646-4673. doi:10.1002/2015WR018030.
- 454 Alizadeh Choobari, O., Zawar-Reza, P., and Sturman, A. (2014). The "wind of 120 days" and dust
455 storm activity over the Sistan Basin. *Atmospheric Research*, 143; 328-341.
456 <http://dx.doi.org/10.1016/j.atmosres.2014.02.001>
- 457 Baddock, M. C., Bullard, J. E., and Bryant, R. G (2009). Dust source identification using MODIS: a
458 comparison of techniques applied to the Lake Eyre Basin, Australia. *Remote Sens Environ*,
459 113:1511-28.
- 460 Barring, L., Jonsson, P., Mattsson, J. O. & Ahman, R. 2003. Wind erosion on arable land in Scania,
461 Sweden and the relation to the wind climate - a review. *Catena*, 52, 173-190.
- 462 Beven, K. and Binley, A. (1992). The future of distributed models: Model calibration and uncertainty
463 prediction. *Hydrological Processes*, 6(3), 279-298. doi: 10.1002/hyp.3360060305.
- 464 Breckle, S.W., Wucherer, W., Liliya, A., Dimeyeva, L. A., Nathalia, P., and Ogar, N.P. (2012). Aralkum -
465 a man-made desert: the desiccated floor of the Aral Sea (Central Asia). Springer; 2012486.
- 466 Bullard, J., Baddock, M., Mctainsh, G. & Leys, J. 2008. Sub-basin scale dust source geomorphology
467 detected using MODIS. *Geophysical Research Letters*, 35.

827
828
829
830
831
832
833
834
835
836
837
838
839
840
841
842
843
844
845
846
847
848
849
850
851
852
853
854
855
856
857
858
859
860
861
862
863
864
865
866
867
868
869
870
871
872
873
874
875
876
877
878
879
880
881
882
883
884
885

468 Buschiazzo, D. E. & Zobeck, T. M. 2008. Validation of WEQ, RWEQ and WEPS wind erosion for
469 different arable land management systems in the Argentinean Pampas. *Earth Surface*
470 *Processes and Landforms*, 33, 1839-1850.

471 Cao, H., Amiraslani, F., Liu, J., and Zhou, N. (2015). Identification of dust storm source areas in West
472 Asia using multiple environmental datasets. *Science of the Total Environment*, 502; 224-235.
473 <http://dx.doi.org/10.1016/j.scitotenv.2014.09.025>

474 Cao, J. J., Zhu, C. S., Chow, J. C., Liu, W. G., Han, Y. M., and Watson, J. G. (2008). Stable carbon and
475 oxygen isotopic composition of carbonate in fugitive dust in the Chinese Loess Plateau.
476 *Atmospheric Environment*, 42; 9118-9122. doi:10.1016/j.atmosenv.2008.09.043

477 Chavagnac, V., Lair, M., Milton, J. A., Lloyd, A., Croudace, I. W., Palmer, M. R., Green, D. R. H., and
478 Cherkashev, G. A. (2008). Tracing dust input to the Mid-Atlantic Ridge between 14°45'N and
479 36°14'N: Geochemical and Sr isotope study. *Marine Geology*, 247; 208-225.
480 doi:10.1016/j.margeo.2007.09.003

481 Chen, J., Li, G., Yang, J., Rao, W., Lu, H., Balsam, W., Sun, Y., and Ji, J. Nd and Sr isotopic
482 characteristics of Chinese deserts: Implications for the provenances of Asian dust.
483 *Geochimica et Cosmochimica Acta*, 71; 3904-3914.

484 Cherboudj, I., Beegum, S. N., and Ghedira, H. (2016). Identifying natural dust source regions over the
485 Middle-East and North-Africa: Estimation of dust emission potential. *Earth Science Review*.
486 <http://dx.doi.org/10.1016/j.earscirev.2016.12.010>

487 Collins, A. L., and Walling, D. E. (2007). Sources of fine sediment recovered from the channel bed of
488 lowland groundwater-fed catchments in the UK. *Geomorphology*, 88, 120-138.
489 doi:10.1016/j.geomorph.2006.10.018

490 Collins, A.L., Walling, D.E., and Leeks, G.J.L. (1997). Fingerprinting the origin of fluvial suspended
491 sediment in larger river basins: combining assessment of spatial provenance and source
492 type. *Geografiska Annaler*, 79, 239-254.

493 Collins, A.L., Zhang, Y., Walling, D.E., Grenfell, S.E., Smith, P., Grischeff, J., ... Brogden, D. (2012).
494 Quantifying fine-grained sediment sources in the River Axe Catchment, southwest England:
495 Application of a Monte-Carlo numerical modelling framework incorporating local and
496 genetic algorithm optimisation. *Hydrological Processes*, 26 (13), 1962-1983.
497 doi:10.1002/hyp.8283.

498 Cooper, R. J., Krueger, T., Hiscock, K. M., & Rawlins, B. G. (2014). Sensitivity of fluvial sediment
499 source apportionment to mixing model assumptions : A Bayesian model comparison. *Water*
500 *Resources Research*, 9031-9047. doi:10.1002/2014WR016194.

501 Cooper, R. J., Krueger, T., Hiscock, K. M., & Rawlins, B. G. (2015). High-temporal resolution fluvial

886
887
888
889
890
891
892
893
894
895
896
897
898
899
900
901
902
903
904
905
906
907
908
909
910
911
912
913
914
915
916
917
918
919
920
921
922
923
924
925
926
927
928
929
930
931
932
933
934
935
936
937
938
939
940
941
942
943
944

502 sediment source fingerprinting with uncertainty: A Bayesian approach. *Earth Surface*
503 *Processes and Landforms*, 40(1), 78–92. doi:10.1002/esp.3621

504 Cowie, S. M., Knippertz, P. & Marsham, J. H. 2013. Are vegetation-related roughness changes the
505 cause of the recent decrease in dust emission from the Sahel? *Geophysical Research Letters*,
506 40, 1868-1872.

507 Dahmardeh Behrooz, R., Esmaili-Sari, A., Bahramifar, N., and Kaskaoutis, D. G. (2017a). Analysis of
508 the TSP, PM10 concentrations and water-soluble ionic species in airborne samples over
509 Sistan, Iran during the summer dusty period. *Atmospheric Pollution Research*, 8; 403-417.
510 <http://dx.doi.org/10.1016/j.apr.2016.11.001>

511 Dahmardeh Behrooz, R., Esmaili-Sari, A., Bahramifar, N., and Kaskaoutis, D. G., Saeb, K., and Rajaei,
512 F. (2017b). Trace-element concentrations and water-soluble ions in size-segregated dust-
513 borne and soil samples in Sistan, southeast Iran. *Aeolian Research*, 25; 87-105.
514 <http://dx.doi.org/10.1016/j.aeolia.2017.04.001>

515 Del Rio-Salas, R., Ruiz, J., De la O-Villanueva, M., Valencia-Moreno, M., Moreno,-Rodriguez, V.,
516 Gomez-Alvarez, A., Grijalva, T., Mendivil, H., Paz-Moreno, F., and Meza-Figueroa, D. (2012).
517 Tracing geogenic and anthropogenic sources in urban dusts: Insights from lead isotopes.
518 *Atmospheric Environment*, 60; 202-210. <http://dx.doi.org/10.1016/j.atmosenv.2012.06.061>

519 Esmaeili, A. and Omrani, M. (2007). Efficiency analysis of fishery in Hamoon lake using DEA
520 approach. *J. Appl. Sci*, 7; 2856-2860.

521 Ge, Y., Abuduwaili, J., Ma, L., Wu, N., and Liu, D. (2016). Potential transport pathways of dust
522 emanating from the playa of Ebinur Lake, Xinjiang, in arid northwest China. *Atmospheric*
523 *Research*, 178-179; 196-206. <http://dx.doi.org/10.1016/j.atmosres.2016.04.002>

524 Gelaro, R., McCarty, W., Suárez, M. J., Todling, R., Molod, A., Takacs, L., Randles, C. A., Darmenov, A.,
525 Bosilovich, M. G. & Reichle, R. (2017) 'The modern-era retrospective analysis for research
526 and applications, version 2 (MERRA-2)'. *Journal of Climate*, 30 (14), pp. 5419-5454.

527 Gholami, H., Middleton, N., Nzari Samani, A., and Wasson, R. (2017a). Determining contribution of
528 sand dune potential sources using radionuclides, trace and major elements in central Iran.
529 *Arab J Geosci*, 10:163. doi. 10.1007/s12517-017-2917-0.

530 Gholami, H., Telfer, M. W., Blake, W. H., and Fathabadi, A. (2017) Aeolian sediment fingerprinting
531 using a Bayesian mixing model. *Earth Surf. Process. Landforms*, 42: 2365–2376. doi:
532 10.1002/esp.4189.

533 Gong, Y., Shen, Zh, Hong, Q., Liu, R., and Liao, Q. (2011). Parameter uncertainty analysis in watershed
534 total phosphorus modeling using the GLUE methodology. *Agriculture, Ecosystems and*
535 *Environment* 142; 246-255. doi:10.1016/j.agee.2011.05.015

945
946
947 536 Goossens, D. (2003). On-site and off-site effects of wind erosion. In: Warren A (ed) Wind erosion on
948 agricultural land in Europe. European Commission, Luxembourg, pp. 29–38
949 537
950 538 Goudie, A. S. and Middleton, N. J. (2006). Desert dust in the global system. Springer.
951
952 539 Grousset, F. E. and Biscaye, P. E. (2005). Tracing dust sources and transport patterns using Sr, Nd and
953 Pb isotopes. *Chemical Geology*, 222; 149-167. doi:10.1016/j.chemgeo.2005.05.006
954 540
955 541 Hamidi, M., Kavianpour, M. R., and Shao, Y. (2014). Numerical simulation of dust events in the
956 Middle East. *Aeolian Research*, 13; 59-70. <http://dx.doi.org/10.1016/j.aeolia.2014.02.002>
957 542
958 543 Hassan, A. E., Bekhit, H. M., and Chapman, J. B. (2008). Uncertainty assessment of a stochastic
959 groundwater flow model using GLUE analysis. *Journal of Hydrology*, 362; 89-109.
960 544
961 545 doi:10.1016/j.jhydrol.2008.08.017
962
963 546 Kaskaoutis, D.G., Rashki, A., Francois, P., Dumka, U.C., Houssos, E.E., and Legrand, M. (2015).
964 547 Meteorological regimes modulating dust outbreaks in southwest Asia: the role of pressure
965 anomaly and Inter-Tropical Convergence Zone on the 1–3 July 2014 case. *Aeolian Research*.
966 548 18, 83–97.
967 549
968
969 550 Kaskaoutis, D. G., Houssos, E. E., Rashki, A., Francois, P., Legrand, M., Goto, D., Bartzokas, A.,
970 551 Kambezidis, H. D. & Takemura, T. (2016) 'The Caspian Sea–Hindu Kush Index (CasHKI): a
972 552 regulatory factor for dust activity over southwest Asia'. *Global and Planetary Change*, 137
973 pp. 10-23.
974 553
975 554 Kaskaoutis, D. G., Rashki, A., Houssos, E. E., Legrand, M., Francois, P., Bartzokas, A., Kambezidis, H.
976 555 D., Dumka, U. C., Goto, D. & Takemura, T. (2017) 'Assessment of changes in atmospheric
978 556 dynamics and dust activity over southwest Asia using the Caspian Sea–Hindu Kush Index'.
979 557 *International Journal of Climatology*, 37 (S1), pp. 1013-1034.
980 558
981 558 Kaskaoutis, D.G., Rashki, A., Houssos, E. E., Goto, D., and Nastos, P. T. (2014). Extremely high aerosol
982 559 loading over Arabian Sea during June 2008: the specific role of the atmospheric dynamics
983 560 and Sistan dust storms. *Atmospheric Environment*. Doi: 10.1016/j.atmosenv.2014.05.012
984 561
985 561 King, J., Etyemezian, V., Sweeney, M., Buck, B. J. & Nikolich, G. 2011. Dust emission variability at the
986 562 Salton Sea, California, USA. *Aeolian Research*, 3, 67-79.
987 563
988 563 Krom, M.D., Cliff, R. A., Eijssink, L. M., Herut, B., and Chester, R. (1999). The characterisation of
989 564 Saharan dusts and Nile particulate matter in surface sediments from the Levantine basin
990 565 using Sr isotopes. *Marine Geology*, 155; 319-330.
991 566
992 566 Li, J., Okin, G. S., Alvarez, L. & Epstein, H. 2007. Quantitative effects of vegetation cover on wind
993 567 erosion and soil nutrient loss in a desert grassland of southern New Mexico, USA.
994 568 *Biogeochemistry*, 85, 317-332.
995 569
996 569 Liu, B., Niu, Q., Qu, J., and Zu, R. (2016). Quantifying the provenance of aeolian sediments using
997
998
999
1000
1001
1002
1003

1004
1005
1006 570 multiple composite fingerprints. *Aeolian Research*, 22, 117-122.
1007
1008 571 dx.doi.org/10.1016/j.aeolia.2016.08.002
1009
1010 572 Long, X., Li., N., Tie, X., Cao, J., Zhao, Sh., Huang, R., Zhao, M., Li, G., and Feng, Tian. (2016). Urban
1011 573 dust in the Guanzhong Basin of China, part I: A regional distribution of dust sources retrieved
1012
1013 574 using satellite data. *Science of the Total Environment*, 541; 1603-1613.
1014 575 <http://dx.doi.org/10.1016/j.scitotenv.2015.10.063>
1015
1016 576 Mahowald, N. M., Bryant, R. G., del Corral., J., and Steinberger, L. (2002). Ephemeral lakes and desert
1017 577 dust sources. *Geophys Res Lett*, 30:1074. <http://dx.doi.org/10.1029/2002GL016041>
1018
1019 578 Manjoro, M., Rowntree, K., Kakembo, V., Foster, I., and Collins, A. L. (2017). Use of sediment source
1020 579 fingerprinting to assess the role of subsurface erosion in the supply of fine sediment in a
1021
1022 580 degraded catchment in the Eastern Cape, South Africa. *Journal of Environmental*
1023 581 *Management*, 194, 27-41. dx.doi.org/10.1016/j.jenvman.2016.07.019
1024
1025 582 Massoudieh, A., Gellis, A., Banks, W. S., & Wiczorek, M. E. (2013). Suspended sediment source
1026 583 apportionment in Chesapeake Bay watershed using Bayesian chemical mass balance
1027
1028 584 receptor modeling. *Hydrological Processes*, 27(24), 3363-3374. doi:10.1002/hyp.9429
1029
1030 585 Middleton NJ. (1986). Dust storms in the Middle East. *J Arid Environ*,10:83-96
1031 586 Moghaddamia, A., Ghafari, M.B., Piri, J., Amin, S., and Han, D. (2009). Evaporation
1032 587 estimation using artificial neural networks and adaptive neuro-fuzzy inference
1033
1034 588 system techniques. *Adv. Water Resour.* 32, 88-97
1035
1036 589 Montovan, P. and Todini, E. (2006). Hydrological forecasting uncertainty
1037 590 assessment: Incoherence of the GLUE methodology. *Journal of Hydrology*, 330; 368-381.
1038
1039 591 doi:10.1016/j.jhydrol.2006.04.046
1040
1041 592 Motha, J.A., Wallbrink, P.J., Hairsine, P.B., and Grayson, R.B. (2003). Determining the sources of
1042 593 suspended sediment in a forested catchment in southeastern Australia. *Water Resources*, 39
1043
1044 594 (3), 1056. doi:10.1029/2001wr000794.
1045 595 Nabavi, S. O., Haimberger, L., and Samimi, C. (2016). Climatology of dust distribution over West Asia
1046 596 from homogenized remote sensing data. *Aeolian Research*, 21; 93-107.
1047
1048 597 <http://dx.doi.org/10.1016/j.aeolia.2016.04.002>
1049
1050 598 Nabavi, S. O., Haimberger, L., and Samimi, C. (2017). Sensitivity of WRF-chem predictions to dust
1051 599 source function specification in West Asia. *Aeolian Research*, 24; 115-131.
1052
1053 600 <http://dx.doi.org/10.1016/j.aeolia.2016.12.005>
1054
1055 601 Nakano, T., Yokoo, Y., Nishikawa, M., and Koyanagi, H. (2004). Regional Sr-Ndisotopic ratios of soil
1056 602 minerals in northern China as Asian dust fingerprints. *Atmospheric Environment*, 38; 3061-
1057
1058 603 3067. doi:10.1016/j.atmosenv.2004.02.016
1059
1060
1061
1062

1063
1064
1065 604 Okin, G. S., Murray, B. & Schlesinger, W. H. 2001. Degradation of sandy arid shrubland
1066 environments: observations, process modelling, and management implications. *Journal of*
1067 605 *Arid Environments*, 47, 123-144.
1068 606
1070 607 Rashki, A., Arjmand, A., and Kaskaoutis, D. G. (2017). Assessment of dust activity and dust-plume
1071 pathways over Jazmurian Basin, southeast Iran. *Aeolian Research*, 24; 145-160.
1072 608 <http://dx.doi.org/10.1016/j.aeolia.2017.01.002>
1073 609
1074 610 Rashki, A., Eriksson, P. G., Rautenbach, C. J. D., Kaskaoutis, D. G., Grote, W., and Dykstra, J. (2013a).
1075 Assessment of chemical and mineralogical characteristics of airborne dust in the Sistan
1076 611 region, Iran. *Chemosphere*, 90; 227-236.
1077 612 <http://dx.doi.org/10.1016/j.chemosphere.2012.06.059>
1078 613
1081 614 Rashki, A., Kaskaoutis, D. G., Francois, P., Kosmopoulos, P. G., and Legrand, M. (2015). Dust-storm
1082 615 dynamics over Sistan region, Iran: Seasonality, transport characteristics and affected areas.
1083 *Aeolian Research*, 16; 35-48.
1084 616
1085 617 Rashki, A., Kaskaoutis, D. G., Goudie, A. S., and Kahn, R. A. (2013b). Dryness of ephemeral lakes and
1086 618 consequences for dust activity: The case of the Hamoun drainage basin, southeastern Iran.
1087 *Science of the Total Environment*, 463-464; 552-564.
1088 619 <http://dx.doi.org/10.1016/j.scitotenv.2013.06.045>
1089 620
1090 621 Rashki, A., Kaskaoutis, D. G., Rautenbach, C. J. D., Eriksson, P. G. (2012a). Changes of Permanent Lake
1091 Surfaces, and Their Consequences for Dust Aerosols and Air Quality: The Hamoun Lakes of
1092 622 the Sistan Area, Iran. In: Hayder Abdul-Razzak (Eds.), *Atmospheric Aerosols - Regional*
1093 623 *Characteristics*. DOI: 10.5772/48776
1094 624
1095 625 Rashki, A., Kaskaoutis, D. G., Rautenbach, C. J. D., Eriksson, P. G., Qiang, M., and Gupta, P. (2012b).
1096 626 Dust storms and their horizontal dust loading in the Sistan region, Iran. *Aeolian Research*, 5;
1097 627 51-62. doi:10.1016/j.aeolia.2011.12.001
1098 628
1099 629 Reheis, M. C., Budahn, J. R. & Lamothe, P. J. 2002. Geochemical evidence for diversity of dust
1100 630 sources in the southwestern United States. *Geochimica Et Cosmochimica Acta*, 66, 1569-
1101 631 1587.
1102 632
1103 633 Reheis, M., Budahn, J. R., Lamothe, P. J., and Reynolds, R. L. (2009). Compositions of modern dust
1104 634 and surface sediments in the Desert Southwest United States. *J Geophys Res*, 114: F01028.
1105 635 <http://dx.doi.org/10.1029/2008JF001009>
1106 636
1107 637 Reynolds, R.L., Yount, J.C., Reheis, M., Goldstein, H, Chavez Jr, P., Fulton, R, Whitney, J., Fuller, C.,
1108 638 Forester, R.M. (2007). Dust emission from wet and dry playas in the Mojave Desert, USA.
1109 639 *Earth Surface Processes and Landforms*, 3; 1811-1827. <https://doi.org/10.1002/esp.1515>
1110 640
1111
1112
1113
1114
1115
1116
1117
1118
1119
1120
1121

1122
1123
1124 637 Rezazadeh, M., Irannejad, P., and Shao, Y. (2013). Climatology of the Middle East dust events.
1125
1126 638 Aeolian Research, 10; 103-109. <http://dx.doi.org/10.1016/j.aeolia.2013.04.001>
1127
1128 639 Schepanski, K., Tegen, I., and Macke, A. (2012). Comparison of satellite based observations of
1129 640 Saharan dust source areas. *Remote Sensing of Environment*, 123; 90-97.
1130 641 [doi:10.1016/j.rse.2012.03.019](https://doi.org/10.1016/j.rse.2012.03.019)
1131
1132 642 Sepehr, A., Hassanli, A. M., Ekhtesasi, M. R. & Jamali, J. B. 2007. Quantitative assessment of
1133 643 desertification in south of Iran using MEDALUS method. *Environmental Monitoring and*
1134 644 *Assessment*, 134, 243.
1135
1136 645 Shen, Z., Caquineau, S., Cao, J., Zhang, X., Han, Y., Gaudichet, A., and Gomes, L. (2009). Mineralogical
1137 646 characteristics of soil dust from source regions in northern China. *Particology*, 7; 507-512.
1138 647 [doi:10.1016/j.partic.2009.10.001](https://doi.org/10.1016/j.partic.2009.10.001)
1139
1140 648 Sherriff, S. C., Franks, S. W., Rowan, J. S., Fenton, O., & Ó'hUallacháin, D. (2015). Uncertainty-based
1141 649 assessment of tracer selection, tracer non-conservativeness and multiple solutions in
1142 650 sediment fingerprinting using synthetic and field data. *Journal of Soils and Sediments*,
1143 651 15(10), 2101–2116. [doi:10.1007/s11368-015-1123-5](https://doi.org/10.1007/s11368-015-1123-5)
1144
1145 652 Smith, H.G., and Blake, W.H. (2014). Sediment fingerprinting in agricultural catchments: A critical re-
1146 653 examination of source discrimination and data corrections. *Geomorphology*, 204, 177–191.
1147 654 [doi:10.1016/j.geomorph.2013.08.003](https://doi.org/10.1016/j.geomorph.2013.08.003).
1148
1149 655 Stein, A. F., Draxler, R. R., Rolph, G. D., Stunder, B. J. B., Cohen, M. D. & Ngan, F. (2015) 'NOAA's
1150 656 HYSPLIT atmospheric transport and dispersion modeling system'. *Bulletin of the American*
1151 657 *Meteorological Society*, 96 (12), pp. 2059-2077.
1152
1153 658 Stewart, H. A., Massoudieh, A., & Gellis, A. (2015). Sediment source apportionment in Laurel Hill
1154 659 Creek, PA, using Bayesian chemical mass balance and isotope fingerprinting. *Hydrological*
1155 660 *Processes*, 29(11), 2545–2560. [doi:10.1002/hyp.10364](https://doi.org/10.1002/hyp.10364)
1156
1157 661 Stone, M., Collins, A.L., Silins, U., Emelko, M.B., and Zhang, Y.S. (2014). The use of composite
1158 662 fingerprints to quantify sediment sources in a wildfire impacted landscape, Alberta, Canada.
1159 663 *Science of the Total Environment*, 473-474, 642–650. [doi:10.1016/j.scitotenv.2013.12.052](https://doi.org/10.1016/j.scitotenv.2013.12.052).
1160
1161 664 Sweeney, M. R., McDonald, E. V. & Etyemezian, V. 2011. Quantifying dust emissions from desert
1162 665 landforms, eastern Mojave Desert, USA. *Geomorphology*, 135, 21-34.
1163
1164 666 Sweeney, M. R., Zlotnik, V. A., Joeckel, R. M. & Stout, J. E. 2016. Geomorphic and hydrologic controls
1165 667 of dust emissions during drought from Yellow Lake playa, West Texas, USA. *Journal of Arid*
1166 668 *Environments*, 133, 37-46.

1181
1182
1183 669 Torres, O. O. (2006) 'OMI/Aura Near UV Aerosol Optical Depth and Single Scattering Albedo. 1-orbit
1184 L2 Swath 13x24 km V003'. [in Greenbelt, MD, USA: Goddard Earth Sciences Data and
1185 670 Information Services Center (GES DISC). (Accessed: 6/11/18)
1186 671
1187
1188 672 United Nations Environment Programme (UNEP) (2006). History of environmental change in
1189 673 the Sistan basin based on satellite image analysis: 1976–2005; 200660.
1190
1191 674 Vale, S. S., Fuller, I. C., Procter, J. N., Basher, L. R., and Smith, I. E. (2016). Characterization and
1192 675 quantification of suspended sediment sources to the Manawatu River, New Zealand. *Science*
1193 676 of the Total Environment, 543, 171–186. doi:10.1016/j.scitotenv.2015.11.003
1194
1195 677 Viola, F., Noto, L. V., Cannarozzo, G., and Loggia, G. L. (2009). Daily streamflow prediction with
1196 678 uncertainty in ephemeral catchments using the GLUE methodology. *Physics and Chemistry of*
1197 679 *the Earth* 34; 701-706.
1200 680 Voli, M.T., Wegmann, K.W., Bohnenstiehl, D.R., Leithold, E., Osburn, C.L., and Polyakov, V. (2013).
1201 681 Fingerprinting the sources of suspended sediment delivery to a large municipal drinking
1202 682 water reservoir: Falls Lake, Neuse River, North Carolina, USA. *Journal of Soils and Sediments*,
1203 683 13 (10), 1692–1707. doi:10.1007/s11368-013-0758-3.
1204
1205 684 Walling, D.E. (2005). Tracing suspended sediment sources in catchments and river systems. *Science*
1206 685 of the Total Environment, 344 (1-3), 159–184. doi:10.1016/j.scitotenv.2005.02.011.
1207
1208 686 Walling, D.E. (2013). The evolution of sediment source fingerprinting investigations in fluvial
1209 687 systems. *Journal of Soils and Sediments*, 13 (10), 1658–1675. doi:10.1007/s11368-013-0767-
1210 688 2.
1211
1212 689 Wang, Y. Q., Zhang, X. Y., Arimoto, R., Cao, J. J., and Shen, Z. X. (2005). Characteristics of carbonate
1213 690 content and carbon and oxygen isotopic composition of northern China soil and dust aerosol
1214 691 and its application to tracing dust sources. *Atmospheric Environment*, 39; 2631-2642.
1215 692 doi:10.1016/j.atmosenv.2005.01.015
1216
1217 693 Washington, R., Todd, M., Middleton, N.J., and Goudie, A. S. (2003). Dust storm source areas
1218 694 determined by the Total Ozone Monitoring Spectrometer and surface observations. *Ann*
1219 695 *Assoc Am Geogr*, 93: 297–313.
1220
1221 696 Wei, T., Dong, Z., Kang, Sh., Qin, X., and Guo, Zh. (2017). Geochemical evidence for sources of
1222 697 surface dust deposited on the Laohugou glacier, Qilian Mountains. *Applied Geochemistry*;
1223 698 79; 1-8. http://dx.doi.org/10.1016/j.apgeochem.2017.01.024
1224
1225 699 Whitney, J. W., Breit, G. N., Buckingham, S. E., Reynolds, R. L., Bogle, R. C., Luo, L., Goldstein, H. L. &
1226 700 Vogel, J. M. 2015. Aeolian responses to climate variability during the past century on
1227 701 Mesquite Lake Playa, Mojave Desert. *Geomorphology*, 230, 13-25.
1228
1229
1230
1231
1232
1233
1234
1235
1236
1237
1238
1239

1240
1241
1242
1243
1244
1245
1246
1247
1248
1249
1250
1251
1252
1253
1254
1255
1256
1257
1258
1259
1260
1261
1262
1263
1264
1265
1266
1267
1268
1269
1270
1271
1272
1273
1274
1275
1276
1277
1278
1279
1280
1281
1282
1283
1284
1285
1286
1287
1288
1289
1290
1291
1292
1293
1294
1295
1296
1297
1298

702 Wiggs, G. & Holmes, P. 2011. Dynamic controls on wind erosion and dust generation on west-central
703 Free State agricultural land, South Africa. *Earth Surface Processes and Landforms*, 36, 827-
704 838.

705 World Health Organisation (2016). WHO Global Urban Ambient Air Pollution Database. URL:
706 http://www.who.int/phe/health_topics/outdoorair/databases/cities/en/ (Accessed
707 23/06/2018).

708 Worster, D. 2004. *Dust bowl: the southern plains in the 1930s*, Oxford University Press.

709 Xu, H. (2006). Modification of normalised difference water index (NDWI) to enhance open water
710 features in remotely sensed imagery. *International Journal of Remote Sensing*, 27; 3025-
711 3033. doi: 10.1080/01431160600589179

712 Yan, Y., Sun, Y., Ma, L., and Long, X. (2015). A multidisciplinary approach to trace Asian dust storms
713 from source to sink. *Atmospheric Environment*, 105; 43-52.
714 <http://dx.doi.org/10.1016/j.atmosenv.2015.01.039>

715 Yang, J., Li, G., Rao, W., and Ji, J. (2009). Isotopic evidences for provenance of East Asian Dust.
716 *Atmospheric Environment*, 43; 4481-4490. doi:10.1016/j.atmosenv.2009.06.035

717 Zhang, D., Zhou, Z. H., Zhang, B., Du, S. H. & Liu, G. C. 2012. The effects of agricultural management
718 on selected soil properties of the arable soils in Tibet, China. *Catena*, 93, 1-8. Prospero, J. M.,
719 Ginoux, P., Torres, O., Nicholson, S. E., and Gill, T. E. (2002). Environmental characterization
720 of global sources of atmospheric soil dust identified with the Nimbus 7 total ozone mapping
721 spectrometer absorbing aerosol product. *Rev Geophys*, 40: 2-31

722 Zhou, H., Chang, W., and Zhang, L. (2016a). Sediment sources in a small agricultural catchment: A
723 composite fingerprinting approach based on the selection of potential sources.
724 *Geomorphology*, 266, 11-19. dx.doi.org/10.1016/j.geomorph.2016.05.007

725 Zhou, R., Li, Y., Lu, D., Liu, H., and Zhou, H. (2016b). An optimization based sampling approach for
726 multiple metrics uncertainty analysis using generalized likelihood uncertainty estimation.
727 *Journal of Hydrology*, 540; 274-286. <http://dx.doi.org/10.1016/j.jhydrol.2016.06.030>.

1299
1300
1301
1302
1303
1304
1305
1306
1307
1308
1309
1310
1311
1312
1313
1314
1315
1316
1317
1318
1319
1320
1321
1322
1323
1324
1325
1326
1327
1328
1329
1330
1331
1332
1333
1334
1335
1336
1337
1338
1339
1340
1341
1342
1343
1344
1345
1346
1347
1348
1349
1350
1351
1352
1353
1354
1355
1356
1357

729 **Figure Captions**

730 Figure 1: Sampling sites in the Sistan region: the dry-bed of Hamoun Puzak (HP); the dry-bed of
731 Hamoun Saberi (HS); uncultivated range Land (RL); and cultivated Land (CL). Inset shows the hourly
732 averaged wind regime for the period June-October 2014 (data source: National Climatic Data Centre,
733 Climate Data Online).

734
735 Figure 2. Typical examples of the land surfaces we sampled. a) Hamoun Puzak dry lake-bed, b) Hamoun
736 Saberi dry lake-bed, c) close-up view of cultivated agricultural land surface during the summer months,
737 and d) sparsely vegetated, uncultivated rangeland.

738
739 Figure 3. Scatterplot constructed from the first and second functions derived from a stepwise DFA for
740 the source groups including the four land (i.e. Hamoun Puzak (HP), Hamoun Saberi (HS), cultivated
741 land (CL) and uncultivated rangeland (RL)). Five optimum fingerprints (Fe, Sr, Mn, Cr and Pb) were
742 used to construct the scatterplot and 87% of the source samples are discriminated correctly.

743
744 Figure 4. GLUE results for dust source contributions yielding 95% confidence limits (with percentiles
745 2.5, 25, 50, 75 and 97.5). A) Hamoun Puzak; B) Hamoun Saberi; C) uncultivated rangeland; and d)
746 cultivated land.

747
748 Figure 5. Summary of all source contributions plotted as a probability density function.

749
750 Figure 6. Decadal scale changes in the Hamoun Lakes. Following lake-full conditions in the late 1990s
751 (a), a sustained decade of drought resulted in the exposure of large areas of dry lake-beds (b and c)
752 and therefore potential dust sources. Since then, levels have varied and often changed rapidly (d, e
753 and f). All images are infrared/red/green composites based on Landsat 5 and 8 imagery, using Bands
754 4/3/2 and 5/4/3 respectively. Vegetation is shown as red tones.

1358
1359
1360 755
1361
1362 756 Figure 7. Changes in the surface extent of the Hamoun Lakes between June and September, 2014.
1363
1364 757 Note the rapid desiccation during June and July, and resultant exposure of new surfaces for potential
1365
1366 758 deflation.
1367
1368 759
1369
1370 760 Figure 8. The relative contributions of a) and b) Hamoun Puzak and c) and d) Hamoun Saberi, plotted
1371
1372 761 alongside a) and c) the surface area of the lakes (expressed as a percentage of the 1996 lake-full
1373
1374 762 conditions) and b) and d) the absolute surface area of the lakes. There is no consistent trend in dust
1375
1376 763 provenance, despite the changing area of the potential sources. Solid lines indicate the median
1377
1378 764 estimate, dashed lines the first and third quartiles and dotted lines the 2.5% and 97.5% bounds.
1379
1380 765
1381
1382 766 Figure 9. The dominant dust contribution from Hamoun Puzak (top; key for lines as in Figure 8), shown
1383
1384 767 alongside the magnitude of dust collected at Zabol (bars), and the mean daily wind speed (thin solid
1385
1386 768 line) and variance in mean wind direction (bold dashed line).
1387
1388 769
1389
1390 770 Figure 10. The dust plume affecting Zabol from the north is evident in remotely-sensed data from July
1391
1392 771 2014. a) The MODIS Corrected Reflectance Imagery (Red:Green:Blue) 500 m colour composite clearly
1393
1394 772 shows the plume as a brown streak emanating from near the Hamoun Lakes and tracking
1395
1396 773 southeastwards. b) The MERRA-2 PM2.5 monthly dust deposition reanalysis data also highlight the
1397
1398 774 plume to the southeast of the Hamoun Lakes, as does c) the AURA OMI UV-derived Aerosol Index for
1399
1400 775 July 4th, 2014.
1401
1402 776
1403
1404 777 Figure 11. Hysplit back trajectories for three dust events during the observation period in summer
1405
1406 778 2014 (4th July – white triangles, 14th August – grey circles, 4th September – black squares). a) Regional
1407
1408 779 tracks over the 24 hours preceding the observations demonstrate the long-distance transport of dust,
1409
1410 780 with a likely source in the Karakum Desert of Turkmenistan. b) Local dust transport pathways over the
1411
1412
1413
1414
1415
1416

1417
1418
1419 781 Hamoun Lakes to Zabol demonstrate different pathways during the summer dust season, with early
1420
1421 782 summer pathways (white triangles and grey circles) routing over the still-inundated Hamoun Saberi,
1422
1423 783 and the September trajectory (black squares) coming over the desiccated Hamoun Baringak and
1424
1425 784 Puzak.
1426
1427
1428 785
1429
1430
1431
1432
1433
1434
1435
1436
1437
1438
1439
1440
1441
1442
1443
1444
1445
1446
1447
1448
1449
1450
1451
1452
1453
1454
1455
1456
1457
1458
1459
1460
1461
1462
1463
1464
1465
1466
1467
1468
1469
1470
1471
1472
1473
1474
1475

1476
1477
1478
1479
1480
1481
1482
1483
1484
1485
1486
1487
1488
1489
1490
1491
1492
1493
1494
1495
1496
1497
1498
1499
1500
1501
1502
1503
1504
1505
1506
1507
1508
1509
1510
1511
1512
1513
1514
1515
1516
1517
1518
1519
1520
1521
1522
1523
1524
1525
1526
1527
1528
1529
1530
1531
1532
1533
1534

786 *Table 1: Summary characteristics of dust samples collected in Zabol during 21 June to 4 October,*
787 *2014.*

788

dust sample no	Sampling date	W V* (m/s)	dust mass (ug/m ³)	dust sample no	Sampling date	W V* (m/s)	dust mass (ug/m ³)
1	23 June 2014	7.1	270.2	30	24 August 2014	6.5	300.15
2	25 June 2014	8.6	1180.5	31	25 August 2014	9	695.65
3	26 June 2014	6.3	380	32	26 August 2014	10.4	1100.15
4	29 June 2014	8.1	500.6	33	27 August 2014**	9.8	1052
5	30 June 2014	9	458	34	27 August 2014***	9.8	922.39
6	4 July 2014	9.5	7800	35	28 August 2014	8	606.29
7	5 July 2014	8.9	570.2	36	29 August 2014	7.4	271.3
8	11 July 2014	10.3	724	37	3 Sep 2014	10	3594.92
9	12 July 2014	10.5	1700.7	38	4 Sep 2014	11.4	3594.92
10	13 July 2014	10.5	831	39	5 Sep 2014	8.1	339.56
11	14 July 2014	8.9	370.3	40	6 Sep 2014	8.5	1243.88
12	18 July 2014	11.3	740.2	41	8 Sep 2014	6.1	186.21
13	19 July 2014	8.3	1800	42	10 Sep 2014	9.1	3188.85
14	21 July 2014	4.8	320.8	43	13 Sep 2014	7.4	296.8
15	3 August 2014	12.3	715.3	44	16 Sep 2014	4.6	213.77
16	4 August 2014	10	1600	45	17 Sep 2014	4.3	192.4
17	5 August 2014	5.1	216	46	19 Sep 2014	10.1	10785.5
18	6 August 2014	6.6	246.4	47	20 Sep 2014	8.5	1013.43
19	7 August 2014	10	1500	48	21 Sep 2014	4.9	111.76
20	8 August 2014	10	1803	49	22 Sep 2014	2.8	179.61
21	9 August 2014	10	480.04	50	24 Sep 2014	3.4	155.98
22	10 August 2014	8	560.04	51	26 Sep 2014	2.3	165.52
23	11 August 2014	9.1	4500	52	27 Sep 2014	5.5	274.83
24	12 August 2014	8.3	720	53	29 Sep 2014	4	90.31
25	13 August 2014	8.3	1480	54	30 Sep 2014	7.1	814.46
26	14 August 2014	11.5	9004.58	55	1 Oct 2014	5.1	413.15
27	16 August 2014	10.9	3529.4	56	2 Oct 2014	5.3	331.67
28	18 August 2014	5.1	126.74	57	3 Oct 2014	7.5	597.6
29	21 August 2014	8.3	498.5				

* W V indicates Wind Velocity; ** Sample collected on the day; *** Sample collected on the night.

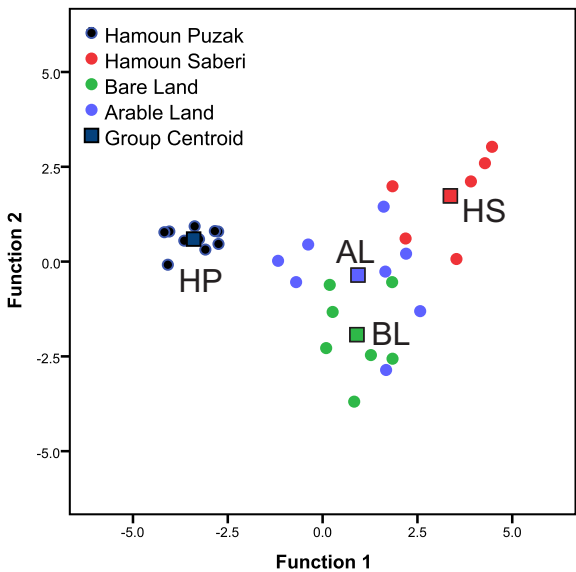
789
790
791
792

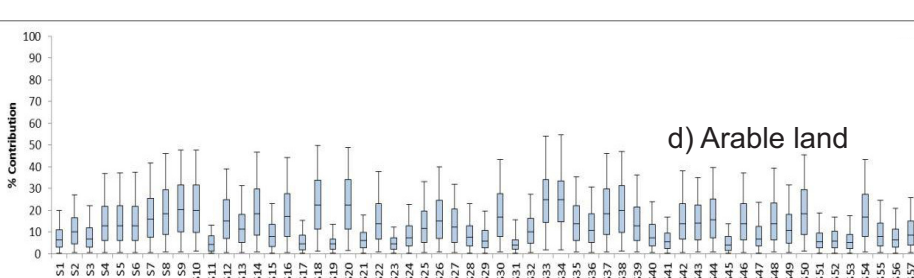
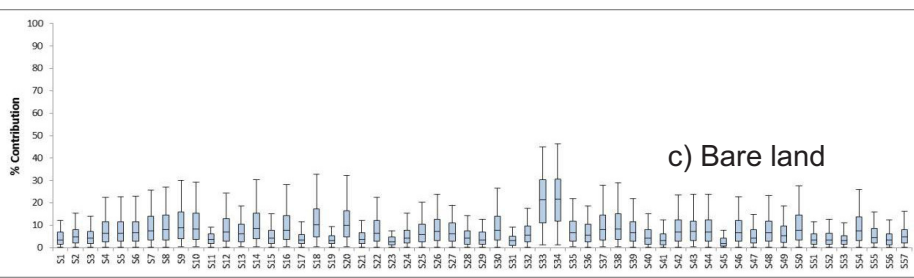
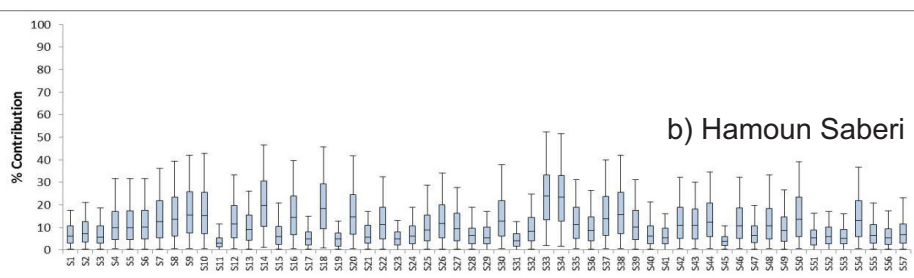
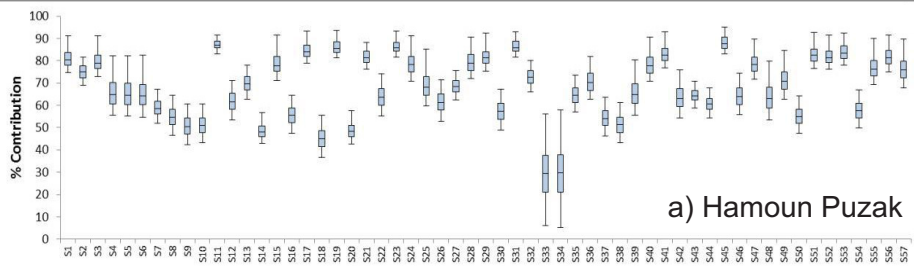
1535
1536
1537
1538
1539
1540
1541
1542
1543
1544
1545
1546
1547
1548
1549
1550
1551
1552
1553
1554
1555
1556
1557
1558
1559
1560
1561
1562
1563
1564
1565
1566
1567
1568
1569
1570
1571
1572
1573
1574
1575
1576
1577
1578
1579
1580
1581
1582
1583
1584
1585
1586
1587
1588
1589
1590
1591
1592
1593

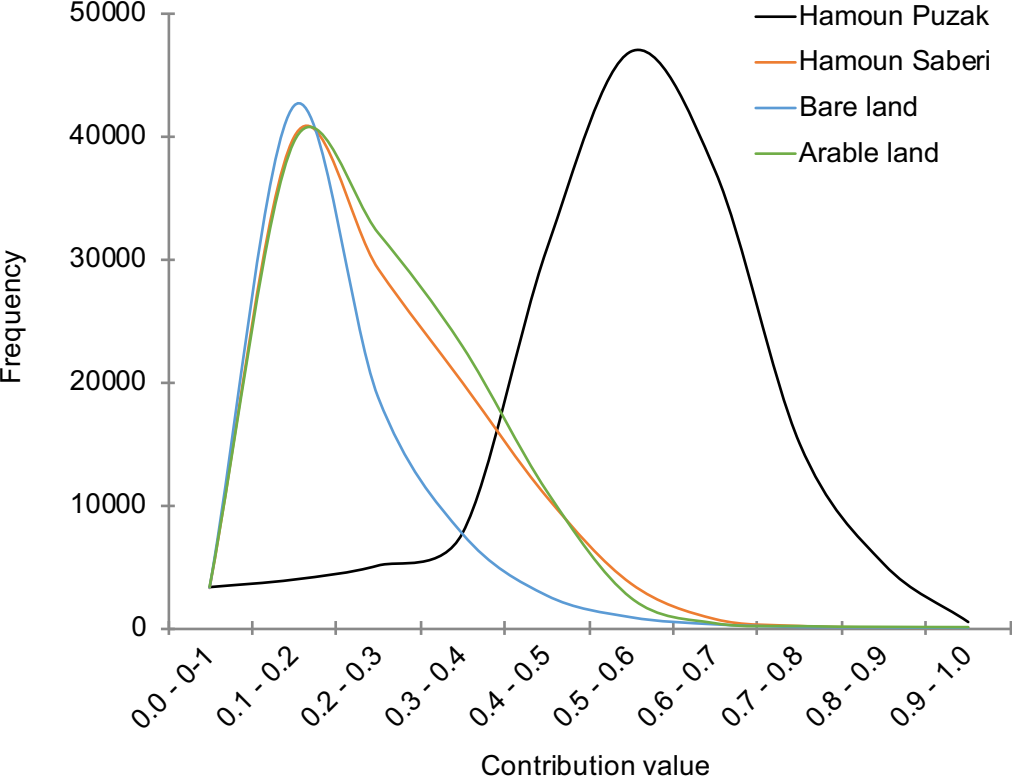
793 *Table 2: Results of a two-stage statistical process for selecting optimum composite fingerprints for*
794 *distinguishing sources of dust.*

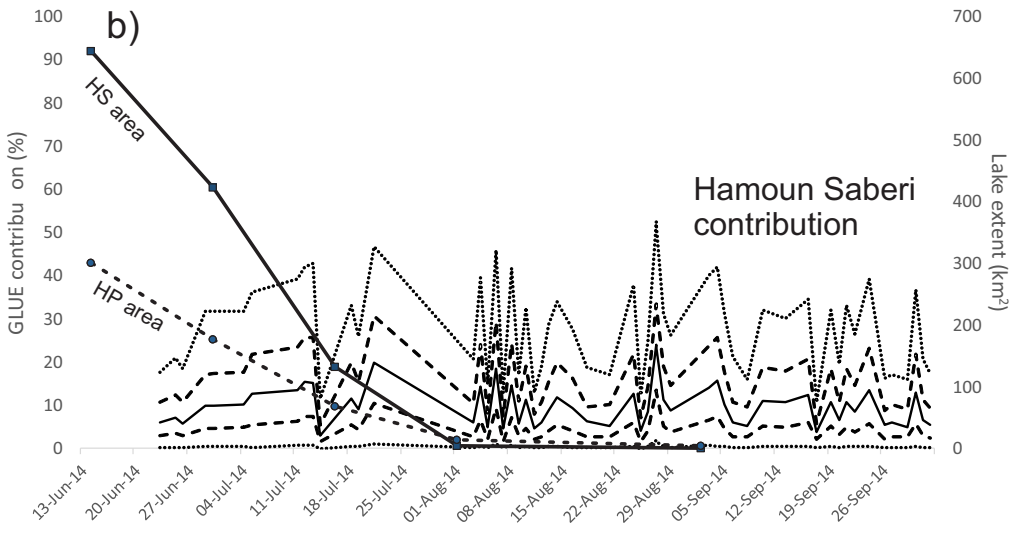
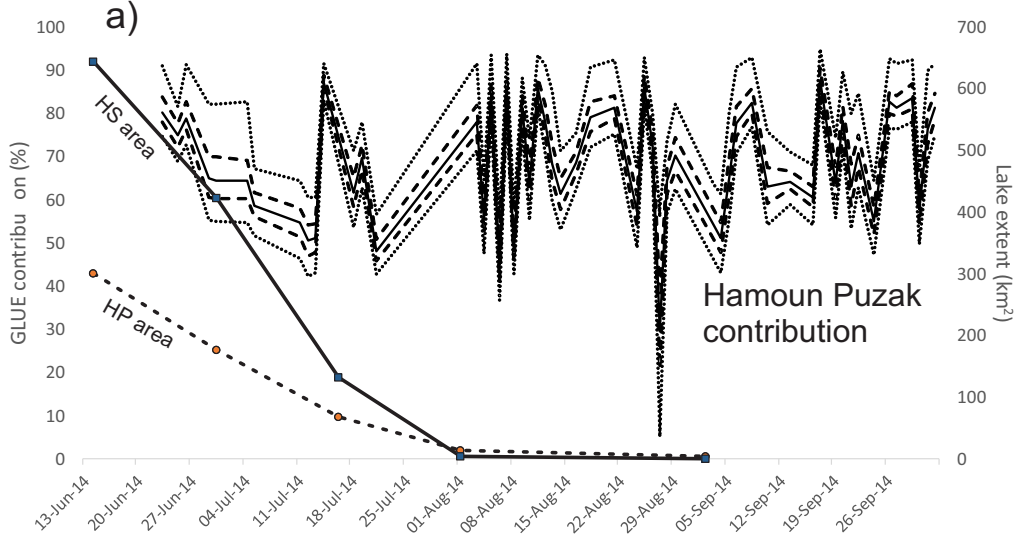
Kruskal-Wallis H test			Stepwise DFA		
Fingerprint property	Chi-Square	P-value	Step	Entered fingerprint	Wilk's lambda
Trace elements			1	Fe	0.356
Au	6.79	0.079	2	Sr	0.188
Pt	1.58	0.664	3	Mn	0.081
Mg	20.83	0.000**	4	Cr	0.053
Al	1.48	0.686	5	Pb	0.033
Sr	20.6	0.000**	*Statistically significant at P<0.05 ** Statistically significant at P<0.01		
Li	22	0.000**			
Fe	20.9	0.000**			
Cr	19.5	0.000**			
Cu	19.5	0.000**			
Zn	5.16	0.16			
As	9.9	0.019*			
Ni	20.75	0.000**			
Pb	9.58	0.022*			
Mn	20.24	0.000**			
Co	18.73	0.000**			
Sn	12.9	0.005**			
Ions					
Na ⁺	7.24	0.065			
NH ₄ ⁺	2.6	0.456			
K ⁺	4	0.254			
Cl ⁻	0.4	0.941			
NO ₂ ⁻	3.3	0.358			
NO ₃ ⁻	7.01	0.072			
Mg ²⁺	1.38	0.709			
Ca ²⁺	14.5	0.002**			

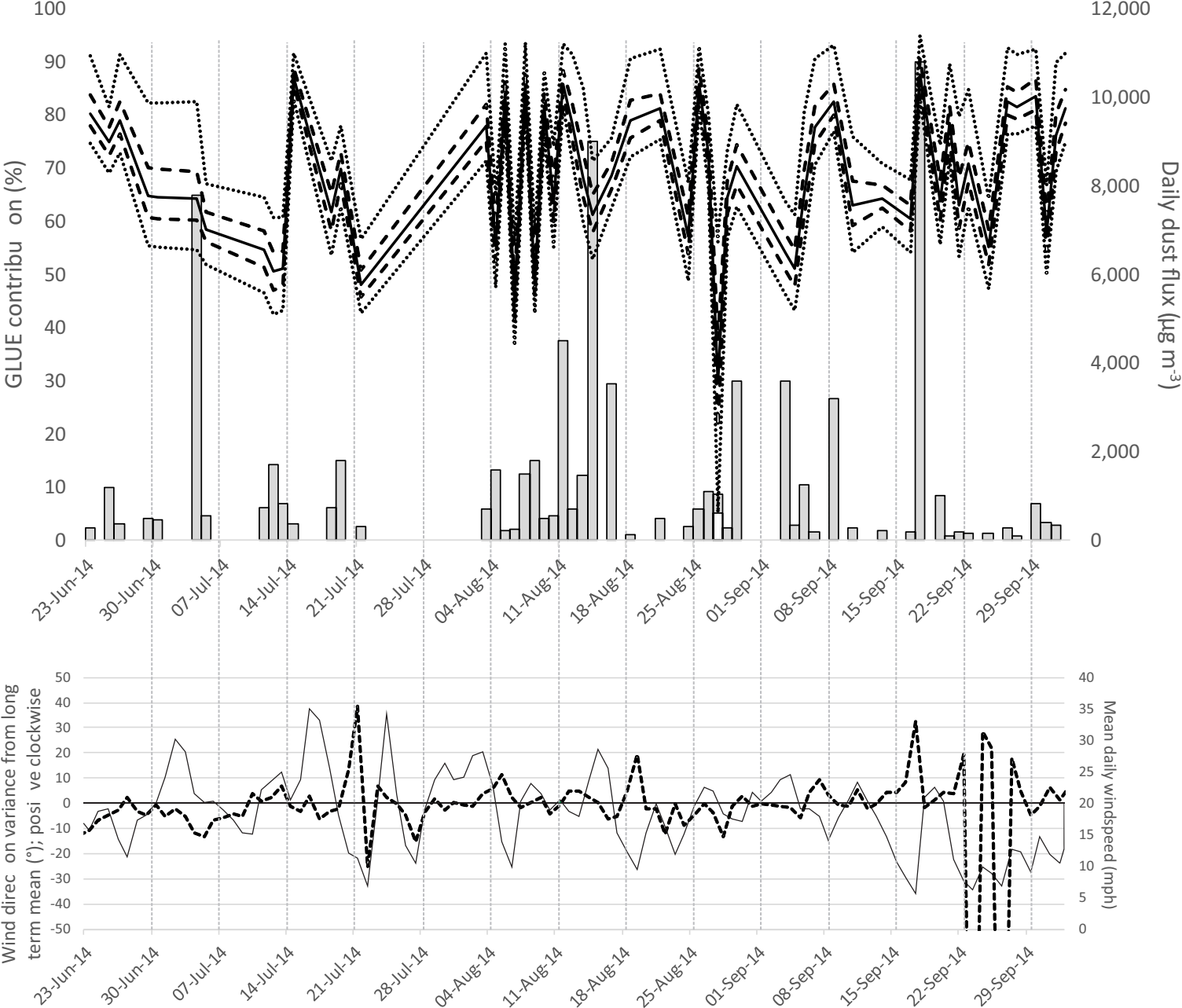
1594
1595
1596 795
1597
1598
1599
1600
1601
1602
1603
1604
1605
1606
1607
1608
1609
1610
1611
1612
1613
1614
1615
1616
1617
1618
1619
1620
1621
1622
1623
1624
1625
1626
1627
1628
1629
1630
1631
1632
1633
1634
1635
1636
1637
1638
1639
1640
1641
1642
1643
1644
1645
1646
1647
1648
1649
1650
1651
1652











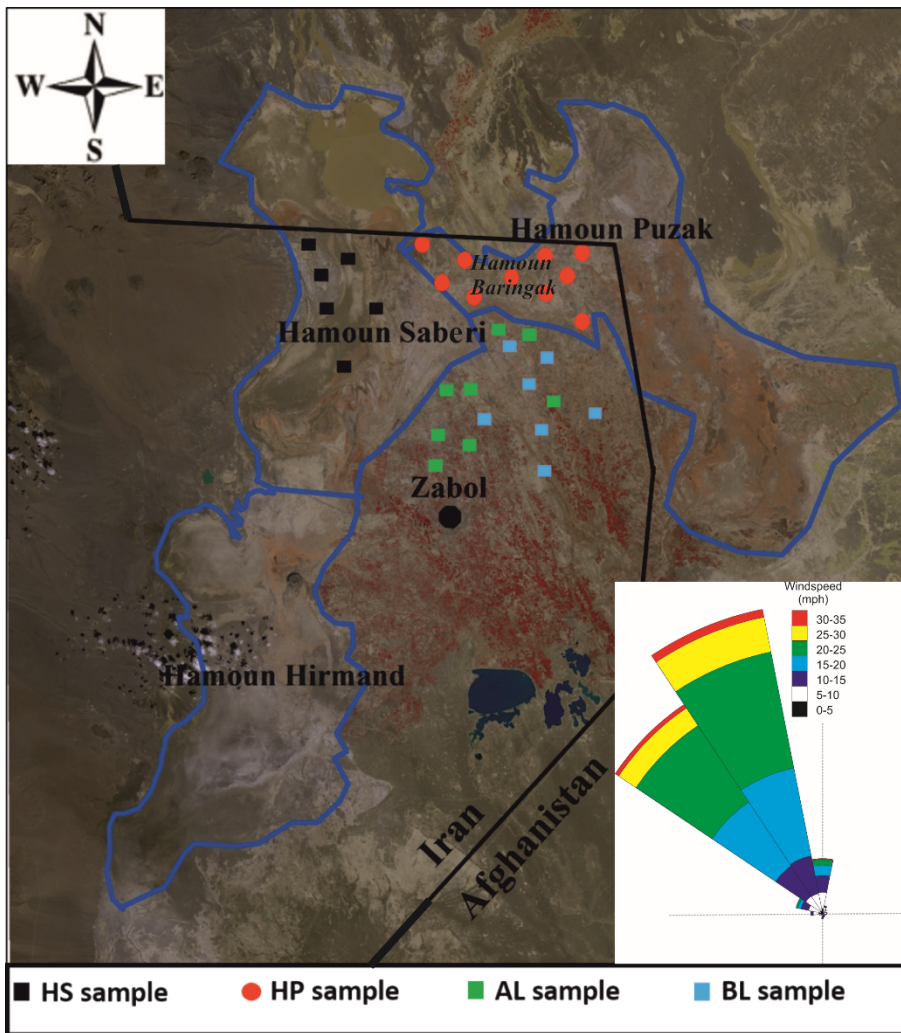


Figure 1

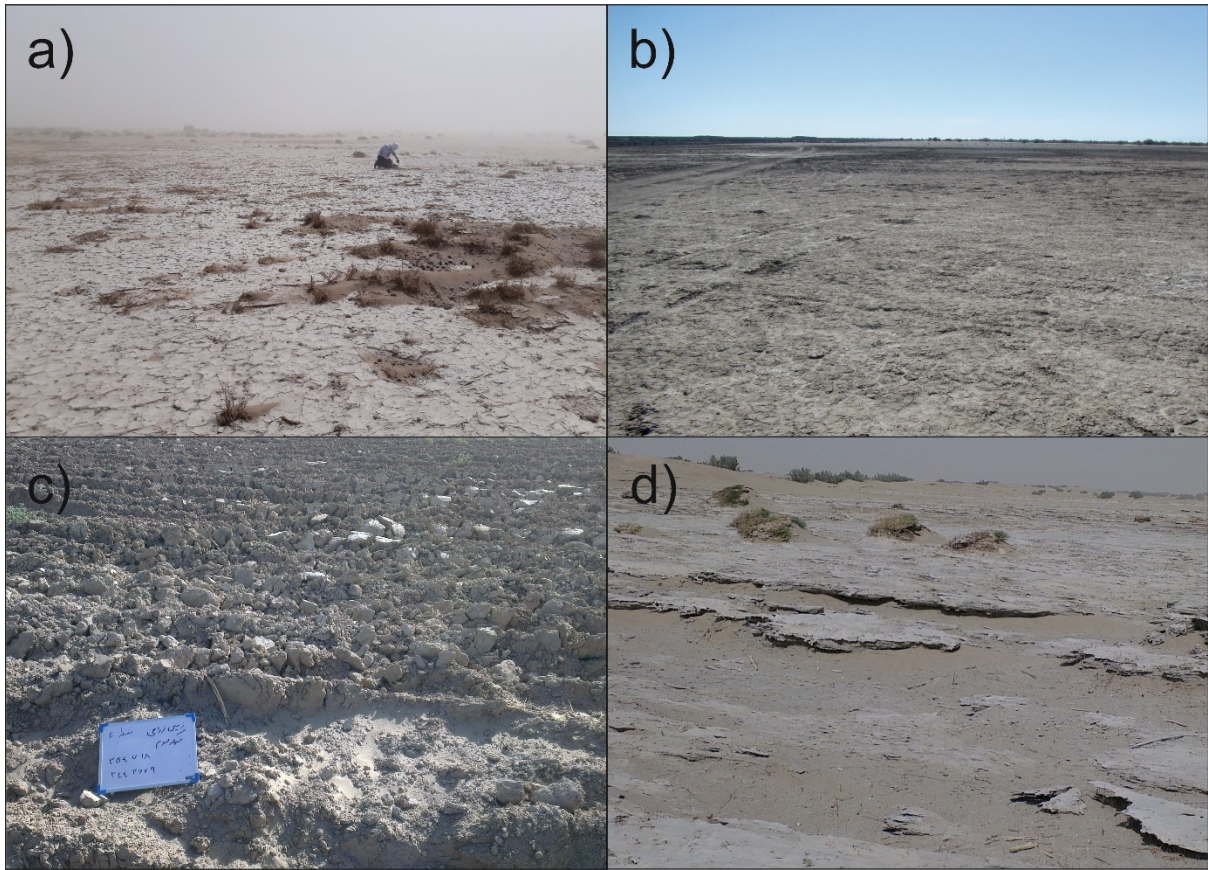


Figure 2.

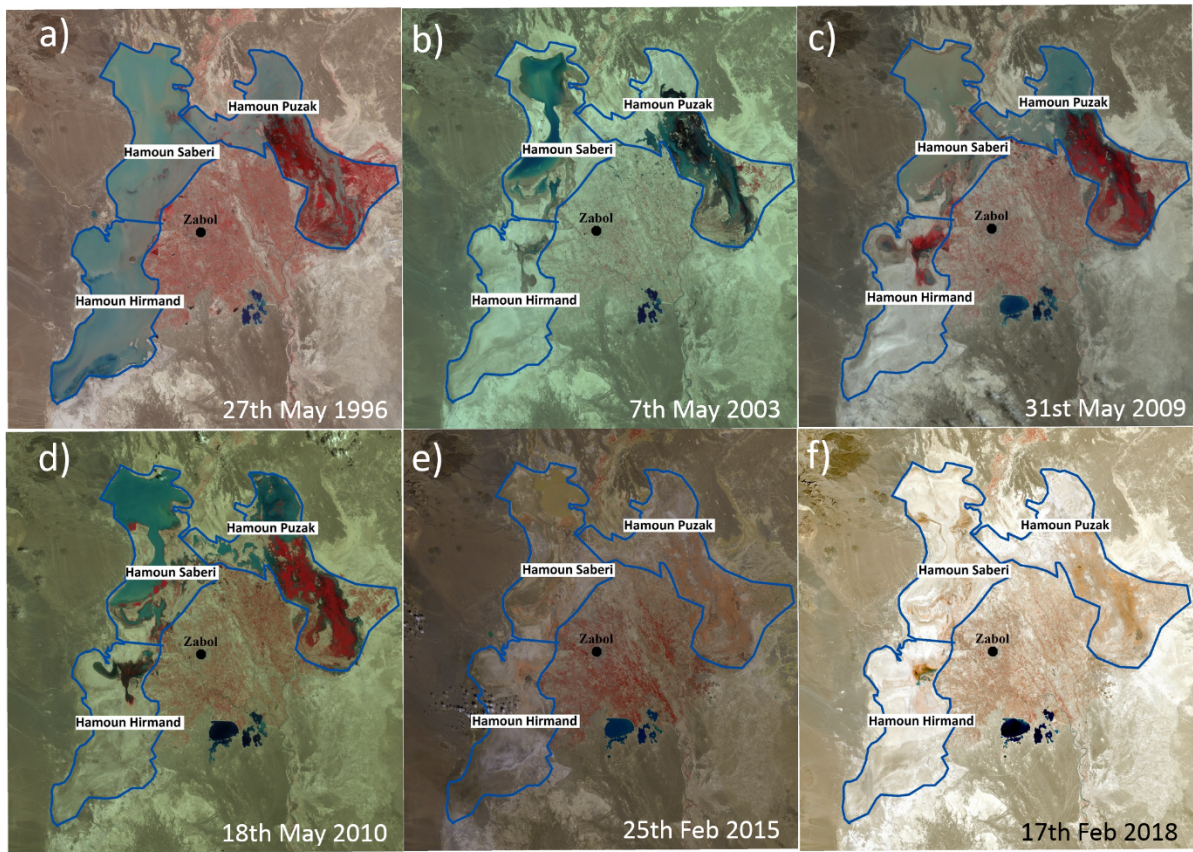


Figure 6.

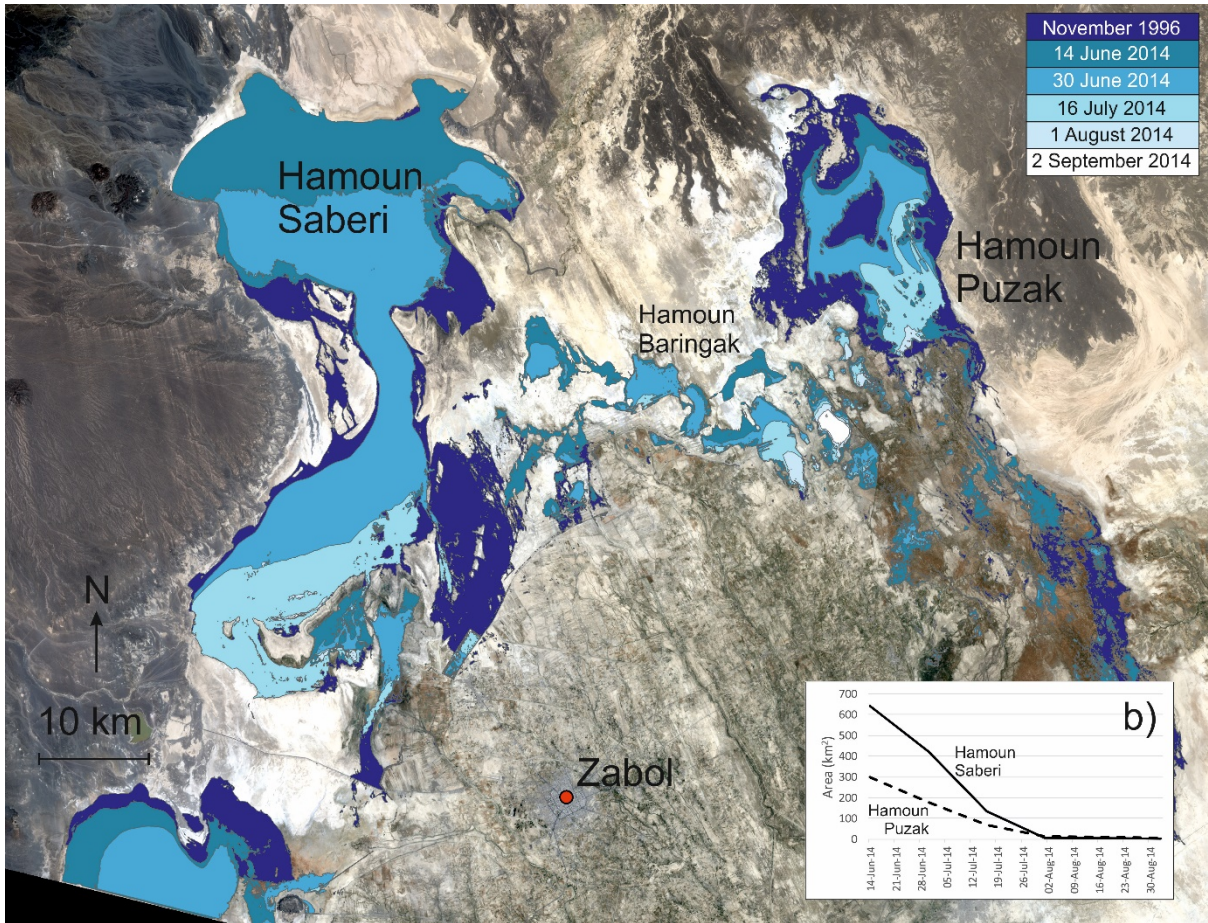


Figure 7.

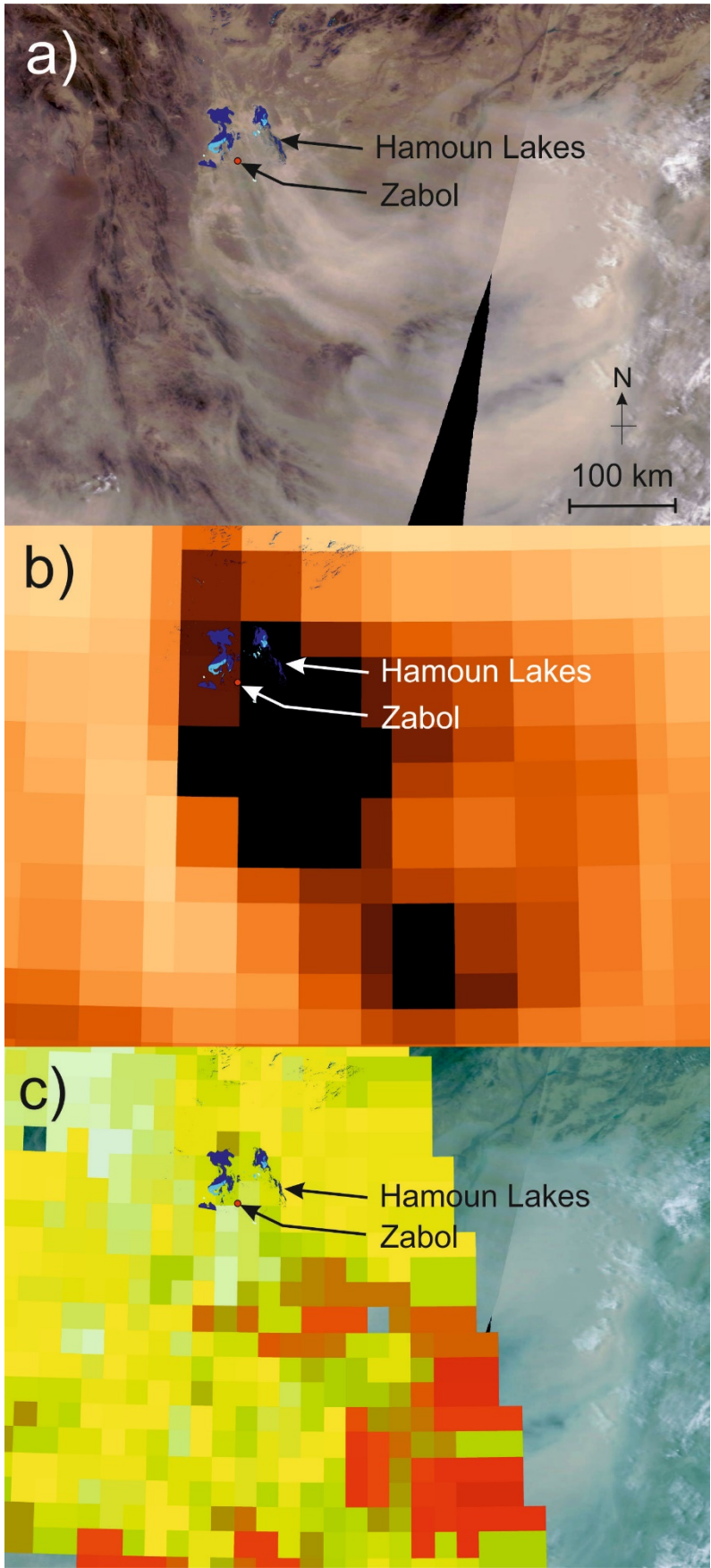


Figure 10.

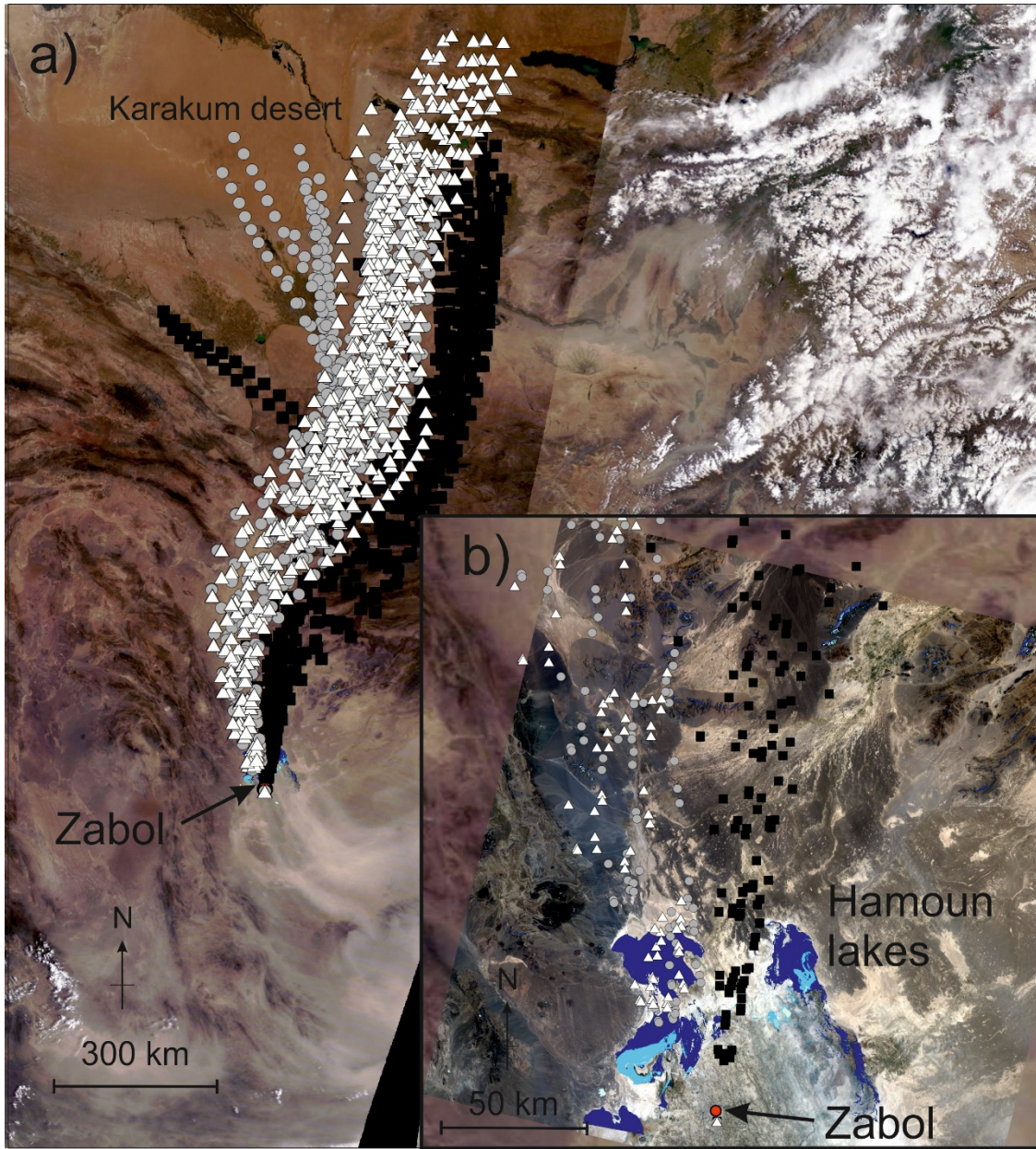


Figure 11.

CRediT Author statement

Reza Dahmardeh Behrooz: Software, Formal Analysis, Investigation, Visualization, Writing – Original Draft Preparation. **Hamid Gholami:** Software, Formal Analysis, Investigation, Visualization , Writing – Original Draft Preparation Supervision, Project Administration. **Matt W. Telfer:** Formal Analysis, Investigation, Visualization , Writing – Review & Editing. **John D. Jansen:** Investigation, Visualization, Writing – Review & Editing. **Abolhassan Fathabadi:** Conceptualization, Supervision, Project Administration